CELLULAR ROLE OF THE *DROSOPHILA* EFR3, ROLLING BLACKOUT (RBO) IN SYNAPTIC TRANSMISSION

By

Niranjana Vijayakrishnan

Dissertation

Submitted to the Faculty of the

Graduate School at Vanderbilt University

in partial fulfillment of the requirements

for the degree of

DOCTOR OF PHILOSOPHY

In

Neuroscience

May, 2010

Nashville, Tennessee

Approved by :

Professor Roger J.Colbran

Professor Kendal S.Broadie

Professor Randy D.Blakely

Professor Todd R.Graham

To Sri Akka, my parents, Raji and Dr.K.G.Vijayakrishnan and my husband

Ramadass Prabhakar,

with my love and gratitude.

ACKNOWLEDGEMENTS

I am grateful to my thesis advisor Dr. Kendal Broadie for letting me join his lab and work on this project. I am thankful for his support and input during the course of this study. I must acknowledge Elvin A. Woodruff III, the lab EM technician for his vital contribution to this project. I am deeply grateful to Drs. Jeffrey Rohrbough and Heinrich Matthies who taught me much about this project in my initial years in the lab. Jeff has a keen eye for detail and very patiently and painstakingly taught me several experimental techniques I used during the course of this study. Heiner initiated me into this project, I am extremely thankful to him for his mentorship, his infectious enthusiasm for science, and for his critical comments on my data. I also acknowledge Drs. Ralf Mohrmann, Fu-de Huang, Scott Phillips, Cheryl Gatto and Charles Tessier for useful discussion on data quantification and experimental design. I am grateful to Dr. Elaine Sanders-Bush for accepting me into the Neuroscience program and funding me during my first two years in the program. I thank the National Institutes of Health (NIH) for funding support during the course of this study.

I am thankful to my dissertation committee members for their keen involvement in this project and for their critical comments on my dissertation.

I thank Vandana Grover, for our daily ritual coffee break and discussions of life in graduate school and Joshua Decker for proofreading this dissertation.

TABLE OF CONTENTS

Page

LIST OF TABLES

Table Page

LIST OF FIGURES

LIST OF ABRREVIATIONS

A	Alanine
ADP	Adenosine Diphosphate
AP2	Adaptor Protein 2
AP180	Adaptor Protein 180
ANTH	AP180 N Terminal Homology
ARF	ADP Ribosylation Factor
ATP	Adenosine Triphosphate
AU	Arbitrary Units
BAR	Bin-Amphiphysin-Rvs
BRP	Bruchpilot
C/COOH	Carboxy Terminus
Ca^{2+}	Calcium
CALM	Clathrin Assembly Lymphoid Myeloid Leukemia
CCV	Clathrin Coated Vesicle
CDK5	Cyclin Dependent Kinase 5
CDP	Cytidine Diphosphate
CDS	CDP-Synthase
CIP4	CDC42 Interacting Protein 4
CME	Clathrin-Mediated Endocytosis
CMP44E	Conserved Membrane Protein 44E
CNS	Central Nervous System

CSP	Cysteine String Protein
D	Aspartic Acid
DAB	3’3’ Diaminobenzidine
DAG	Diacylglycerol
DIV	Days In Vitro
DLG	Disc Large
DLM	Dorsal Longitudinal Muscle
DNA	Deoxyribonucleic Acid
E	Glutamic Acid
EAS	Easily Shocked
EH	Eps15 Homology
EJP	Excitatory Junction Potential
ENTH	Epsin N Terminal Homology
EM	Electron Microscopy
EMS	Ethyl Methanesulfonate
ER	Endoplasmic Reticulum
ESI	Electrospray Ionization
F	Phenylalanine
FCH	FER/CIP4 Homology
FER	Fes Related Protein
FM	Fei Mao
GAP	Guanosine Triphosphatase Activating Protein
GED	GTPase Effector Domain

GEF	Guanine nucleotide-Exchange Factor
GFP	Green Fluorescent Protein
GPCR	G Protein Coupled Receptor
GPI	Glycophosphatidylinositol
GTP	Guanosine 5' Triphosphate
H	Histidine
HAS	High Acuity System
HRP	Horse Radish Peroxidase
HRS	Hepatocyte Growth Factor Regulated Tyrosine Kinase Substrate
HSS	High Sensitivity System
INAD	Inactivation No AfterPotential D
INAE	Inactivation No Afterpotential E
IP_3	Inositol 1,4,5,Trisphosphate
K	Lysine
L	Leucine
LAP	Like-AP 180
LCRP	Light Coincident Receptor Potential
N	Asparagine
N/NH_2	Amino Terminus
NMJ	Neuromuscular Junction
NORP A	No Receptor Potential A
NP40	Nonidet P40

NSF N-Ethylmaleimide–Sensitive Factor or N-Ethylmaleimide Sensitive Fusion Protein

NT Neurotransmittor

MALDI Matric Assisted Laser Desorption Ionization

Mg^{2+} Magnesium

MS Mass Spectrometry

P Proline

PA Phosphatidic Acid

PBS Phosphate Buffered Saline

PBS-TX Phosphate Buffered Saline-Triton X

PC Phosphatidylcholine

PE Phosphatidylethanolamine

PH Pleckstrin Homology

PI Phosphatidyl Inositol

PIP_2 Phosphatidyl Inositol 4,5 Bisphosphate

PKC Protein Kinase C

PLC Phospholipase C

PRD Proline-Rich Domain

PSD 95 Post Synaptic Density 95

PUFA Poly Unsaturated Fatty Acid

Q Glutamine

R Arginine

RBO Rolling Blackout

RDG A	Retinal Degeneration A
RDG B	Retinal Degeneration B
RME	Receptor-Mediated Endocytosis
RNA	Ribonucleic Acid
RVS	Reduced Viability Upon Starvation
S	Serine
SDS	Sodium Dodecyl Sulfate
SM	Sec1p-Like/Munc-18
SMC	Sub Microvillar Compartment
SMS	Stiff-Man Syndrome
SH3	Src Homology 3 Domain
SNAP	Soluble N-Ethylmaleimide-Sensitive Factor Attachment Protein
SNAP 25	Synaptosomal Associated Protein of 25 KDa
SNARE	Soluble *N*-Ethylmaleimide-Sensitive Fusion Protein Attachment Protein Receptor
STMA	Stambha A
SV	Synaptic Vesicle
TAP	Tandem Affinity Purification
TBS	Tris Buffered Saline
TEV	Tobacco Etch Virus
TGN	Trans Golgi Network
TLC	Thin Layer Chromatography
TPR	Tetratrico Peptide Repeat

TRP	Transient Receptor Potential
TRPL	Transient Receptor Potential Like
TS	Temperature-Sensitive
UAS	Upstream Activating Sequence
VAMP	Vesicle Associated Membrane Protein
VNC	Ventral Nerve Cord

CHAPTER I

INSIGHTS INTO THE SYNAPTIC VESICLE CYCLE: *DROSOPHILA* TEMPERATURE-SENSITIVE PARALYTIC MUTATIONS

Introduction to the synaptic vesicle cycle

Synaptic transmission is the basic mode of information exchange between nerve cells in the brain. Electrical activity produced by the flow of ions across the nerve cell plasma membrane results in an all-or-none binary signal, an action potential that propagates to the nerve terminal. At the presynaptic terminal this signal serves to activate specialized voltage-gated Ca^{2+} channels in the vicinity of the presynaptic active zone leading to the Ca^{2+}-triggered release of chemical transmitter into the synaptic cleft. Exocytosis at the synapse is coupled to compensatory mechanisms to recycle and refill vesicles so that synapses may cope with high demand conditions. This membrane-trafficking cycle in the presynaptic compartment is schematically depicted in Figure 1. Thus the chemical synapse is a highly evolved secretory apparatus, which relies on specialized molecular machinery for rapid translation of an excitatory electrical signal into neurotransmitter secretion. The synaptic vesicle (SV) cycle is a tightly regulated version of a cellular transport pathway conserved from yeast to humans and across various non-excitable cells. Regulation of this process requires the elaborate orchestration of both protein-protein and protein-lipid interactions coupling exocytosis and endocytosis (Littleton et al., 1998; Sudhof,

1995; Sudhof, 2004). Elucidating the molecular pathways involved in this process provides a mechanistic basis for understanding higher cognitive function.

Synaptic Vesicle Exocytosis

Our understanding of the process of neurotransmitter release by exocytosis comes from a convergence of genetic studies of vesicular transport in budding yeast *Saccharomyces cerevisiae*, *in vitro* reconstitution assays, and biochemical characterization of trafficking proteins from nerve terminal preparations. SVs filled with transmitter molecules are 'docked' to morphologically and molecularly specialized fusion sites within pre-synaptic active zones. The SNARE (soluble *N*-ethylmaleimide-sensitive fusion protein attachment protein receptor) complex forms, linking the vesicle to the terminal plasma membrane. Vesicles undergo priming and are poised to fuse in response to a Ca^{2+} transient (Sudhof, 2004). Fusion involves regulatory lipids, lipid partitioning/remodeling and the action of fusogenic proteins, possibly including SNAREs, Rab GTPases and their effectors, and SM (Sec1p-like/Munc-18) proteins (Dulubova et al., 1999; Rohrbough and Broadie, 2005). SV docking and fusion follow an evolutionarily conserved pathway for constitutive secretion that occurs in all eukaryotic cells, with the addition of neuron-specific regulatory proteins that ensure temporal specificity of fusion.

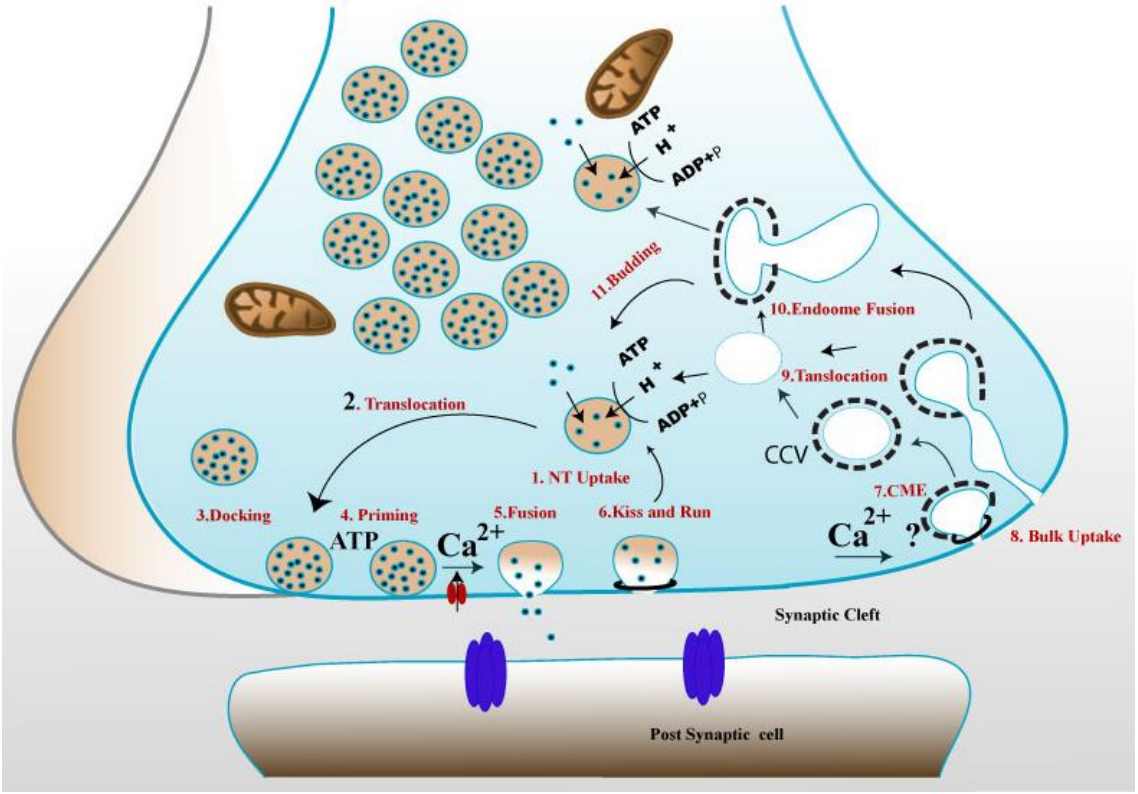

Figure 1: **The synaptic vesicle cycle.** Pathway of SVs in the nerve terminal are labelled in numerical order. 1: Neurotransmittor (NT) is pumped into the lumen of empty vesicles by active transport. 2: Filled vesicles translocate to specialized active zones. 3: The vesicle undergoes docking. 4: Vesicles undergo a prefusion priming reaction. 5: Vesicles undergo fusion or exocytic release following Ca^{2+} entry. Following exocytosis vesicle membrane may be retrieved in several ways. 6: Vesicles may undergo incomplete fusion through the opening and closing of a transient fusion pore -Kiss and run endocytosis. 6: Vesicles may be retrieved through clathrin-mediated endocytosis (CME), involving clathrin, AP2, AP180, dynamin and several other accessory proteins. This process may involve Ca^{2+}. 8: Following conditions of tonic stimulation, large portions of plasma membrane can be take up by bulk-endocytosis.9: Empty synaptic vesicles translocate into the terminal after shedding their clathrin coat. 10: After uncoating vesicles formed by CME or bulk uptake may fuse with early endosomes. This process may eliminate aged or mis-sorted proteins. 11: Vesicles are generated by budding from endosomes by a clathrin mediated mechanism. This step is not obligatory for all vesicles, SVs may go from step 9 directly to step 1 where they are acidified filled and retranslocated into the nerve terminal. Adapted from Sudhof , 1995.

The SNARE Hypothesis

The current working model for vesicle fusion is a modified version of the SNARE hypothesis originally proposed by Jim Rothman in 1993. Epitope tagged recombinant NSF (N-ethylmaleimide sensitive factor) a soluble hexameric protein known to be required for transport vesicle fusion in the Golgi, and SNAPs (Soluble N-ethylmaleimide sensitive factor attachment protein), cytoplasmic proteins required for NSF function, were bound to protein G beads and incubated with detergent-treated brain membrane fractions. The three proteins that bound and were eluted off the NSF-SNAP protein complex, were identified as the v–(vesicle) SNARE synaptobrevin or VAMP (vesicle associated membrane protein), and t-(target) SNARES, syntaxin 1A and SNAP 25 (synaptosomal associated protein of 25 kDa) (Sollner et al., 1993). Syntaxin itself had been previously identified as a 35kDa neurally enriched plasma membrane protein from rat brain that bound to synaptotagmin (Bennett et al., 1992). Each of the SNARE proteins identified has a SNARE domain, a heptad repeat that facilitates the formation of a four helix anti-parallel bundle, the SNARE complex.

The original model posited that the SNARE complex formation determined the directional specificity of vesicle targeting or docking to the presynaptic plasma membrane. However studies in *Drosophila* and the Squid have shown that perturbing the SNARE complex does not eliminate vesicle docking (Broadie et al., 1995; Hunt et al., 1994). Bacterial neurotoxins, tetanus and botulinum toxin have been shown to inhibit Ca^{2+} dependent exocytosis in femtomolar concentrations by proteolytic cleavage of SNARE proteins. Nervous system-

specific overexpression of tetanus toxins to disrupt synaptobrevin, and genetic null mutants for syntaxin 1A demonstrated the loss of synaptically evoked responses (Broadie et al., 1995; Sweeney et al., 1995). Ultrastructural analyses revealed the presence of presynaptically docked but arrested vesicles following SNARE proteins disruption. At the neuromuscular junction (NMJ), by ultrastructural criteria these vesicles are in close apposition of the presynaptic active zone, often in morphologically specialized areas on the presynaptic plasma membrane juxtaposed to the postsynaptic membrane (Couteaux and Pecot-Dechavassine, 1970). In *Drosophila* these morphological specializations of the active zones are demarcated by an electron-dense 'T' bar. Vesicles that are less than half a vesicle diameter on the presynaptic plasma membrane under the T bar are deemed to be docked. The accumulation of docked vesicles in boutons of syntaxin 1A null embryos suggested that the vesicles are unable to fuse and undergo exocytosis. They can however be forced to fuse using hyperosmotic saline, a treatment that triggers the release of docked vesicles (Broadie et al., 1995). Thus data from *Drosophila* using genetically targeted neural specific expression of neurotoxins strongly indicates that SNARE proteins have a post-docking fusion role in SV exocytosis. However using two different serotypes botulinum toxin, A and E that show differential effects on secretion due to their cleavage of t-SNARE SNAP25, it was the shown that Ca^{2+} dependent-binding of synaptotagmin to SNAP25 is essential for docking of neuroendocrine vesicles to the plasma membrane (Gerona et al., 2000). Similarly syntaxin 1A also seems essential for docking of dense core vesicles (de Wit et al., 2006). Other factors

may also be necessary in vesicle docking. Therefore it appears that the original hypothesis has now been modified - SNARE complex formation is the minimal machinery for membrane fusion both *in vitro* and *in vivo*, it may in addition have a role in vesicle docking.

During SNARE complex formation, synaptobrevin and syntaxin1A provide one helix each and SNAP25 provides two helices, making up the four helix core complex or SNAREpin. SNARE pairing is promiscuous *in vitro*, however when reconstituted into liposomes, SNARE pairing is a specific reaction that can only occur if the SNARE components are in the correct orientation (Weber et al., 2000). SNARE complex formation is therefore necessary and sufficient for membrane fusion *in vitro*. After docking, vesicles undergo a priming reaction. The molecular requirements of this reaction are not fully known, but the SNARE proteins zipper into a sodium dodecyl sulfate (SDS) and heat resistant stable complex, biochemically identified based on its sedimentation coefficient as a 7s complex. This complex may allow the vesicle membrane to be closely juxtaposed with the synaptic plasma membrane. Fusion is triggered following Ca^{2+} entry and binding to SV protein and Ca^{2+} sensor synaptotagmin1. The energy released from the formation of the SNARE complex may provide the mechanical force to facilitate membrane fusion. The steps involved in SNARE complex assembly and disassembly are depicted in Figure 2. Additional proteins bind to one or more of the SNARE proteins and regulate the temporal specificity of the fusion reaction.

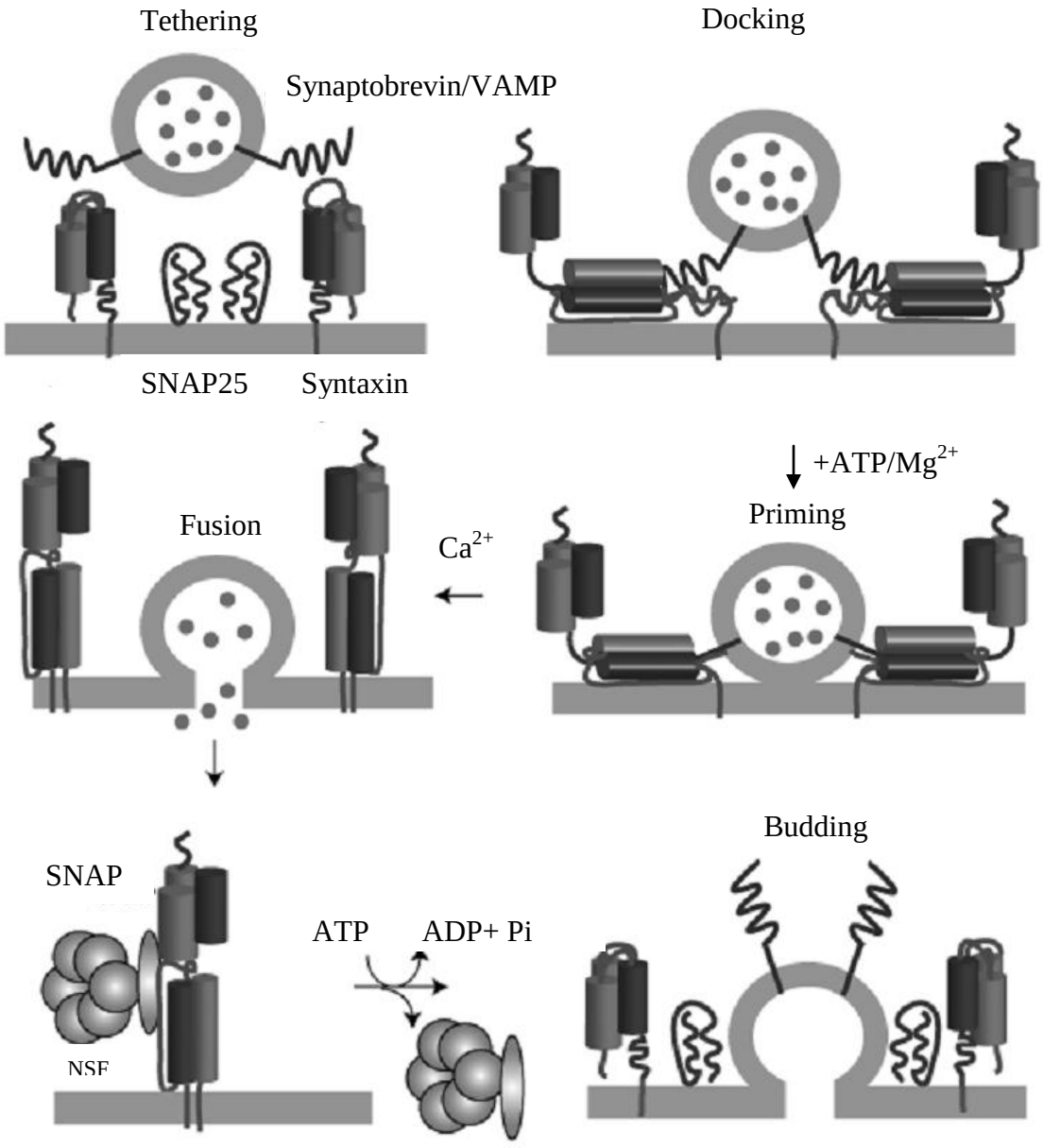

Figure 2: **SNARE assembly and disassembly during exocytosis.** The conformation of syntaxin changes from 'closed' to 'open' during SNARE complex formation. The four SNARE bundles of the complex zipper bringing the vesicles closer to the plasma membrane. This may lead to fusion. Following fusion the ATPase N-ethylmaleimide sensitive fusion protein (NSF) and soluble NSF attachment proteins (SNAPs) disassemble and recycle cis-SNARES on the plasma membrane. Adapted from (Rizo and Sudhof, 2002)

Syntaxin 1A

To date 15 syntaxin genes have been identified in mammals and 7 in yeast. Syntaxin 1A and 1B are neural specific isoforms involved in SV exocytosis. Syntaxin 1-4 are plasma membrane proteins. Other syntaxins are more ubiquitously expressed and involved in transport of organelles intracellularly. (syntaxins 7, 8, 12,13 are endosomal, syntaxin 5 is at the ER-Golgi boundary, syntaxin 6 is at the trans-Golgi network, for review (Teng et al., 2001)). As opposed to vertebrates, in *Drosophila* only one known syntaxin 1A gene exists. It maps to the cytological region 95E1-2 on the 3rd chromosome (Schulze et al., 1995). The protein shows about 82% homology to rat syntaxin. In addition to being associated with plasma membrane fractions, it is also associated with vesicle fractions (possibly SV or endosomal) (Schulze et al., 1995).

Syntaxin 1A is a 35 kDa protein with a C terminal transmembrane domain, a coiled-coil SNARE domain, a linker region and an N terminal autoinhibitory domain. The autoinhibitory domain or the H_{abc} domain comprises three α helices, HA/H1, HB/H2 and HC. Studies using NMR spectroscopy revealed that in its default position, the three helices of H_{abc} are autonomously folded onto the SNARE domain and in this conformation syntaxin is said to be “closed” conformation (Fernandez et al., 1998). Binding of syntaxin1A to other proteins varies depending on whether it is in a ‘closed’ or ‘open’ state. Syntaxin 1A interacts with several proteins through the N terminus, including Unc-13,

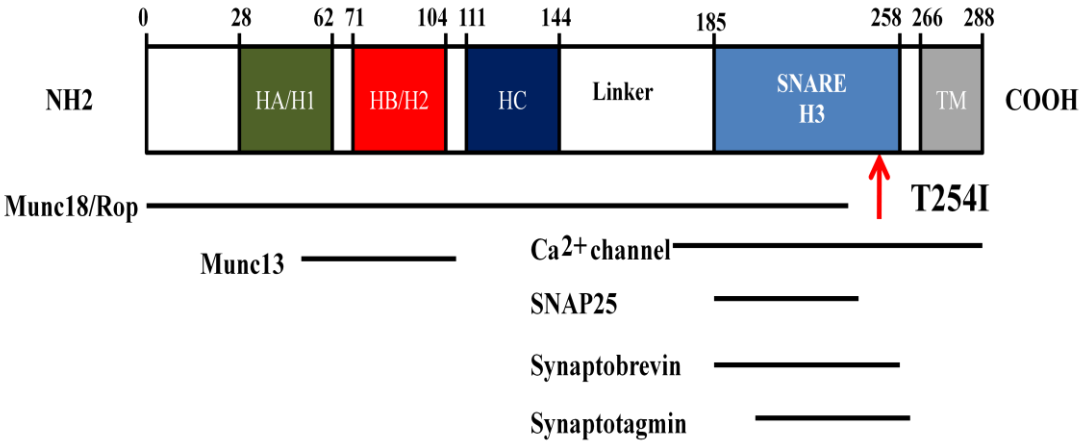

Figure 3 : **Domain structure of syntaxin 1A.** The C terminal region contains a transmembrane domain in plasmamembrane syntaxins (shown in grey). The N terminus contains three helices as observed by NMR spectroscopy, the HA, B and C domains (shown in green, red and blue respectively). These domains are involved in Munc18/ROP and Munc13 binding and determine 'closed' and 'open' confirmations of the protein. The C terminal cytoplasmic region (shown in light blue) contains a SNARE motif and is involved in core complex formation. The red arrow points to the TS mutation in *syx* $^{3\text{-}69}$, T254I. The numbers above the bar indicate protein sequence. Adapted from (Fernandez et al., 1998; Littleton et al., 1998; Wu et al., 1999).

(Betz et al., 1997), synaptotagmin (Shao et al., 1997), and Munc18 (Hata et al., 1993). The C terminal SNARE domain binds several proteins including SNAP25 and synaptobrevin to form the core SNARE complex. The domain structure of syntaxin1A and its binding partners are shown in Figure 3.

A temperature-sensitive mutation in the *Drosophila syntaxin* gene, $syx^{3\text{-}69}$, was isolated by ethylmethane sulfonate (EMS) mutagenesis (Littleton et al., 1998). Mutant animals paralyze reversibly when exposed to a restrictive temperature of 35^{o}C. The molecular lesion was identified as a T-I substitution at position 254 in the amino acid sequence (Figure 3). This lesion appears at the C terminal end of the SNARE motif close to the transmembrane domain of the protein. Although initial studies reported that these mutants showed a loss of synaptic transmission in electroretinogram (ERG) recordings from the eye, and a defect in the formation of the 7S SNARE complex, a recent reevaluation of this mutant has contradicted these results (Lagow et al., 2007; Littleton et al., 1998). This study showed that synaptic responses are not lost in the eye at restrictive temperature (38^{o}C). The giant fiber neurons are a pair of large bilateral interneurons that relay information from the eye to the musculature in thorax. They are known to mediate a light-dependent escape response, defined by stereotypical leg and wing movements. $syx^{3\text{-}69}$ animals show repetitive leg movements at both permissive and restrictive temperature following giant fiber stimulation. This would not be expected in a condition in which synaptic transmission is blocked. Furthermore, intracellular recordings from the dorsal longitudinal flight muscles (DLM), one of several muscle targets of the

polysynaptic escape circuit, show the persistence of action potentials, both spontaneous and evoked in response to stimulation in these mutants at restrictive temperature. Based on these results the authors concluded that synaptic transmission was not blocked in these mutants at restrictive temperature.

The threonine residue that is mutated is conserved in all plasma membrane syntaxins (except syntaxin4), however, isoleucine, valine or leucine are found in other constitutive syntaxins involved in intracellular trafficking. Based on structural modeling experiments, and the evolutionary conservation of isoleucine in constitutive syntaxins, the authors propose that the T254I mutation acts in a dominant positive fashion. It is proposed to increase the hydrophobicity of the +7 core layer of the SNARE complex, thereby removing a molecular break on fusion and enhancing the fusion rate at restrictive and permissive temperature.

Lipids in Exocytosis

While SNAREs mediate fusion by bringing apposing lipid bilayers together, the efficiency of fusion is increased by fusogenic lipids that alter the membrane topology such as phosphatidic acid (PA), PIP_2 and lipid modifying enzymes such as phosphatidylinositol 4 phosphate 5 kinase (Di Paolo et al., 2004).

The geometry of the lipid as determined by the charge and size of the head group may be of crucial importance in the fusion reaction. Cone shaped

lipids such as PA can bring about the formation of the hemifusion intermediate that precedes the fusion step in vitro when present on apposing membranes. PIP_2 when present on the outer leaflet of the vesicle, and PA when present on the inner leaflet of the plasma membrane can increase fusion rate. In addition PIP_2 may be distributed non-uniformly, enriched in raft-like domains that serve as foci for vesicle exocytosis.

Endocytosis

In neurons, compensatory recycling of lipids and proteins must be coupled to transmitter release to frugally and faithfully maintain subsequent rounds of release during sustained transmission. A failure of such a mechanism would result in vesicle pool depletion.

Endocytosis is an umbrella term for a wide variety of processes that refer to the mechanisms by which the cell internalizes macromolecules and particles into vesicles, derived from the plasma membrane. It is involved in a variety of physiological roles such as neurotransmission, signal transduction, development, antigen presentation and immune surveillance, cell-cell communication and pathological processes such as the entry of viral particles in to the cell. Broadly endocytic processes can be divided into two groups

1)Phagocytosis

2) Pinocytosis

Phagocytosis involves the engulfment of relatively large particulate matter such as bacteria, yeast, arterial fat deposits and dead cells by specialized cells such a macrophages, monocytes and neutrophils.

Pinocytosis includes four basic mechanisms- clathrin-mediated endocytosis (CME), caveolae–mediated endocytosis, macropinocytosis and clathrin and caveolin-independent endocytosis. At the synapse, due to the increased need for recycling, three specialized but different variations on some of the aforementioned pathways of endocytosis have been proposed for SV recovery (see Figure 1); CME (Heuser and Reese, 1973; Slepnev and De Camilli, 2000), “kiss and run”, which involves a transient fusion pore with the plasma membrane (Ceccarelli et al., 1973; Fesce et al., 1994; Gandhi and Stevens, 2003), and bulk retrieval/macroendocytosis of large portions of membrane to directly form endosomes (Leenders et al., 2002; Takei et al., 1996). SV endocytosis may involve the immediate fission of the fusion pore (‘kiss and run’), or slower recovery following complete fusion involving the clathrin-mediated retrieval of membrane proteins and lipids from the plasma membrane.

Clathrin-Mediated Endocytosis

At the molecular level, CME is by far the best characterized pathway (Hinshaw, 2000; Koenig and Ikeda, 1989; Narita et al., 1989; Wenk and De Camilli, 2004).It is a highly conserved pathway in species ranging from yeast to humans and is involved in a variety of processes such as synaptic vesicle retrieval, cell surface receptor internalization, nutrient uptake and internalization

of viruses. Clathrin a trimeric protein, serves as a mechanical scaffold to the budding membrane during endocytosis. Clathrin coats, seen as “bristle-coated vesicles”, were first observed in ultrastructural studies from *Mosquito* Oocytes by Roth and Porter in 1964. In 1975, Barbara Pearse biochemically purified clathrin from bovine brain extracts and named it ‘clathrin’, as a reference to its ‘lattice-like structure. Although clathrin coated pits are hard to find in a resting nerve terminal, several coated structures appear following depolarizing stimulation, indicative of the coupling of exo and endocytosis at the synapse. The presence of coated vesicles was shown at the Frog NMJ by John Heuser. Elegant studies using the ‘freeze slammer’, a device that allowed the rapid freezing of samples by slamming them against a copper block, allowed Heuser to obtain ‘snapshots’ of hexagonal networks of clathrin surrounding nerve terminal plasma membrane in different stages of invagination. These groundbreaking contributions began a new focus of interest in the field of membrane recycling and provided a widely accepted model for the process of endocytosis. Much of our knowledge of the structure of the clathrin lattice comes from subsequent cryoelectron microscopy and X ray crystallography studies by Tomas Kirchchausen. The basic unit of a clathrin lattice, the triskelion, is a spider-like molecule with three legs radiating away from a central hub (Figure 6).

The steps involved in coat formation and disassembly can be divided into coat nucleation or pit formation, propagation of the clathrin lattice, cargo recruitment (in the case of endocytosis of transmembrane ligands), pinching off of the coated vesicle or budding followed by transport of the vesicle away from

the membrane and uncoating (Brodsky et al., 2001). The sequence of events involved in CME are depicted in Figure 4.

The nucleation of the clathrin coat is a highly cooperative process in which the recruitment of one molecule leads to the recruitment and binding of several others. Adapter protein AP-2, is recruited to endocytic domains via protein-lipid interactions to link the membrane to the budding clathrin lattice (Gaidarov and Keen, 1999; Gonzalez-Gaitan and Jackle, 1997; Honing et al., 2005). Membrane lipids such as PIP_2 generated by phosphorylation and dephosphorylation of the inositol ring, provide the spatial and temporal signal to trigger endocytosis by facilitating target membrane recognition via interaction with AP2.

Accessory Factors Involved in CME

The domain structures of clathrin and accessory proteins involved in synaptic CME is depicted in Figure 5.

AP-2

AP-2 is a heterotetrameric protein complex consisting of α, β2, μ2 and σ2 adaptins. The N terminus of the α subunit binds PIP_2, thus facilitating target membrane recognition (Collins et al., 2002; Gaidarov and Keen, 1999). The C terminus then recruits other endocytic accessory proteins (Slepnev and De Camilli, 2000). While the β2 subunit binds clathrin via a clathrin-box domain

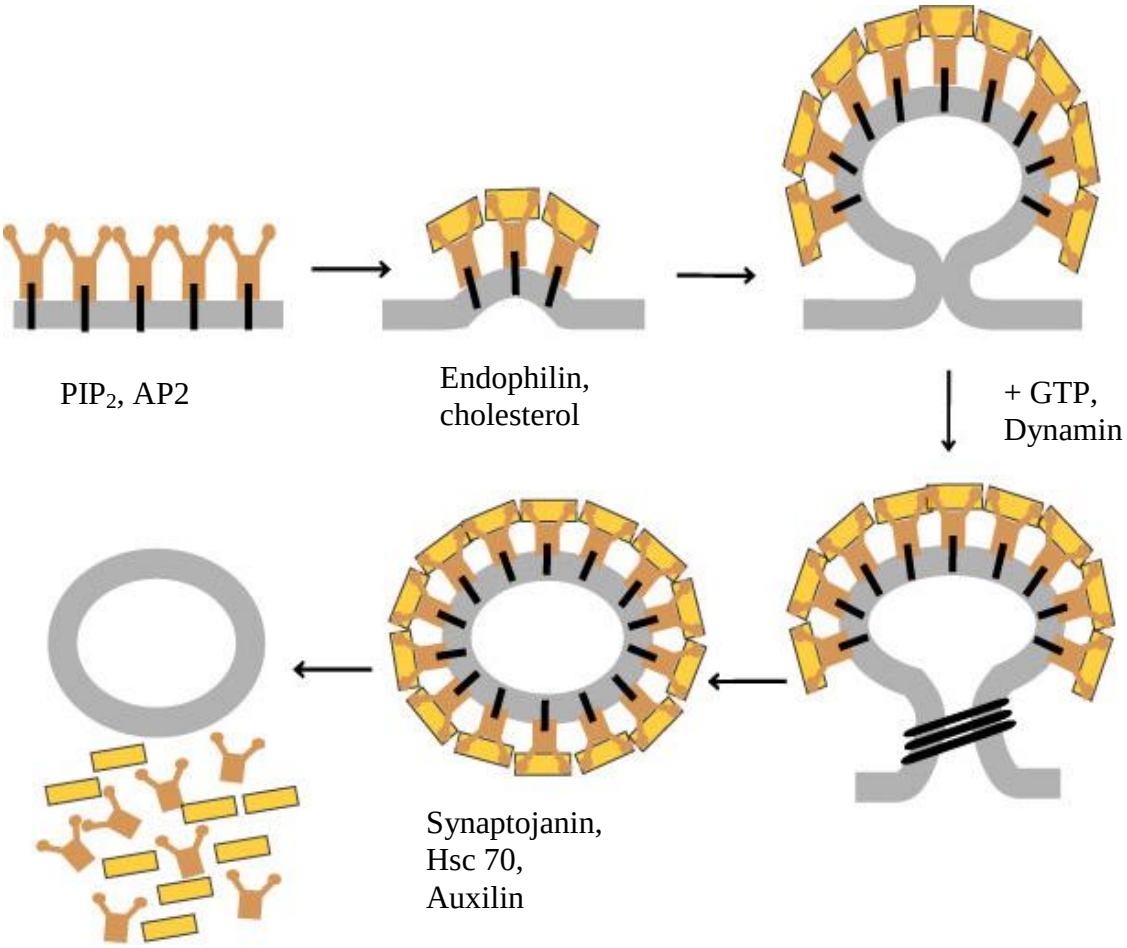

Figure 4: **Steps involved in clathrin-mediated endocytosis.** Adaptor recruitment and oligomerization at the site of endocytosis. This step may depend on the binding of membrane phosphatidylinositol 4,5, bis phosphate (PIP_2) by AP2. Membrane budding following clathrin recruitment. This may require membrane cholesterol and endophilin. Membrane curvature to form a deeply invaginated pit following coat expansion. The neck of the coated pit elongates. Dynamin mediated scission to generate a clathrin coated vesicle. Vesicle uncoating may be mediated by synaptojanin, heat shock cognate protein 70 (Hsc 70), and auxilin. Adapted from (Narayanan et al., 2005; Slepnev and De Camilli, 2000).

(Owen et al., 2000), μ2 can also interact with PIP_2 (Collins et al., 2002; Rohde et al., 2002). The current model holds that the recruitment and oligomerization of the adaptor protein in a highly cooperative process leads to the recruitment and polymerization of clathrin.

As the coated pit expands, the membrane acquires curvature to form a vesicle shaped structure. Accessory proteins like dynamin, AP-180/CALM, synaptotagmin, epsin, eps15, amphyphysin, intersectin and syndapin are recruited to the budding coated vesicle (Figure 6).

AP180/CALM (Alternatively called NP185, F1-20 or AP-3)

AP180 is one of the many clathrin accessory proteins required for coat formation (Ahle and Ungewickell, 1986). The C terminal portion of the protein contains 12 repeats, each 23 amino acids in length, and often containing a DLL motif that binds clathrin (Morgan et al., 1999). This repeat is also found in CALM (clathrin assembly lymphoid myeloid leukemia protein), a closely related homolog of AP180 thought to be required for a clathrin assembly in non-neuronal cells (Tebar et al., 1999). Clathrin binding by AP180 is a cooperative process further increased following binding of AP-2 (Hao et al., 1999). The N terminal portion of AP180 contains an ANTH (AP180 N-terminal homology) domain that can bind membrane PIP_2 (Ford et al., 2001). This has been proposed to mediate nucleation of the clathrin coat at endocytic hotspots. Studies from the *Drosophila* AP180 homolog, *lap* (Like AP180) null mutant revealed reduced vesicle number and defects in activity-dependent FM dye uptake. Excitatory junction potentials

(EJPs - which measure muscle depolarization in response to excitatory nerve stimulation, at the NMJ), were of decreased amplitude consistent with a decrease in the readily releasable vesicle pool size in the presynaptic terminal (Zhang et al., 1998). Notably the median SV diameter is shifted in the mutants from 40 nm in control terminals to ~80 nm. In line with a role in reforming vesicles, clathrin, synaptotagmin, synatobrevin/VAMP, and CSP (Cysteine String Protein) are mislocalized in AP 180 mutants (Bao et al., 2005; Nonet et al., 1999; Zhang et al., 1998). It is proposed that AP180 functions to regulate vesicle size and reform and sort proteins into SVs.

Amphiphysin

Amphiphysin is 75kDa neuronally enriched highly acidic protein conserved from yeast to humans. It was originally identified in chicken synaptic membrane preparations (Lichte et al., 1992). The protein has a N terminal BAR domain (BIN-amphiphysin-RVS), a central domain implicated in clathrin binding and a C terminal SH3 (Src homology 3) domain (Figure 6). The C terminal SH3 domain is implicated as an autoantigen in a rare neurological condition called Stiff-man syndrome (SMS), characterized by rigidity of musculature. Mammalian amphiphysins (both 1 and 2) show weak homology to yeast proteins rvs161 and rvs167 (reduced viability on nutrient starvation), two genes that are implicated in endocytosis (Munn et al., 1995). A role for amphiphysin in endocytosis first emerged when it was shown to bind to dynamin via its C terminal SH3 domain (David et al., 1996). Microinjecting live neuronal synapses with a recombinant

fluorophore-tagged SH3 domain peptide from human amphiphysin produced an arrest in synaptic endocytosis. As is the case with most endocytic phenotypes this phenotype was exacerbated under conditions of increased exocytosis. Large clathrin coated pits were found to decorate the plasma membrane by ultrastructure. This condition was phenocopied by injecting the proline-rich C terminal portion of dynamin, indicating that the amphiphysin-dynamin interaction is necessary *in vivo* for endocytosis (Shupliakov et al., 1997). The C terminal SH3 domain also mediates interactions with the PRD domain of synaptojanin. The N terminal portion of amphiphysin contains a BAR domain that interacts with membrane lipids. *In vitro* experiments have shown that the BAR domain can bind to liposomes, evaginate and convert them into high curvature tubules (Ren et al., 2006). BAR domains are known to form homo/heteromers with highly positively charged residues. This may help a BAR domain containing protein like amphiphysin to bind to the negatively charged membrane and dynamically induce bending and curvature in endocytic microdomains. The middle clathrin binding domain of amphiphysin mediates binding to the ear domain of α adaptin (David et al., 1996).

Amphiphysin is proposed to function as a multifunctional adaptor protein linking clathrin coat proteins to the budding lipid membrane and recruiting proteins such as synaptojanin and dynamin to the budding coated pit, and in the generation of highly curved membrane structures during vesicle scission (Slepnev and De Camilli, 2000). In addition work on amphiphysin-like proteins in yeast and *Drosophila* reveals a strong nexus with the actin cytoskeleton,

endocytosis, cell proliferation and polarity. Amphiphysin may be involved in suppressing tumor growth by integrating signals from these various pathways

Data from *Drosophila*, however, appear to show no role for amphiphysin in synaptic vesicle retrieval. In *Drosophila*, a single amphiphysin gene (*damph*) is present with four splice isoforms (Zelhof et al., 2001). Amphiphysin is expressed in distinct membrane microdomains, both in epithelial and neural cells. However contrary to data from vertebrates, in *Drosophila* it is expressed postsynaptically in muscle transverse (T) tubules and colocalizing with muscle membrane marker DLG (disc large), but is conspicuous in its absence from presynaptic structures, (Razzaq et al., 2001). *damph* null animals are viable, have pleiotropic defects but no observable defects in presynaptic endocytosis. They are reported to be sluggish as larvae and adult animals do not fly. They have defects in postsynaptic protein localization and function (Zelhof et al., 2001). Importantly SH3 domain of *Drosophila* Amph does not bind dynamin, *damp* mutants do not show any observable genetic interaction with the *shibire* mutants, and Amph does not colocalize with dynamin (Zelhof et al., 2001). Amph in *Drosophila* appears to be required for SNARE-dependent postsynaptic exocytosis, in T-tubule biogenesis and in recruiting and maintaining proteins involved in membrane curvature.

Dynamin

The GTPase dynamin is part of a superfamily consisting of classical dynamins, dynamin-like proteins, OPA, Mx proteins, mitofusins and guanylate-

binding proteins/atlastins. Dynamin and dynamin-like proteins are involved in the scission of a wide variety of vesicles and organelles ranging from clathrin-coated vesicles (CCV), caveolae, phagosomes and mitochondria (Marks et al., 2001; Praefcke and McMahon, 2004). *Drosophila* possess one dynamin gene with 6 splice variants while there are three mammalian isoforms (dynamin 1-neuronal, 2-ubiquitous and 3) and several splice variants. Fundamental to our understanding of dynamin and how it function in synaptic vesicle endocytosis was the discovery of the *Drosophila* temperature-sensitive (TS) paralytic mutation, *shibire* by David Suzuki (Grigliatti et al., 1973). The mutant flies become paralyzed when the temperature is raised to 28^{o}C, but resume activity after they are returned to 25^{o}C. This behavior is mirrored at the ultrastructural level in nerve terminals of *shibire* animals by the depletion of vesicles, and the occurrence of apparently arrested invaginated endocytic membrane intermediates with an electron dense collar around the necks of the coated pits both in neuronal and non-neuronal tissues (Kosaka and Ikeda, 1983; Poodry and Edgar, 1979). The *shibire* gene was shown to encode dynamin, previously characterized as a protein that could bind microtubules *in vitro* (Chen et al., 1991; van der Bliek and Meyerowitz, 1991).

After nearly 20 years of study the precise mechanism of action is still a matter of debate. Dynamin is a multidomain protein. It contains a N terminal GTPase domain, a “middle” domain which promotes self-assembly, a PIP_2 binding PH domain, a GED (GTPase enhancing domain) and a C terminal PRD (Figure 5). Dynamin is a noncanonical GTPase, it has a low affinity for GTP,

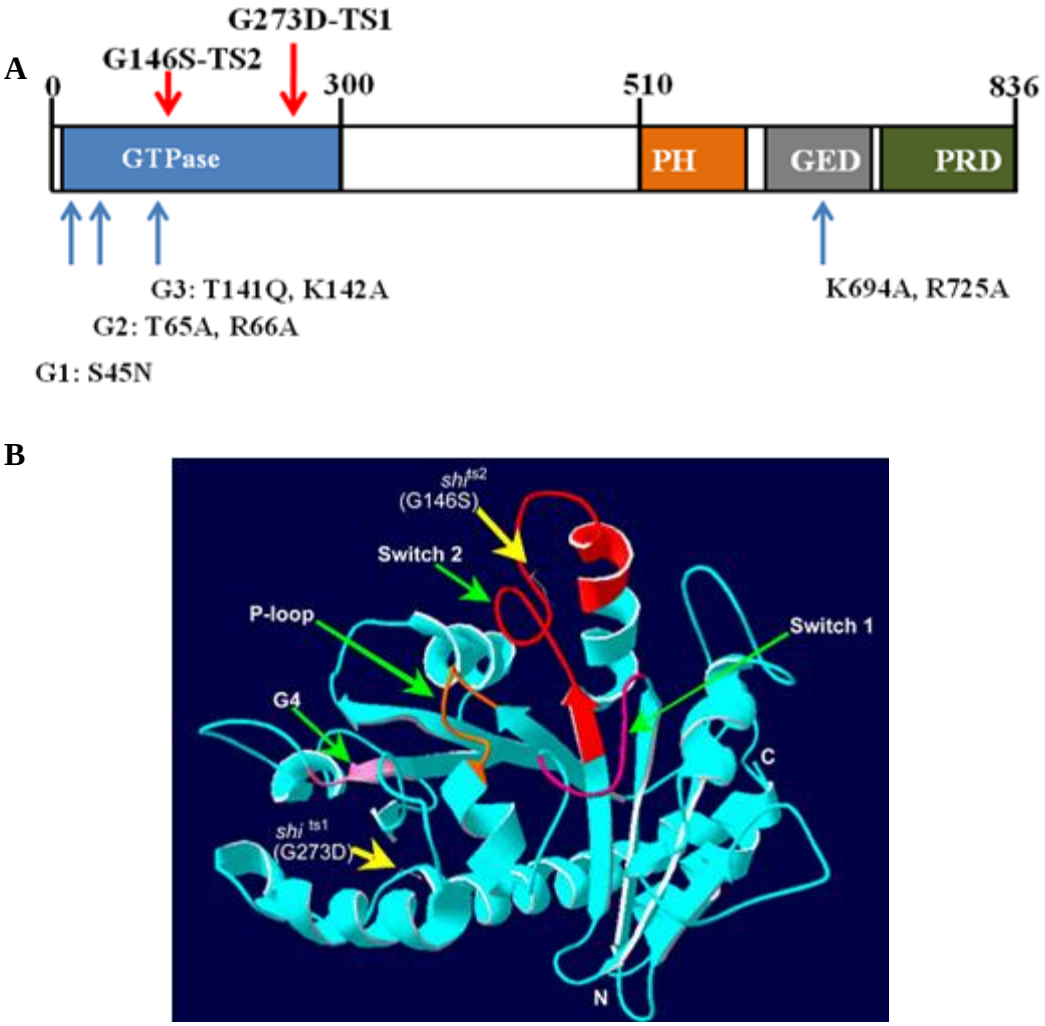

Figure 5: **Domain structure of dynamin**. **A,** N terminal GTPase domain, middle region, PIP_2 binding Pleckstrin homology (PH) domain, GTPase effector domain (GED) which promotes oligomerization and GTP hydrolysis, and a proline rich domain (PRD) which binds to SH3 domain containing Amphiphysin and Endophilin. 3 out of 4 nucleotide binding sequences (G1-G4) are shown in the GTPase domain. Positions of *shi*^{ts1} and *shi*^{ts2}, shown (red arrows) along with several available point mutations in mammalian Dynamin (blue arrows). **B,** Thread diagram model of the GTPase domain of human Dynamin-1, showing the locations of the ts1 and ts2 mutation and the nucleotide bindings regions, (G1-G4). Reproduced with permission from (Creative Commons Attribution-Noncommercial-Share Alike 3.0 Unported license)
Adapted from (Narayanan et al., 2005; Slepnev and De Camilli, 2000)

a high GTP hydrolysis rate(basal rate of ~1min^{-1}) which is increased 50-100 fold by self-assembly and the formation of higher order ring or spiral structures. Self-assembly and oligomerization are mediated by the GED a putative intramolecular GAP (GTPase activating protein) (Binns et al., 1999; Muhlberg et al., 1997; Song et al., 2004). It has been shown that the GTPase activity of dynamin is enhanced by protein oligomerization facilitated by its GED (GTP Enhancing Domain). The following models have been proposed to explain the mechanistic basis of dynamin function.

1) A mechanochemical enzyme, dynamin effectively converts the chemical energy produced by GTP hydrolysis into the mechanical shearing force necessary to sever the membrane. Two variants of this model have been proposed

a) "Pinchase" model – scission occurs due to constriction the neck of the invaginating vesicle (Sweitzer and Hinshaw, 1998)

or

b) "Poppase"model – Scission occurs by stretching or increasing the helical pitch of the dynamin spirals (Stowell et al., 1999).

2) A regulatory protein, dynamin functions as a canonical GTPase. GTP hydrolysis facilitates recruitment of downstream effectors that constrict the neck of the budding vesicle and bring about scission.

3) A third model aiming to reconcile the above two posits that the initial rate limiting step of GTP hydrolysis constricts the necks of budding vesicles, this

promotes self-assembly which further enhances GTPase activity facilitating the final steps in the formation of a CCV (Narayanan et al., 2005).

Most studies aiming to elucidate the mechanism of action of dynamin have relied on making molecular lesions (see Figure 5) in the protein structure and analyzing the nature of the endocytic arrest produce by electron microscopy (EM). In spite of this the mechanism remains much debated. It has been suggested that GTP binding but not hydrolysis are necessary for endocytosis, based on mutation that decrease self-assembly (K694A) and mutations that are defective for GAP activity (R725A) (Sever et al., 2000). An alternate view is that both GTP binding and hydrolysis are necessary for fission (Marks et al., 2001).The molecular lesion in the *shi*^{ts1} mutant a G273D substitution in the amino acid sequence of the protein that may disrupt coordination with GTP or one of the helices in the GTPase domain (Figure 5). It is still not known how this protein is able to function at permissive temperature. *shi*^{ts2}, (G146S) also occurs in the GTPase domain and is thought to disrupt a loop region (switch2) in the protein that affects its ability to bind GTP (Narayanan et al., 2005). Interestingly two suppresors of the *shi*^{ts2} mutation (*sushi*-suppresor of *shibire*-G146S/A738T and G146S/T749I) both mapping to the GED domain, completely rescue the TS paralytic and endocytic defects seen in *shi*^{ts2} without affecting the GTP binding defect suggesting that reduced GTP hydrolysis can compensate for a reduced ability to bind GTP (Figure 5).

Overexpression of a mutation in mammalian Dynamin analogous to *shi*^{ts1} (K44A) in cell lines leads to the accumulation of coated pit, similar to those seen

in *Drosophila* (Damke et al., 2001). The mutation is thought to act as a dominant negative and inhibit some types of endocytosis (transferrin receptor uptake (Damke et al., 1995)) but not others (toxin and tracer uptake GPI-anchored proteins and Dopamine D2 receptor) (Chatterjee and Mayor, 2001; Damke et al., 1995; Vickery and von Zastrow, 1999). Mammalian groups have suggested that uptake of tracers and toxins by fluid-phase endocytosis is dynamin-independent and persists even after overexpression of dominant-negative dynamin (Damke et al., 1995). In *Drosophila* however, the uptake of tracers like avidin and HRP (horse radish peroxidase), also described as fluid phase uptake, seems to require clathrin and dynamin function and is blocked in *shi*^{ts1} mutants at restrictive temperature (Kosaka and Ikeda, 1983) Mammalian cells may have dynamin-independent mechanisms of endocytosis or alternatively this may be due to compensation by dynamin 2 and 3.

Several lines of evidence suggest that in addition to its role in SV scission dynamin may play additional roles in endocytosis, including coated pit formation and vesicle uncoating. Dynamin recruitment to a coated pit is an early event even before membrane indentation (Merrifield et al., 2002).The use of K44A dominant negative dynamin peptide to block uptake reveals that the endocytic intermediates formed still have a large pore, are connected to the plasma membrane and accessible to large molecular probes such as avidin and HRP (Damke et al., 1995) (Carter et al., 1993). A novel small molecule dynamin inhibitor, dynasore non-competitively and reversibly inhibits GTP hydrolysis without affecting binding affinity. Dynasore treatment of cells shows inhibition of

endocytosis at 2 stages at the ultrastructural level. ‘U’ shaped half formed pits and ‘O’ shaped pits that were fully formed and ready to pinch off were seen (Macia et al., 2006). These data suggest that dynamin may function at 2 stages during endocytosis, the O-shaped pit is formed by an arrest at the pre-constriction stage in a deeply invaginated vesicle with the pore still accessible to the extracellular surface. The U-shaped structure has not been previously reported but may be an intermediate stage after early invagination before constriction. Therefore dynamin may be required at an earlier stage in the endocytic pathway. However studies using *shi*^{ts1} and the analogous K44A mutation in mammalian cell lines (both of which inhibit GTP hydrolysis and binding) reveal only fully formed O-shaped structures (Kosaka and Ikeda, 1983). It is therefore possible that the block produced by dynasore may be the result of blocking other GTPases that play a role in the early steps of membrane invagination. Alternatively it may be mechanistically similar to the block produced by nonhydrolyzable GTPγS, by increasing self-assembly and promoting the formation of curved U-shaped structures possibly due to recruitment of curvature inducing BAR domain containing proteins like endophilin (Nankoe and Sever, 2006).

Dynamin may be required for later stages of endocytic trafficking from internal endocytic compartments, for example from late endosome to the trans Golgi network (TGN) (Llorente et al., 1998; Nicoziani et al., 2000). Dynamin independent modes of endocytosis have been proposed to exist by the use of nonhydrolyzable GTP analogues, measures of membrane surface area

(capacitance), RNAi mediated knock down, the use of the dominant negative K44A peptide and optical imaging using styryl dye uptake. A Rac – dependent pathway for the internalization of nicotinic acetylcholine receptors, an ARF1 and cdc42 dependent pathway for the internalization of GPI anchored proteins, a pathway for internalization of GPI anchored proteins, a fluid phase pathway for internalization of dextrans in cultured *Drosophila* larval hemocytes and a protein kinase A dependent pathway in dorsal root ganglion neurons are some forms of endocytosis proposed to be dynamin independent (Guha et al., 2003; Kumari et al., 2008; Kumari and Mayor, 2008; Zhang et al., 2004). However, it is not known what the scission mechanism is precisely for these forms of retrieval.

The use of recombinant dynamin in affinity chromatography studies has lead to the identification of multiple interactors (Takei et al., 1996). The C terminal PRD can bind multiple SH3 domain containing effectors including intersectin, amphiphysin, endophilin, synaptojanin, syndapin and cortactin. Dynamin can thereby act as a molecular scaffold and connect the budding vesicle to the actin cytoskeleton.

Endophilin and Synaptojanin

Dynamin is stabilized by endophilin, which may help generate membrane curvature and serve as an adaptor to recruit other proteins to the lipid domains of endocytosis (Ringstad et al., 1999). The synaptojanin phosphoinositide phosphatase, with two distinct phosphatase domains, facilitates clathrin

Clathrin triskelion

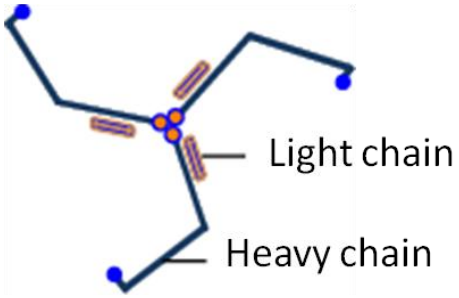

Coat protein formed by trimerization of three heavy(170kDa) and light chains (33-35kDa)The heavy chain is non-essential in yeast but essential in *Drosophila*. The NH_2 portion of the heavy chain (blue) is involved in membrane attachment and interacts with adaptor proteins. The COOH domain (orange) acts as a hub

Adaptor Protein 2 (AP-2)

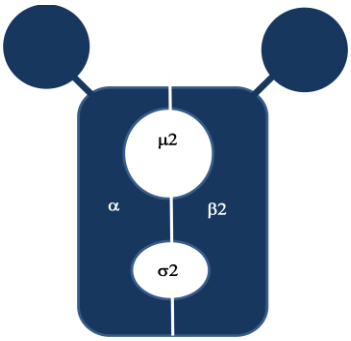

A heteroterameric protein complex consisting of α (100kDa), β2 (100kDa), μ2 (50kDa) and σ2 (19kDa) subunits. Interacts with several clathrin accessory factors and lipids through the ear domains. Non-essential in yeast but essential in *Drosophila*. Binds phosphoinositides.

AP180

An accessory adaptor for clathrin. Contains a Asp-Leu-Leu (DLL) in the COOH terminus that binds clathrin, also binds ear domain of AP-2. Binds phosphoinositides. Proposed to control vesicle size. *Drosophila* homologue, LAP (Like-AP-180),yeast YP1801, YP1802. Ubiquitously expressed isoform CALM.

Dynamin

A 100kDa GTPase, encoded by the *shibire* gene in *Drosophila*, Vps1 in yeast and 3 genes dynamin 1,2 and 3.in mammals Showed to be required for the scission of vesicles.

Figure 6: **Domain structure of clathrin and accessory protein involved in clathrin-mediated endocytosis.**

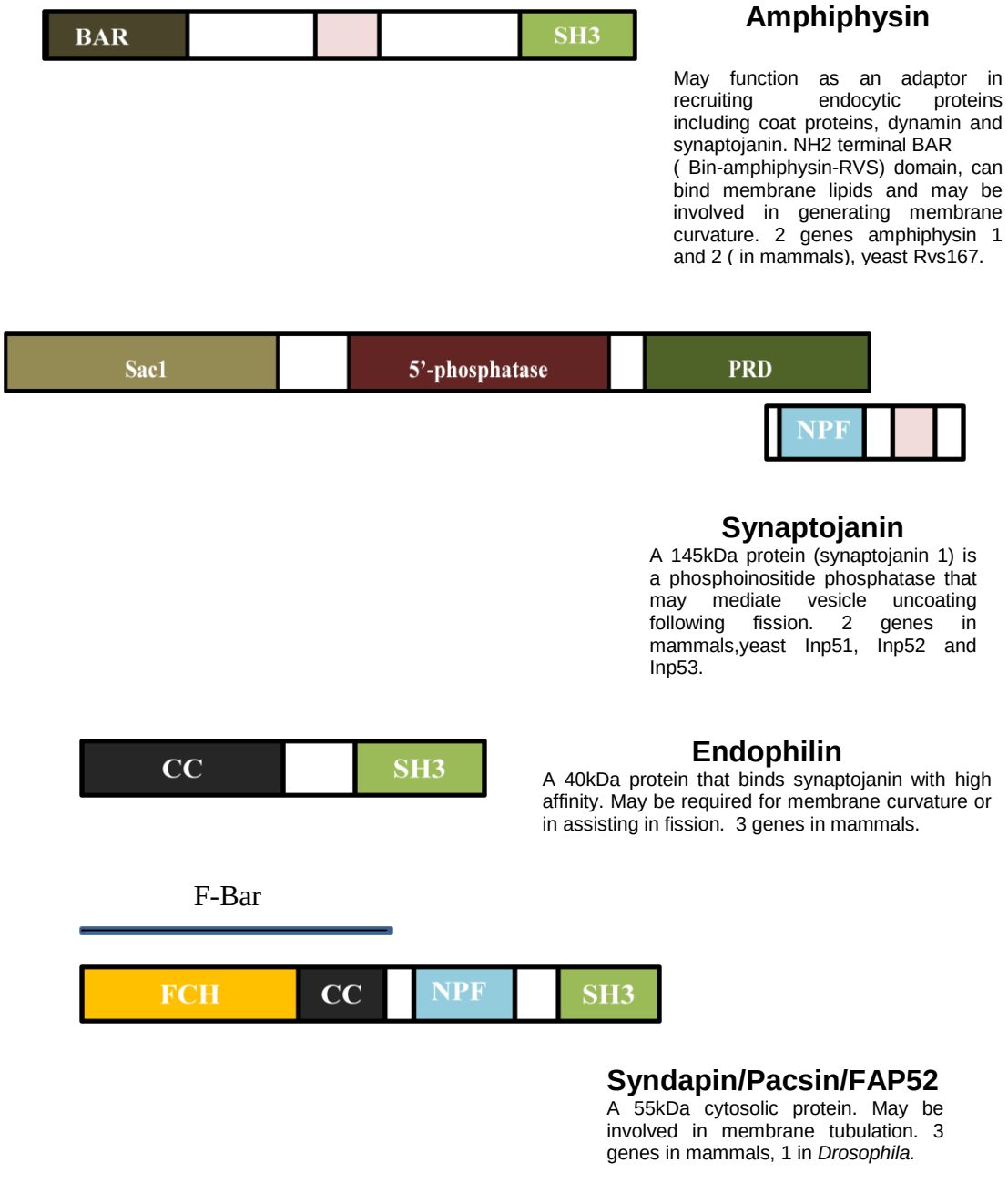

Figure 6: **Domain structure of clathrin and accessory protein involved in clathrin-mediated endocytosis.** CC coiled coil, SH3, src homology 3, NPF, Asp-Pro-Phe motif, PRD, proline rich domain GED, GTPase enhancing domain, EH, EPS15 homology, ENTH, epsin amino-terminal homology, BAR, Bin-Amphiphysin, Rvs, PH, pleskstrin homology, FCH, FER/CIP4 homology. Adapted from (Narayanan et al., 2005; Slepnev and De Camilli, 2000).

uncoating (Haffner et al., 2000). After uncoating vesicles may directly return to a fusion competent pool and/or fuse with sorting endosomes from which new vesicles bud.

Bulk Endocytosis

This involves the formation of large invaginations from the plasma membrane and the subsequent formation of large endosomal-like endocytic intermediates from which smaller vesicles may be pinched off in a clathrin-dependent mechanism (Figure 1). This pathway is recruited during periods of long and intense stimulation and allows the synaptic terminal to recover large amounts of vesicle membrane from which more than one SV can be formed (Royle and Lagnado, 2003). This form of retrieval has been reported in a variety of systems, the NMJ (Richards et al., 2000; Teng et al., 2007), the calyx of Held (de Lange et al., 2003), retinal bipolar synapses (Holt et al., 2003) and lamprey reticulospinal synapses (Gad et al., 1998). Bulk uptake may be activated physiologically in the CNS under conditions of long term potentiation or burst firing during epileptic seizures and is linked to macropinocytosis of fluid phase uptake in non-neuronal cells. The molecular mechanisms involved in this pathway are not as well elucidated as they are for CME. A group of structurally unrelated endocytic proteins termed dephosphins, due to their ability to be dephosphorylated by the calcium-dependent phosphatase calcineurin, play a critical role in bulk endocytosis. Dephosphins consists of dynamin I, synaptojanin, amphiphysin I and II, epsin, eps15, AP180 and PIP kinase γ (Cousin and

Robinson, 2001; Evans and Cousin, 2007). Dynamin I is dephosphorylated at S774 and S778 during endocytosis. Cyclin-dependent kinase 5 (CDK5) has been identified as an endogenous dephosphin kinase, shown to be required for the rephosphorylation of dynamin I, synaptojanin, PIP kinase γ and amphiphysin I (Cousin and Robinson, 2001; Lee et al., 2005; Tan et al., 2003). Some of the abovementioned dephoshins may be involved in bulk endocytosis, and their deposphorylation by calcineurin may be the activity-dependent trigger for initiating the process. The intracellular Ca^{2+} concentration required to activate calcineurin and maximally deposhorylate the dephosphins is in the range of 1μM (Sihra et al., 1992). It remains to be determined if dephosphorylation of dynamin and other dephosphins only occurs at stimulation frequencies that trigger bulk uptake.

Drosophila Temperature-sensitive Paralytic Mutants

To reveal novel mechanisms involved in SV cycling, screens in the soil nematode *Caenorhabditis elegans* and the fruitfly *Drosophila melanogaster* have used a 'phenotype-to-genotype' approach, relying on behavioral manifestations caused by disruption of genes required for synaptic function. In *C.elegans,* screens for mutations that disrupt the normal undulating sinuous worm movement, or that confer resistance to inhibitors of choline esterase, have identified uncoordinated ('unc') and 'ric' phenotypes respectively. Two seminal examples of genes identified in this way are *unc-13* and *unc-18*, which encode syntaxin-binding proteins critical for SV priming/ fusion.

In the fly, a powerful genetic strategy pioneered over 30 years ago involves screening for TS (temperature sensitive) paralytic mutants. The assumption is that, at restrictive temperature, a heat-labile form of a protein acutely required for neuronal signaling/neurotransmission should quickly terminate nerve–muscle communication and result in paralysis. One important caveat is the introduction of an additional variable (temperature) in the mutant analysis; the interaction between mutant and temperature in neurotransmission cannot always be predicted. TS mutants provide conditional, temporal control of assaying protein function *in vivo* and greatly reduce concerns of pleiotropy. Most TS mutants behave normally at 'permissive' temperatures (e.g. 25^{o}C), but are paralyzed upon a shift to a 'restrictive' temperature (e.g. 37^{o}C) at a rate that tends to reflect the temporal requirement of the gene product. Flies with mutations of ion channels and their regulators paralyze very rapidly (seconds), whereas those with mutations affecting the SV cycle usually paralyze more slowly (minutes). The most highly exploited example of the synaptic TS paralytic mutant approach is *shibire*^{ts}. This mutation first identified the Dynamin family of GTPases and established the essential role of Dynamin in neurotransmission and SV endocytosis. Other TS paralytic mutants have been similarly informative and have added enormously to our understanding of neurotransmission and synaptic function (Table 1). These unique tools continue to hold great promise to further unravel the mechanisms of the SV cycle. Forward genetic screens identifying TS conditional paralytic mutants have been a particularly fruitful phenotypic paradigm in *Drosophila melanogaster* to help identify the

physiological roles of novel genes encoding proteins involved in neuronal signaling or neurotransmission. This strategy was first developed in the early 1970's (Grigliatti et al., 1973; Siddiqi and Benzer, 1976; Suzuki et al., 1971). These mutants typically develop and behave normally when raised at a permissive temperature, but paralyze when given an acute heat shock at a restrictive temperature such that the functional consequences of perturbing the function of the protein can be studied.

Rolling Blackout (RBO): Acute Requirement in Neurotransmission

The Broadie Lab reported the cloning of a novel TS paralytic mutant, *rbo (Huang et al., 2004; Huang et al., 2006),* which was first identified 20 years ago by EMS mutagenesis (Shyngle and Sharma, 1985). The recessive TS paralysis in *rbo*^{ts} mutants is due to a single point mutation resulting in a glycine-to-aspartate mutation (G487D) (Huang et al., 2004). A single copy of the wild-type *rbo* gene introduced by germ line transformation into *rbo*^{ts} flies rescues all behavioral and neural signaling defects. The *rbo* gene encodes a predicted transmembrane protein, previously identified as *cmp*44E (conserved membrane protein at cytological map position 44E) (Faulkner et al., 1998). RBO protein is expressed within both sensory and central neurons. In the central nervous system, RBO is expressed in synaptic neuropil. RBO is similarly enriched at NMJ synaptic terminals, with a subcellular expression consistent with pre-synaptic membrane localization (Figure 7).

Table 1 *Drosophila* TS paralytic mutants

ERG, *ether-a-go-go* (*eag*)-related gene;. *paralytic* (*para*)

Mutant	Gene Product	Phenotype	Proposed Function
Neuronal excitability			
paralytic (*para*)	*α*1 Na+ channel subunit	Impaired nerve conduction	Action potential propagation
no action potential (*nap*ts)	Double-stranded RNA helicase	Decrease in Na**+** channels	Regulation of Na+ channel expression
temperature-induced paralysis E *(tipE)*	Na+ channel auxillary subunit	Impaired nerve conduction	Action potential propagation
slowpoke (*slo*)	Ca2+-activated K+ channel	Action potentials lengthened	Action potential repolarization
seizure (*sei*)	ERG family K+ channel	Action potentials lengthened	Action potential repolarization
shab	Delayed rectifier K+ channel	Muscle contraction dysfunction	Action potential repolarization
cacophony (*cac*ts)	*α*1 Ca2+ channel subunit	Decreased evoked release	Presynaptic Ca2+ influx
RNA adenosine deaminase (adar)	A-I RNA editing	Not characterized	Regulates *para* and *cac* expression
kumbhakarna (*kum*)	Sarco/endoplasmic reticulum Ca2+-ATPase	Severe contraction of body wall musculature	Limits muscle contraction
axotactin (*axo*)	Neurexin family protein	Decreased neuronal excitability	Glial protein that influences electrical properties of axons
kinesin heavy chain (*khc*)	Microtubule ATPase	Loss of mobility and sensory responses	Anterograde transport of vesicles, ion channels, proteins
ATPα	Na+/K+-ATPase *α* subunit	Neuronal hyperexcitability	Maintains membrane potential
orangi (*org*, *sesB*org)	Adenine nucleotide translocase (ANT)	Depressed synaptic transmission	Provides ATP
Endocytosis			
shibire (*shi* ^{ts})	Dynamin GTPase	Depletion of vesicles	'Pinchase' in endocytosis
stoned (*stn*)	Stoned A: novel protein	Reduced vesicles; aberrant SV morphology, trafficking	Unknown endocytosis role
dynamin-associated protein of 160 kDa (*dap160*)	Dynamin-associated protein	Mislocalization of synaptic proteins	Endocytosis scaffolding protein

Mutant	Gene Product	Phenotype	Proposed Function
Exocytosis			
cystine string protein	Molecular chaperone (DNA J domain)	Decreased evoked release	Chaperone during SV cycle. Regulates calcium
synaptosomal-associated protein of 25 kDa (*SNAP25*^{ts})	Plasma-membrane-attached SNARE protein	Release increased at 22◦C, reduced at 37◦C	SNARE protein fusion machinery
comatose (*comt*)	NSF ATPase	Loss of evoked release	Disassembly of *cis* SNAREs after fusion
*syntaxin*ts (*syx*$^{3\text{-}69}$)	Integral T-SNARE	Previously thought to have a post-docking block in vesicle release	Vesicle priming/fusion
rolling blackout (*rbo*^{ts})	Putative transmembrane lipase	Previously thought to have a post-docking block in vesicle release, (shown here to have a role in endocytosis)	Lipid signaling in vesicle retrieval
Biosynthetic degradative enzymes			
Choline acetyltransferase (*ChaT*)	Choline acetyltransferase	Loss of synaptic transmission	Synthesizes acetylcholine
Acetylcholinesterase (*AchE*)	Acetylcholine esterase	Loss of ‘off’ transient in electroretinogram	Degrades acetylcholine
Other			
nervous wreck (*nwk*)	SH3 domain protein	Synaptic overgrowth and decreased function	An adaptor protein controlling actin dynamics
vacuous (*vacu*)	Not known	Neural hyperactivity	Not known
tripped-and-fell (*Taf*)	Not known	TS effects on locomotion and phototransduction	Not known

RBO also shows considerable overlap with markers for the postsynaptic side such the *Drosophila* Postsynaptic Density 95 (PSD 95) homologue, Disc Large. Cellular fractionation assays and cell-surface biotinylation indicate that RBO is an integral plasma membrane protein, and hydropathy plots predict that RBO is a two or three-pass transmembrane protein (Huang et al., 2004). The *rbo*^{ts} mutant paralyses at 37^{o}C in a few minutes, indicating an acute, but not immediate, requirement (F.D.Huang and K. Broadie, unpublished work). The paralysis kinetics are similar but slower to those of *shibire*^{ts} and dissimilar to TS mutants affecting ion channels. For example, *paralytic*^{ts}, a Na^{+} channel mutation that blocks nerve action potential conduction at restrictive temperature, results in paralysis within seconds (Table 1; (Loughney et al., 1989)). Direct recordings of evoked synaptic responses at the adult DLM (dorsal longitudinal flight muscle) NMJ synapse show a reversible block in synaptic transmission in *rbo*^{ts} animals within minutes of shifts to/from the restrictive temperature. In *paralytic*^{ts} mutants, action potential-independent synaptic transmission can still be induced by passive electrotonic depolarization of the nerve terminal (Loughney et al., 1989). In contrast, in *rbo*^{ts} mutants, electrotonic stimulation fails to evoke detectable transmission, indicating that the defect is not due to action potential failure (F.D. Huang and K. Broadie, unpublished work). Ultrastructural analyses of unstimulated heat shocked DLM NMJs show a dramatic accumulation of SVs in *rbo*^{ts} mutants after a few minutes at restrictive temperature. It was therefore hypothesized that exocytosis may be blocked at or near the fusion step itself, as

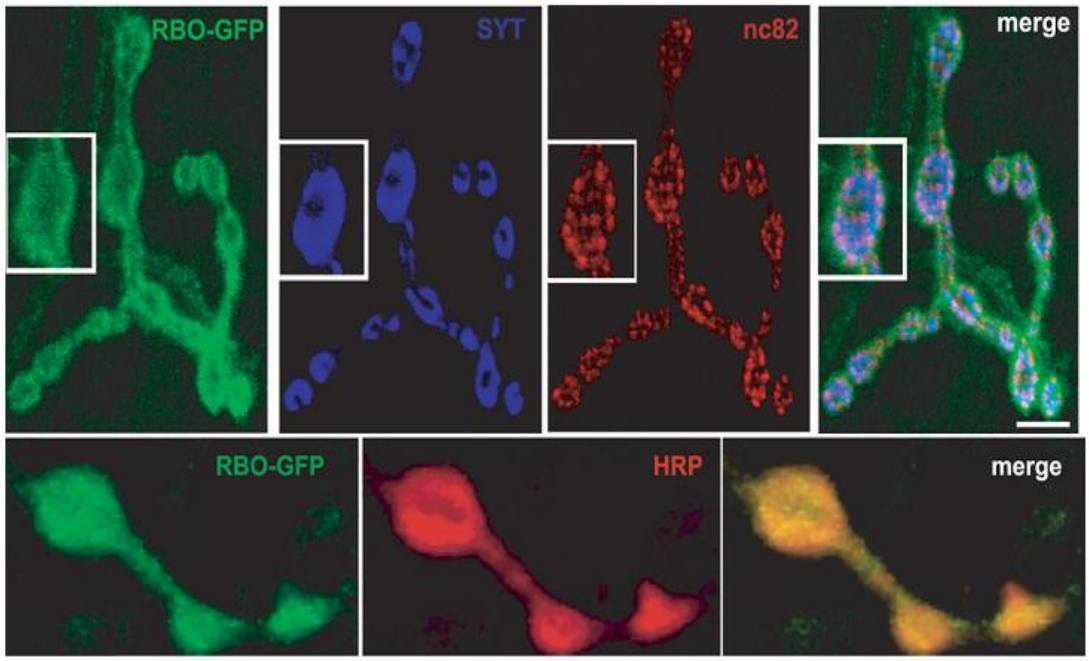

Figure 7: **Localization of RBO at the Drosophila 3rd instar larval neuromuscular junction (NMJ).** Distribution of RBO–GFP in a double labeled third instar larval NMJ with integral SV protein synaptotagmin (SYT;blue) and active zone marker nc82 (bruchpilot or brp red). Scale bar,5 µm.At the bottom, double-labeling with the neuronal plasma membrane marker anti-horseradish peroxidase (HRP; red). Scale bars, 5µm. Image courtesy of Dr. Jeffrey Rohrbough (VanderbiltUniversity).

an increased number of docked vesicles are accumulated at presynaptic active zones. Previous studies from our lab and others had revealed similar post-docking exocytosis defects in SNARE mutants (*syntaxin* and *synaptobrevin*) and. mutants of the SV priming protein *Drosophila* UNC-13 (DUNC-13) (Aravamudan et al., 1999; Littleton et al., 2001). Genetic interaction studies reveal a synergistic interaction between *rbo*^{ts} and *syntaxin*^{ts} mutants, such that the *rbo*^{ts};*syx*$^{3\text{-}69}$ double homozygous mutants paralyze at a lower temperature (33^{o}C) than either of the single mutants (Huang et al., 2006). Since the *syx*$^{3\text{-}69}$ allele was previously believed to be a loss of function mutation, negatively affecting vesicle fusion (Littleton et al., 1998), the synergistic interaction between RBO and Syntaxin was interpreted as meaning that both RBO and Syntaxin acted in the same pathway, i.e., exocytosis, (F.D.Huang and K. Broadie, unpublished work). This would place RBO function downstream of SV docking in an essential priming/fusion mechanism required for SV release.

Drosophila Phototransduction

The phototransduction cascade in *Drosophila* is one of the most well characterized G protein coupled signaling cascades. The absorption of photons by rhodopsin in photoreceptor cells in the compound eye of the fly is very rapidly transduced into a modulation of plasma membrane conductance and voltage. The compound eye of the fly consists of ~800 repeating units known as ommatidia, arranged in a stereotypical hexagonal array giving rise to a faceted honeycomb-shaped appearance. Each ommatidium is a column-like structure

that is akin to a simple eye, consisting of eight photoreceptor neurons (R1-8), cone cells, primary and secondary pigment cells and a cornea.

Photoreceptor cells are specialized sensory cells with a polar morphology. By way of expanding the surface area available for the absorption of photons the apical domain of the photoreceptor cell, called the rhabdomere expands during the later stages of pupal development to form microvilli. Each rhabdomere contains ~30,000 microvilli which effectively contribute ~90% of the membrane area of the photoreceptor cell.

A cross-sectional view of each ommatidium reveals the photoreceptor cells in each ommatidium arranged in a precise asymmetric circular pattern with R1-6 arranged peripherally and R7 and 8 one above the other in the centre . R1-6 are the main photoreceptor class in the fly retina and are akin to rods in the vertebrate eye. They from the high sensitivity (HSS) system in the eye. They express blue absorbing rhodopsin (Rh1) as a visual pigment. R7 and R8 are comparable to cones, contain multiple photopigments (Rh3,4 and Rh2 respectively) and form the low sensitivity, high acuity system (HAS) (Kirschfeld and Franceschini, 1969). This distinct organization of outer and inner photoreceptor cells in the periphery carried on to the subsequent layers as these cells make axonal contact with more central synaptic neuropil. Axonal processes from peripheral retinula cells R1-6 terminate in synaptic contacts with neurons located in the lamina ganglionaris, a layer of neuropil directly below the retina and R7 and 8 traverse the lamina to synapse onto neurons in the medulla (Trujillo-Cenoz, 1965).

Visual Signal Transduction

The visual transduction cascade in *Drosophila* begins with the light dependent isomerization of rhodopsin, a 7 transmembrane spanning G protein coupled receptor (GPCR) to metarhodopsin. This step entails the conversion of the chromophore 3-hydroxy-11 cis-retinal that is covalently bound to opsin to all trans retinal (Wald, 1968) . Metarhodopsin can catalyze the activation of a heterotrimeric G protein by the exchange of nucleotide guanosine diphosphate (GDP) with guanosine triphosphate (GTP). The α subunit of the G protein dissociates from the heterotrimeric complex to activate the effector enzyme phosphoinositide-specific phospholipase C (PLCβ) that is part of a large signaling complex. PLC in turn hydrolyses membrane phospholipid PIP_2 to membrane bound diacylglycerol (DAG) and soluble inositol 1,4,5 triphosphate ($InsP_3$) (Berridge, 1993). Although the precise mechanism is still remains unknown, the hydrolysis event results in the activation of two classes of cation-permeable ion channels, namely transient receptor potential (TRP) and transient receptor potential-like (TRPL). The *Drosophila* genome contains only one IP_3 receptor which was cloned based on homology to the mammalian genes (Hasan and Rosbash, 1992). Somatic mosaic animals null for this IP_3 receptor contain some photoreceoptor cells in the eye that are lacking in this receptor protein. Intracellular recordings of light response made from these null cells do not detectably show impaired phototransduction currents suggesting that TRP/TRPL channels are not gated by store operated or capacitative calcium entry, i.e., the

IP_3–dependent depletion of intracellular Ca^{2+} leading to movement of extracellular Ca^{2+}. Instead they are gated possibly by DAG itself or its downstream metabolite poly unsaturated fatty acids (PUFAs) (Chyb et al., 1999). This idea is also supported by data from (Raghu et al., 2000), who showed that TRP and TRPL channels are constitutively active in *Drosophila rdg*A (*retinal degeneration* A) mutants, which contain elevated levels of DAG due to the lack of DAG kinase, an enzyme involved in the conversion of DAG to phosphatidic acid (PA). The opening of TRP/TRPL channels results in the influx of cations like calcium and sodium which depolarizes the membrane of the photoreceptor cell. The entire cascade is rapid. Time taken from light absorption to depolarization is about 20 milliseconds. The steps involved in light-dependent depolarization of the photoreceptor membrane are depicted in Figure 8.

Response termination involves the endocytic internalization of rhodopsin by arrestin, phosphorylation of DAG by DAG kinase, to phosphatidic acid which is then recycled in a multistep process to regenerate PIP_2 (Figure 9). Rhodopsin becomes unbound from $G\alpha$ and is phosphorylated by rhodopsin kinase, which then signals binding by one of two *Drosophila* arrestins (arrestin 1 and arrestin 2) and the recruitment of endocytic machienary to internalize the receptor (Alloway et al., 2000; Satoh and Ready, 2005). Similarly TRP channels are phosphorylated by PKC which is present in a large signalplex consisting of the scaffolding protein INAD (inactivation no afterpotential D) along with PLC.

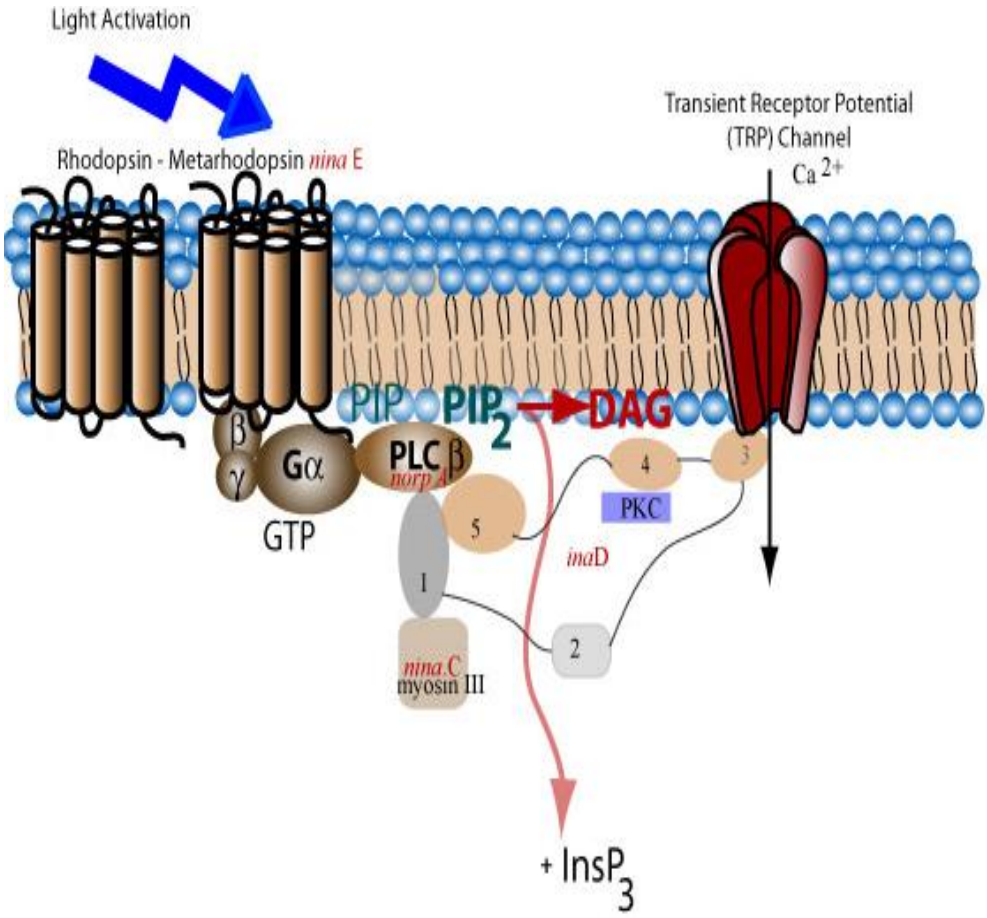

Figure 8: **Phototransduction cascade in Drosophila.** Schematic representation of the microvillar membrane of a photoreceptor cell. Major protein and lipid components of the pathway are shown. *Drosophila* genes involved in the various steps are shown in red. Following the absorption of blue light rhodopsin is converted to the active metarhodopsin which then interacts with the heterotrimeric G protein. GDP is exchanged for GTP by the Gq subunit resulting in the activation of phospholipase C (PLC). PLC cleaves membrane phosphatidyl inositiol 4.5.bisphosphate (PIP_2) to produce diacylglycerol (DAG) and inositol 1,4,5 trisphosphate ($InsP_3$). This leads to activation of the transient receptor potential (TRP) and transient receptor potential-like (TRPL) ion channels and membrane depolarization. Components of the phototransduction cascade are held in place by the PDZ domain (shown as 1-5) containing scaffolding protein InaD

The G protein α subunit is inactivated by its own internal GAP activity and also by that of PLC (Cook et al., 2000).

Genetic Approaches to Studying Drosophila Vision.

The molecular dissection of the visual transduction pathway using electrophysiological analysis of genetic mutations began in the 1960s. These studies have helped further our understanding of not only of the biochemisty of signal transduction complexes and PLC signaling but also underlying synaptic transmission mechanisms.

A vast majority of mutants with defects in signal activation, light adaptation, and signal termination have been identified using electroretinogram (ERG) recordings as a screening method. ERGs measure the summed response or field potential of the cells in the retina to a light stimulus. (Pak et al., 1970). The response to incident light typically consist of light coincident receptor potential (LCRP) which is a sustained depolarization, produced by the opening of TRP and TRPL ions channels in the photoreceptor retinula cells. The beginning and the cessation of the light stimulus are marked by the positive “on” and negative “off” transients respectively, which result from synaptic transmission events in the lamina region post-synaptic to the retinula photoreceptor cells (Alawi et al., 1972; Heisenberg, 1971) . Once mutations affecting ERG response are identified, Further characterization could be done by patch clamping or intracellular recording.

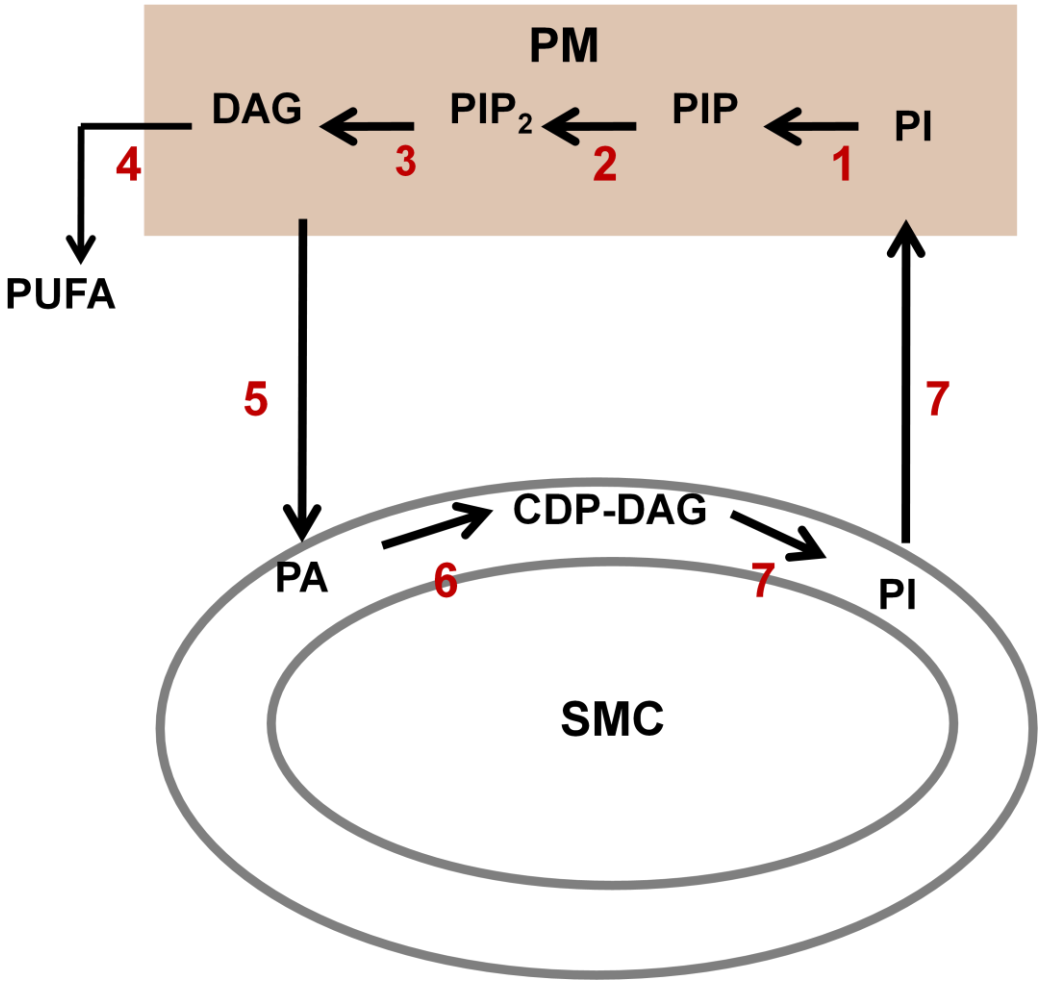

Figure 9: **PI turnover pathway.**The turn over of PIs takes place in the microvillar plasma membrane (PM) and submicrovillar compartment (SMC) below the microvillar surface. The following conversion steps are shown, PI to PIP by PI kinase (1), PIP to PIP_2 by PIP kinase, *skittles* (2), PIP_2 to DAG by PLC, *norp*A (3), DAG to polyunsaturated fatty acids (PUFAs) by DAG lipase, *ina*E (4), DAG to phosphatidic acid (PA) by DAG kinase, *rdg*A (5), PA to cytidine diphosphate –DAG (CGP-DAG) by CDP synthase (cds, 6), and then to PI by PI synthase, PIS (7). PI transporter *rdg*B transfers PI from the SMC to the microvillar membrane.

Phototransduction-related phenotypes in *rbo*^{ts}.

rbo^{ts} mutants show an activity-dependent loss of the phototransduction response (both on, off transients and the sustained response). RBO shows homology to a human sn-1 DAG lipase (Bisogno et al., 2003).These data were interpreted as a the possibility that RBO acts as a DAG lipase or acts at another point in the PLC-dependent PIP_2/DAG signaling pathway to regulate DAG level. To test this prediction, lipid levels in *rbo*^{ts} brain homogenates isolated at permissive and restrictive temperatures were assayed (Huang et al., 2004). Under restrictive conditions, PIP_2 levels were elevated and DAG levels were decreased in the brain. This might suggest a defect in PLC activity, although there was no difference in the ability of PLC to hydrolyze PIP_2 in the mutant, at least when assayed *in vitro* (Huang et al., 2004). Perhaps RBO regulates the environmental control of PLC activation? For example, the products of DAG lipase activity (PUFAs) are known to activate PLC, and so loss of DAG lipase would be predicted to down-regulate PLC function. Alternatively, lipid-binding assays with purified RBO protein show that it binds directly to PIP_2, as well as several other phosphoinositides (N. Vijayakrishnan and K. Broadie, unpublished work). It is therefore possible that RBO may regulate the availability or metabolism of these phosphoinositides.

Based on these data the model shown in Figure 10 was proposed for RBO function at the synapse. It was proposed that RBO may function as a lipase to modulate the local lipid environment at synaptic terminals. The changes seen in

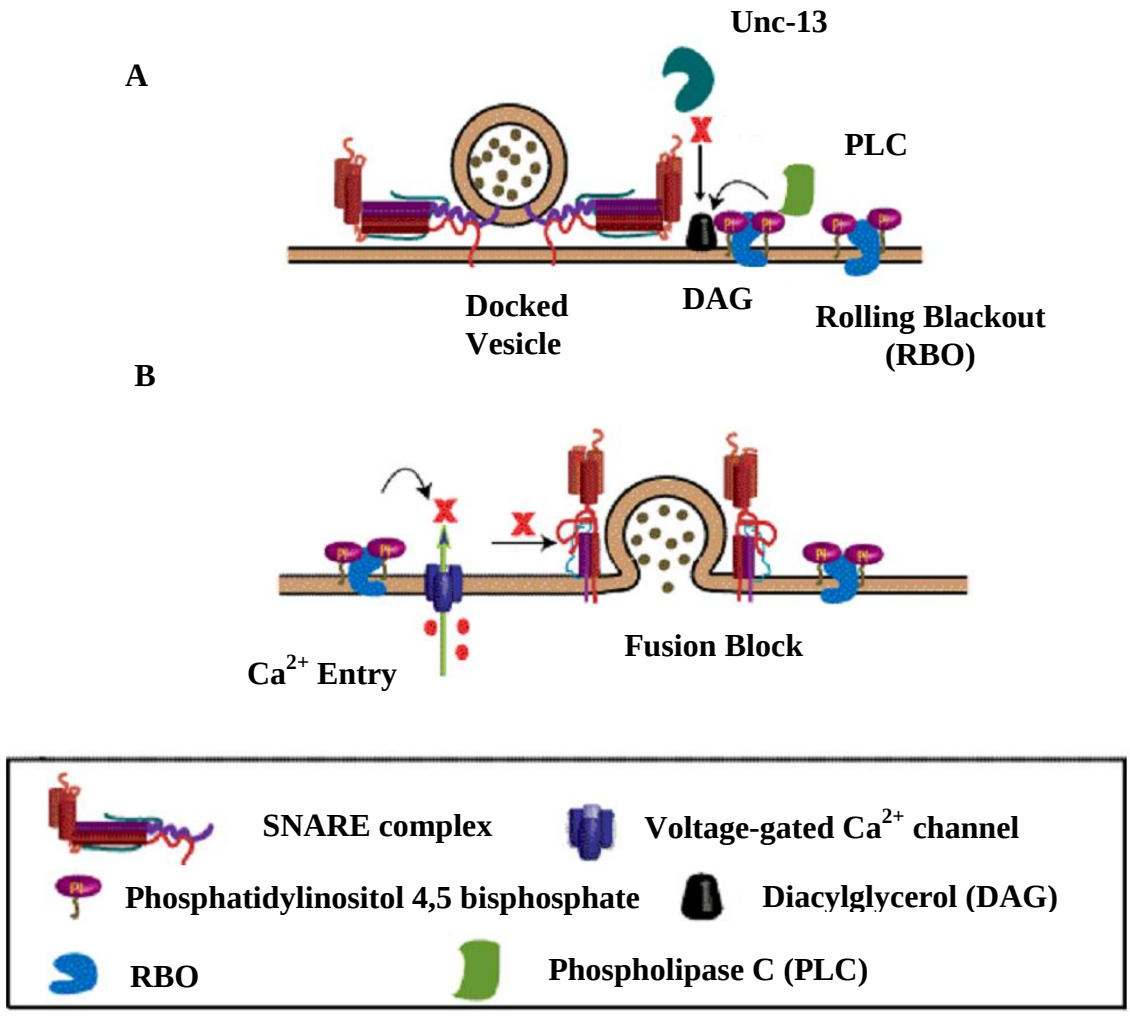

Figure 10: **Initial model for RBO function based on synergism with *syx*$^{3\text{-}69}$. A,** RBO may be required for the local production of DAG, which may bind UNC-13 to mediate SV priming immediately upstream of fusion. **B,** RBO may be required for the local regulation of PIP_2. In *rbo* mutants, elevated PIP_2 concentration may negatively regulate Ca^{2+} channels, blocking Ca^{2+} influx to arrest docked SVs immediately upstream of fusion.

the levels of DAG or PIP_2 could negatively affect synaptic vesicle fusion/exocytosis. The first specific aim of this study was to directly demonstrate this requirement for RBO in the synaptic vesicle cycle at the *Drosophila* 3rd instar larval NMJ using the lipophilic styryl dye FM1-43 by optical imaging assays.

CHAPTER II

THE *DROSOPHILA* EFR3 ROLLING BLACKOUT IS REQUIRED FOR BULK ENDOCYTOSIS IN NON-NEURONAL CELLS AND NEURONAL SYNAPSES

Introduction

Neuronal synapses efficiently couple neurotransmitter release with compensatory mechanisms that recycle the fusion-competent synaptic vesicle (SV) pool. Two full-fusion pathways mediate SV recovery; direct CME (Heuser and Reese, 1973; Slepnev and De Camilli, 2000), and bulk retrieval/macroendocytosis of large portions of membrane to form endosomes (Leenders et al., 2002; Marxen et al., 1999; Takei et al., 1996). SVs internalized via CME may immediately enter the fusion competent pool or fuse with sorting endosomes prior to rebudding (Hinshaw, 2000; Koenig and Ikeda, 1989; Narita et al., 1989; Wenk and De Camilli, 2004). Under high demand conditions, synapses use the bulk plasma membrane retrieval mechanism in parallel with CME (Holt et al., 2003; Richards et al., 2000). This activity-dependent formation of endosomes was first demonstrated in central brain synapses (Takei et al., 1996), and subsequently in many diverse synapses, including *Drosophila* NMJ (Heerssen et al., 2008; Koenig and Ikeda, 1996; Kuromi and Kidokoro, 1998), frog NMJ (Richards et al., 2000), goldfish retinal bipolar synapse (Holt et al., 2003; Neves et al., 2001) and mammalian Calyx of Held synapse (de Lange et al., 2003). Bulk endocytosis commences within 1-2 seconds of strong stimulation (Leenders et al., 2002; Marxen et al., 1999; Teng et al., 2007), but very little is known about the molecular mechanisms involved. Synaptic bulk endocytosis has often been

compared to macropinocytosis in non-neuronal cells, the process is similarly sensitive to disruption of the actin cytoskeleton and requires activation of Rho GTPases (Holt et al., 2003; Richards et al., 2000).

We report here characterization of a new player with a specific role in bulk endocytosis; Rolling Blackout (RBO/EFR3 or Pho Eighty-Five Requiring 3). We previously reported that conditional, temperature-sensitive (TS) *rbo*^{ts} mutants manifest complete blindness and paralysis within minutes upon shift to restrictive temperature (Huang et al., 2004; Huang et al., 2006). RBO is a well conserved integral plasma membrane protein and predicted lipase (Huang et al., 2004; Huang et al., 2006; Vijayakrishnan and Broadie, 2006). In *rbo*^{ts} brain, PIP_2 accumulates and DAG is concomitantly reduced within minutes upon shift to restrictive temperature. However, the exact RBO lipase substrate in the PIP_2-DAG pathway has not been identified, despite exhaustive attempts (Vijayakrishnan and Broadie, 2006). Our previous data pointed to RBO function in SV exocytosis, with vesicles accumulating within minutes at the restrictive temperature, arrested at the docking stage at presynaptic active zones (Huang et al., 2006). Critical to this model, we showed *rbo*^{ts} displays a strong synergistic behavioral interaction with *syntaxin-1A* TS allele, *syx*$^{3\text{-}69}$ (Littleton et al., 1998). Double homozygous mutants paralyze at a lower temperature than either single mutant, suggesting that RBO and Syntaxin-1A act synergistically in SV exocytosis. However, a recently published analysis of *syx*$^{3\text{-}69}$ revealed that this allele is in fact a dominant positive mutation causing elevated Syntaxin-1A function (Lagow et al., 2007). This revelation forced us to question our

hypothesis. We have therefore since performed many additional studies, with better tools, and in multiple cell types, to assess the functional requirements for RBO in both neurons and non-neuronal cells.

In this study, we perform FM1-43 dye cycling assays both at the well-characterized NMJ and the novel setting of central synapses in primary culture. Both synapse classes display severely defective SV endocytosis in *rbo*^{ts} mutants. Nevertheless, ultrastructural analyses of synaptic boutons at rest and post-stimulation show an increase in SV density and accumulation of docked SVs in *rbo*^{ts} synapses, similar to results in adult dorsal longitudinal muscle (DLM) synapse (Huang et al., 2006), posing us a conundrum. We therefore combined FM dye uptake experiments with photoconversion electron microscopy to reveal that loss of RBO function causes a specific blockade in the activity-dependent bulk endocytosis generation of endosomes. We performed parallel fluid phase tracer uptake studies in non-neuronal Garland cells, a well-established constitutive endocytosis assay system (Dermaut et al., 2005; Kosaka and Ikeda, 1983). These studies similarly show a complete arrest in macropinocytosis in *rbo*^{ts} mutants, comparable to the blockade in *shibire*^{ts} Dynamin mutants. Tracer ultrastructure studies in Garland cells also show a complete loss of tracer uptake into endosomes. Together, these results show that RBO is specifically required for the bulk endocytosis pathway only in both neuronal synapses and non-neuronal cells.

Results

RBO Is Required For Endocytosis At The Neuromuscular Synapse

FM1-43 styryl lipophilic dye imaging was used to assay SV cycling at the larval NMJ (Fergestad and Broadie, 2001; Renden and Broadie, 2003; Trotta et al., 2004). Dye can be loaded by a depolarizing stimulus, triggering SV endocytosis, and then unloaded by a second depolarizing stimulus, triggering SV exocytosis. Dye uptake and release assays were performed at staged permissive (25^{o}C) and restrictive (37^{o}C) temperatures to independently examine effects on endocytosis and exocytosis. Four genotypes were assayed under both conditions; wildtype control (OR), *rbo*^{ts} and *syx*$^{3\text{-}69}$ single mutants, and the *rbo*^{ts};*syx*$^{3\text{-}69}$ double homozygous mutant (Figure. 11).

Figure 11A shows a schematic of the two assays employed. To test predicted roles in SV exocytosis, FM dye was loaded with a 60 mM [K^{+}] stimulus for 2 minutes at the permissive 25^{o}C condition, and then shifted to the restrictive 37^{o}C for 10 minutes prior to applying a second depolarizing stimulus (Figure 11A, protocol 1). Under these conditions, the *rbo*^{ts} and *syx*$^{3\text{-}69}$ single mutants showed dye loading comparable to the wildtype control (P=0.98 comparing *rbo*^{ts} to wildtype; Figure 11B). In contrast, *rbo*^{ts};*syx*$^{3\text{-}69}$ double mutants showed a strong dye loading defect even at this permissive temperature (Figure 11B, bottom panel). Quantification of this phenotype revealed a very highly significant (P<0.0001) decrease in FM endocytosis only in the double mutant (OR 64.49 ± 0.96 (N=4), *syx*$^{3\text{-}69}$ 63.39 ± 2.58 (N=6), *rbo*^{ts} 64.31 ± 5.36 (N=5) and *rbo*^{ts};*syx*$^{3\text{-}69}$ 28.81 ± 2.17 (N =11); Figure 11D).

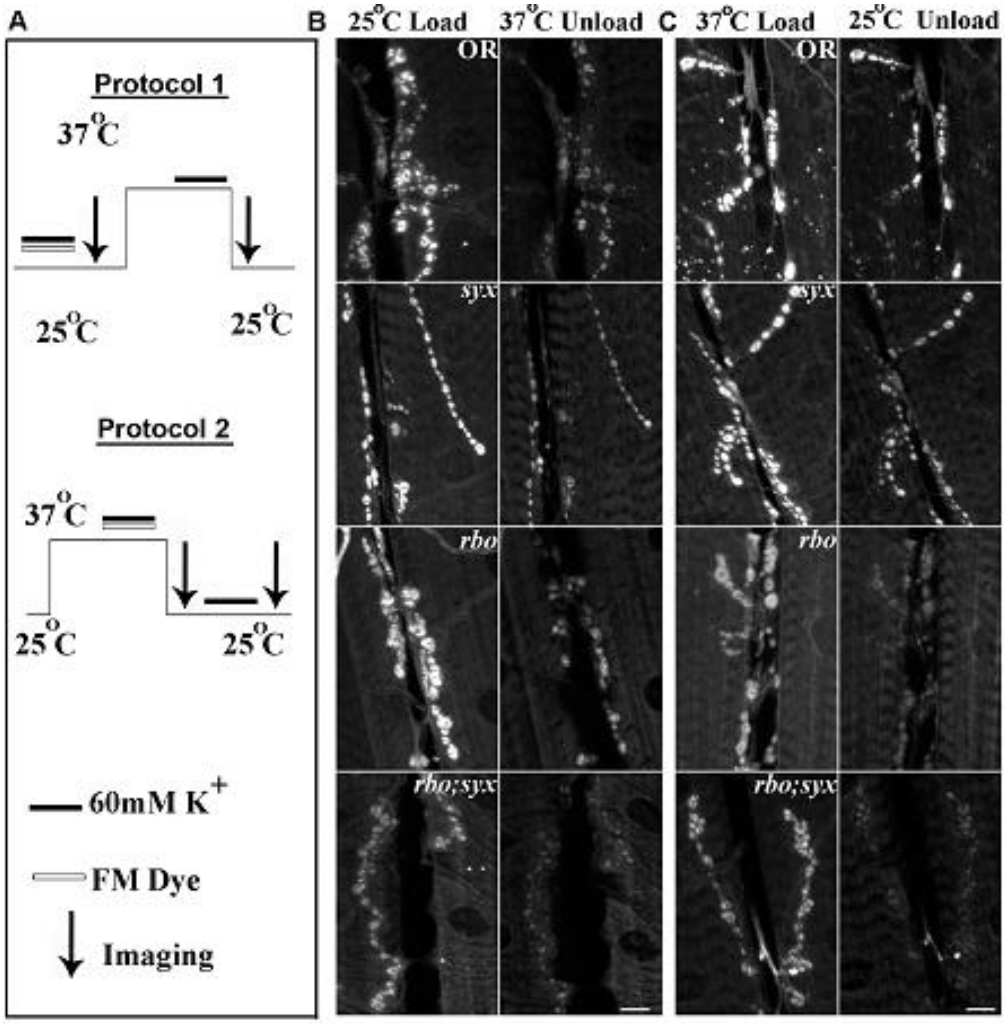

Figure 11: **RBO facilitates FM1-43 dye endocytosis at the neuromuscular synapse. A**, Schematic of dye loading protocols used at the larval NMJ**.** In protocol 1, FM1-43 was loaded for 2 minutes with 60 mM [K^+] at 25°C, and then unloaded with 2 minutes 60 mM [K^+] at 37°C. In protocol 2, following 10 minutes incubation at 37°C, dye was loaded for 2 minutes at 37°C, and then unloaded for 2 minutes at 25°C. **B,** Representative images of wildtype (OR), *syx*$^{3\text{-}69}$ and *rbo*^{ts} single mutants, and *rbo*^{ts};*syx*$^{3\text{-}69}$ double mutant. **C,** Top three panels show representative images comparing FM1-43 loading and unloading. Bottom panel shows *rbo*^{ts};*syx*$^{3\text{-}69}$ 37°C unloading after 5 minutes loading at 25°C. Scale 10μm.

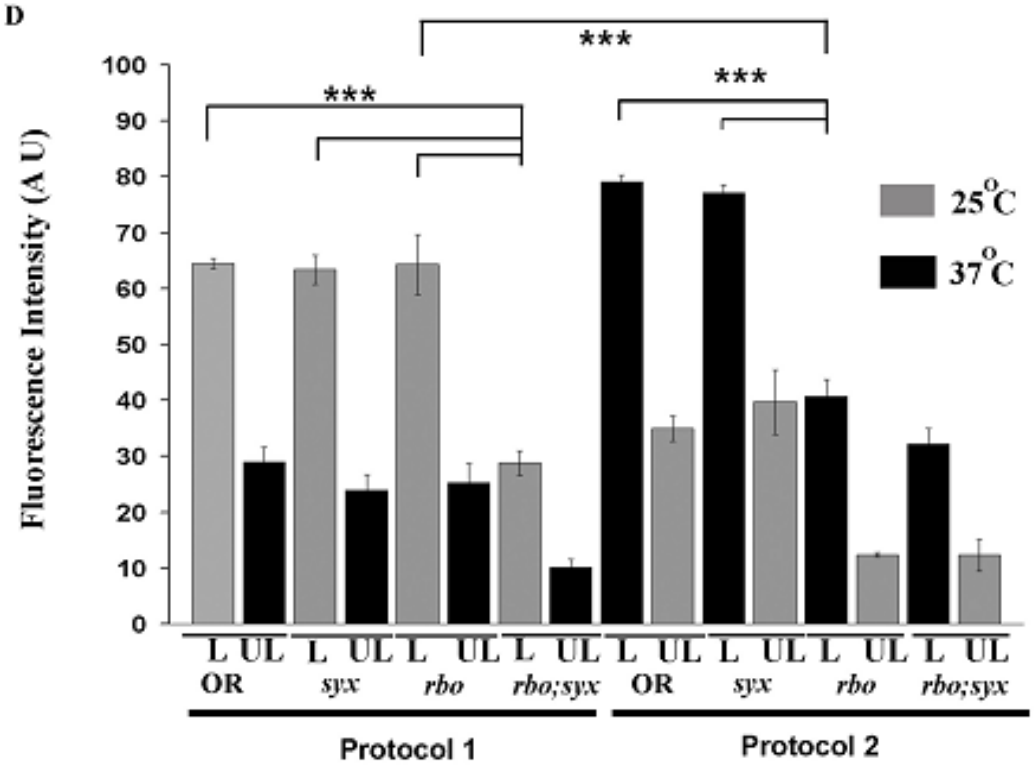

Figure 11: **RBO facilitates FM1-43 dye endocytosis at the neuromuscular synapse. D,** Quantification of loading (L) and unloading (UL) with both protocols. Error bars show mean ± SEM. Significance of $p<0.001$ is indicated (***).

In protocol 2, FM dye was loaded in the restrictive 37^{o}C condition, and then shifted to permissive 25^{o}C for 10 minutes prior to applying the second depolarizing stimulus (Figure 11A, protocol 2). Under these conditions, *syx*$^{3\text{-}69}$ continued to load similarly to wildtype, showing no requirement for Syntaxin 1A in endocytosis (Figure 11C; 11D, right). In contrast, *rbo*^{ts} showed a very significant ($p<0.0001$) impairment (Figure 11C). The mutant takes up ~50% less dye than wildtype controls (OR 79.07 ± 1.28 (N=9), *rbo*^{ts} 40.63 ± 3.07 (N= 11); Figure 11D, right). A wildtype copy of *rbo* in the mutant background completely rescues this loading defect (77.01 ± 1.81 (N=6); Figure 12). The *rbo*^{ts};*syx*$^{3\text{-}69}$ double mutant also showed a severe defect in FM endocytosis; however, the defect at 37^{o}C and 25^{o}C is comparable, suggesting that the interaction is already maximal at the permissive temperature (*rbo*^{ts};*syx*$^{3\text{-}69}$ 32.18 ± 2.85 (N=8), compared to OR $p<0.0001$; Figure 11D, right). Since the double mutant showed such poor loading at 2 minutes, a longer 5 minute load was used to determine if unloading was defective (Figure 11C, bottom panel). Dye loaded remained significantly reduced ($p=0.0064$), but the relative amount of dye unloaded was not significantly different ($p=0.10$) in the double mutant compared to wildtype (OR 43.64%, *rbo*^{ts};*syx*$^{3\text{-}69}$ 55.63%). Together, these data indicate that RBO has a critical role in endocytosis, which is exacerbated by the elevated SV cycling driven by the *syx*$^{3\text{-}69}$ mutant.

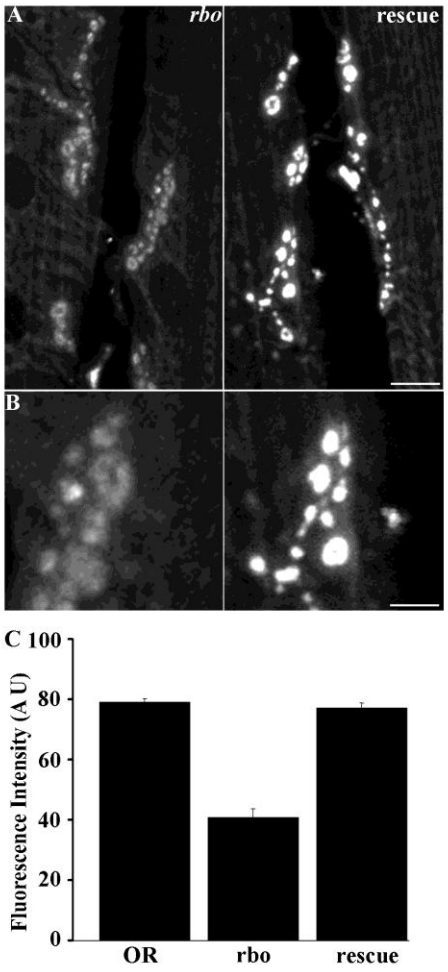

Figure 12: **Endocytic defects in *rbo*^{ts} fully rescued by wildtype *rbo* gene.**
A, Representative images of *rbo*^{ts} and *rbo*^{ts}/*rbo*^{2}; *rboegfp* (rescue) larval NMJs loaded with FM1-43 dye after 10 minutes at 37^{o}C (Protocol 2, Figure 9). Scale bar 10μm. **B,** Magnified loaded synaptic boutons in both genotypes. The wildtype *rbo* transgene rescues the *rbo*^{ts} dye loading defect. Scale 5μm. **C,** Quantification of dye loading in wildtype (OR) and *rbo*^{ts} compared to rescue animals.

RBO Is Required For Endocytosis In Central Brain Synapses

There appeared to be a disparity between our previous results at the adult DLM synapse, which suggest a role for RBO in SV exocytosis (Huang et al., 2006), and our new results at the larval NMJ synapse. Consistently, *rbo*^{ts} at restrictive temperature displays a total blockade of neurotransmission within 3 minutes at the adult DLM synapse, whereas there is no functional block at the larval NMJ (Huang et al., 2006). One possible explanation is that RBO displays a development stage (larval vs. adult) or synapse type-specific differential requirement. To test these possibilities, we wished to perform comparable FM1-43 experiments in a range of synapses. The DLM synapse is not accessible for FM dye assays (Beramendi et al., 2007). We therefore turned to primary neuronal cultures derived from the late-stage pupal brain, using methods pioneered by Jiang et al. (2005). This technique gives excellent access to a large set of diverse central brain synapses (Figures 13 and 14). We sought first to determine whether RBO is expressed in primary culture neurons. We cultured disassociated central brain neurons from *rbo* null mutants rescued to adulthood by an *rbo-egfp* transgene under native *rbo* promoter control (Figure 13). RBO-GFP expression was assayed using anti-GFP antibody staining. At the pupal brain dissection period (~55-70 hours after puparium formation), RBO expression is clearly visible in the brain, where the protein is tightly restricted to the synaptic neuropil (data not shown). In individual disassociated brain neurons at 6 DIV, anti-GFP labeling similarly shows clear RBO expression (Figure 13A). In neurons

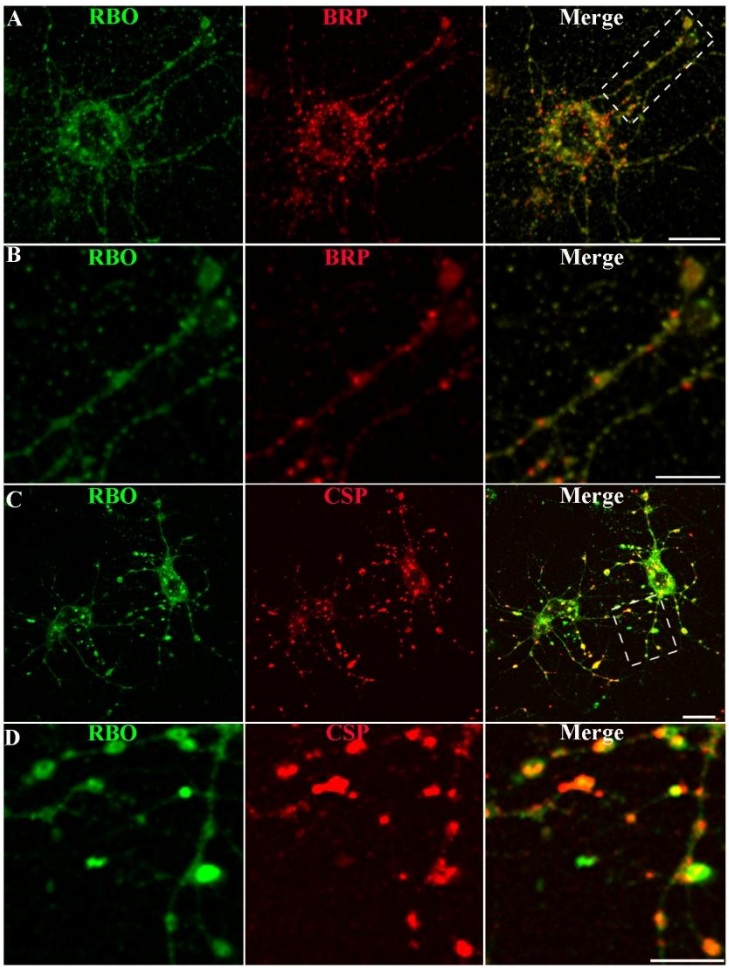

Figure 13: **RBO localizes to synapses in central brain primary neuron culture.** Representative images of neuron cultures of *rbo*^{2}/*rbo*^{2}; *rbo-egfp*/*rbo-egfp*. **A**, RBO-GFP (green) at 6 DIV, double-labeled with anti-BRP (red) marking active zones. Scale 10µm. **B**, Area in dashed box (A) magnified to show RBO-GFP and BRP co-localization in axonal synaptic varicosities. Scale 5µm. **C,** RBO-GFP (green) double-labeled with anti-CSP (red) marking synaptic puncta. Scale 10µm. **D,** Area in dashed box (C) magnified to show RBO-GFP and CSP colocalize in synaptic puncta. Scale 5µm.

double-labeled with the presynaptic marker anti-Bruchpilot (BRP), an overlapping punctate pattern was observed, very similar to that reported by Oh et al. (2008). RBO expression is clearly observed in varicosities along axonal processes, co-localized with BRP and Cysteine-string Protein (CSP) in synapses (Figure 13B-D). These same varicosities have been recently shown to be presynaptic specializations by ultrastructural criteria (Oh et al., 2008). These data show that RBO is expressed in synapses, colocalizing with presynaptic markers in central brain neurons.

It has been recently shown that these primary culture neurons develop mature electrophysiological properties, express ligand-gated neurotransmitter receptors and form functional synaptic contacts indicative of a functional SV release machinery (Campusano et al., 2007; Jiang et al., 2005; Su and O'Dowd, 2003). However, to the best of our knowledge, presynaptic vesicle cycling has not been directly demonstrated in this system (Kuppers-Munther et al., 2004). We therefore next sought to determine whether the presumed synaptic varicosities along axonal processes take up and release FM dye in a depolarization-dependent manner. Neurons were labeled with the membrane marker CD8-GFP, to reveal varicosities, and synaptic markers including anti-Synapsin (Figure 14A). FM1-43 dye cycling was stimulated with depolarizing high [K^+] saline as at the NMJ synapse. FM dye is taken into the stimulated axonal varicosities (Figure 14B, load). Following a second depolarizing stimulus, the loaded FM dye is effectively released again (Figure 14B, unload). Neurons were labeled with FM1-43, imaged live and subsequently fixed and stained for RBO

and synaptic markers such as CSP (Figure 14C). Active synapses clearly localize RBO with other synaptic markers. Quantification of the percentage of BRP or CSP-positive synapses that co-express RBO showed 93.09 ± 2.31% and 85.48 ± 3.36% overlap, respectively (Figure. 14D). Taken together, these data show that RBO is localized to functional presynaptic varicosities.

We therefore performed FM1-43 dye imaging studies to examine the role of RBO in SV cycling in central synapses. To test the restrictive condition, cultured control and *rbo*^{ts} neurons were incubated for 10 minutes at 37^{o}C in Ca^{2+}-free saline after which a 45 second pulse of FM1-43 was applied in depolarizing high [K^{+}] saline (Figure 15). In wildtype (OR) neurons, some cell body dye loading is evident, but most of the dye is endocytosed into the synaptic varicosities along axon processes (Figure 15A, B; right, arrows). In sharp contrast, *rbo*^{ts} neurons display greatly reduced endocytosis. The majority of mutant neurons load poorly, with faintly detectable fluorescent puncta (Figure 15C), and a subset show almost no detectable loading (Figure 15D). A wildtype copy of *rbo* in the mutant background rescues dye loading (Figure 15E), proving that the *rbo* mutation is responsible for this endocytosis defect. To quantify this phenotype, culture fields were selected blind to fluorescence using Nomarski optics and the number of FM1-43 loaded synaptic puncta per 20 μm length of axonal process then counted and calculated as the percentage of total varicosities. This blind quantification showed a very highly significant ($p<0.0001$) decrease in dye loading in *rbo*^{ts} compared to control (OR 80.25 ± 3.74, *rbo*^{ts} 39.48 ± 3.68 and rescue 77.37 ± 2.66; Figure 15F). These results demonstrate

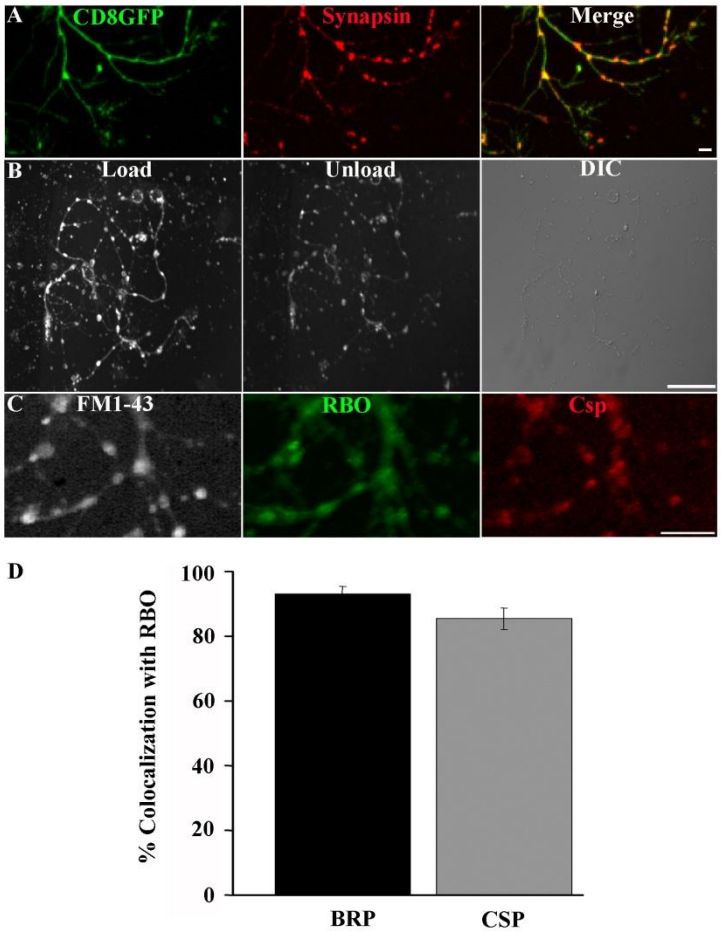

Figure 14: **RBO localizes to functional synapses with cycling synaptic vesicles.**
A, *elav*-GAL4 driven UAS-CD8::GFP (green) doubled-labeled with anti-Synapsin (red) to show axonal varicosities containing presynaptic marker. Scale 2µm. **B,** FM1-43 labeling with 60 mM [K^+] for 45 seconds loads synaptic varicosities (left). A shorter 30 second exposure to 60 mM [K^+] partially unloads dye (middle). Nomarski DIC image showing neuronal structure (right). Scale 20µm. **C**, In rbo^2/rbo^2; *rbo-egfp*/*rbo-egfp* 6 DIV cultures, loaded FM1-43 dye (white) colocalized with RBO-GFP (green) and synaptic marker anti-CSP (red). Scale 5µm. **D,** Quantification of percent colocalization of BRP and CSP with RBO-GFP puncta.

that a strikingly similar endocytosis defect is shared between larval neuromuscular synapses and pupal central brain synapses of *rbo*^{ts} animals. We therefore set out to further investigate the basis of this endocytosis requirement.

RBO Is Required For Endocytosis In Non-Neuronal Cells

Garland or "wreath" cells, involved in rapid fluid-phase endocytic uptake from the haemolymph, are a long-established system used to elucidate mechanistic requirements during endocytosis (Kosaka and Ikeda, 1983; Narita et al., 1989). Several synaptic endocytic mutants show defects in tracer/dye uptake in Garland cells (Chang et al., 2002; Dermaut et al., 2005; Lloyd et al., 2002). Since these cells are much larger than synaptic boutons, they provide excellent visualization of endocytic defects and allow dysfunction to be pin-pointed with greater accuracy. To test whether *rbo*^{ts} mutants and *rbo*^{ts};*syx*$^{3\text{-}69}$ double mutants have a more generalized endocytic defect, we performed texas-red avidin (TR-avidin) uptake experiments on Garland cells (Figure 16).

RBO expression is clearly detected in Garland cells (Figure 16A). The protein is primarily localized to the plasma membrane as at the synapse (Vijayakrishnan and Broadie, 2006). In addition, RBO is also present in a small subset of internal organelles (Figure 16B, arrows). Following application of TR-avidin tracer for 5 minutes at 25^{o}C, internalized vesicles are observed in the cell periphery in both wildtype (Figure 16C) and *rbo*^{ts} (Figure 16D). At this permissive temperature, *rbo*^{ts} cells are indistinguishable from wildtype in the number and

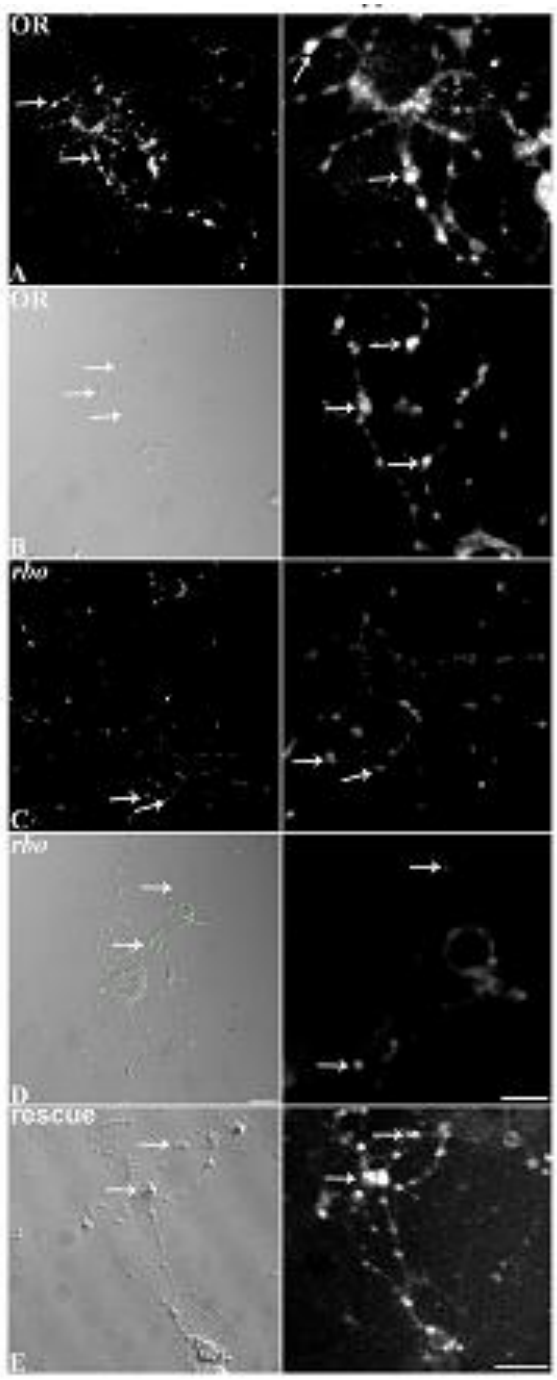

Figure 15: **RBO facilitates FM1-43 dye endocytosis in central brain synapses**.
Dye labeling in cultured neurons from wildtype (OR) and *rbo*^{ts} after 10 minutes at 37^{o}C. Left panels show lower magnification fields and Nomarski DIC images; right panels show higher magnification images of FM1-43 labeled synapses (arrows). The range of loading in wildtype, with more intense (**A**) and less intense (**B**) labeling; and in *rbo*^{ts}, with more intense (**C**) and less intense (**D**) labeling. **E,** Rescue of loading in *rbo*^{ts}/*rbo*^{2}; *rbo-egfp*/*rbo-egfp* neurons. Scale 10μm.

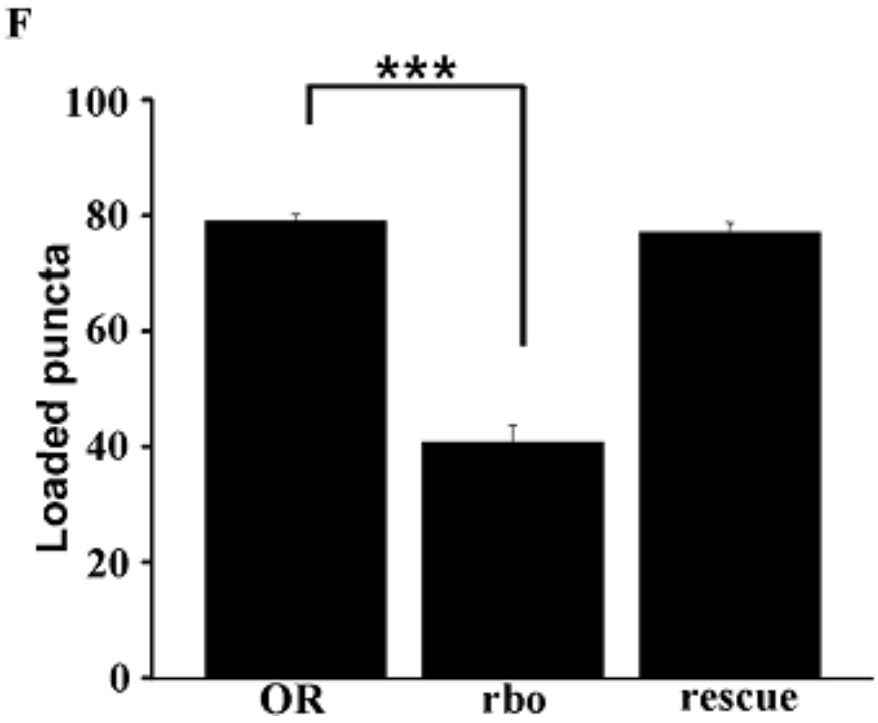

Figure 15: **RBO facilitates FM1-43 dye endocytosis in central brain synapses**. **F,** Quantification of FM1-43 loading. The number of loaded varicosities as a percentage of the total varicosities from DIC images, per 20 μm of axon length**.** Error bars show mean ± SEM for 4 independent trials for each genotype. Significance of $p<0.001$ is indicated (***).

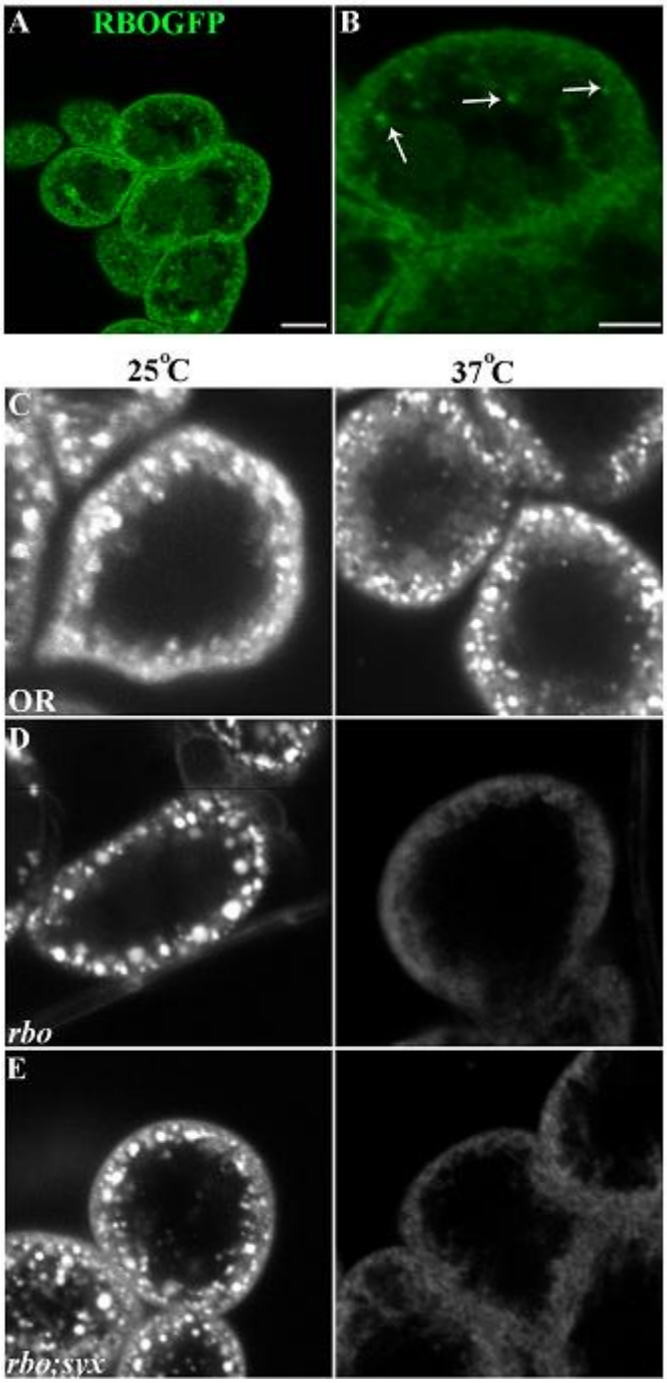

Figure 16: **RBO required for texas-red avidin tracer endocytosis in Garland cells**.
A, RBO-GFP in *rbo*^{2}/*rbo*^{2}; *rbo-egfp*/*rbo-egfp* is expressed at the periphery of Garland cells. Scale 5μm**. B,** Most RBO-GFP is associated with the plasma membrane, but some RBO associates with internal organelles (arrows). Scale 5μm**. C,** Wildtype (OR) cells loaded at 25°C (left) or following 10 minutes at 37°C (right). **D,** *rbo*^{ts} at 25°C (left) is similar control, but at 37°C (right) shows no dye internalization. **E,** *rbo*^{ts};*syx*$^{3\text{-}69}$ also shows block of uptake at 37°C.

distribution of endocytosed vesicles. These results suggest that RBO is essential for endocytosis.

To precisely characterize the defect in *rbo*^{ts}, we performed ultrastructural analyses (Figure 17). Garland cells possess tubular invaginations of the plasma membrane extending ~3 μM into the interior (labyrinthine channels; arrows in Figure 15) and numerous endosomal alpha vacuoles (labeled a in Figure 17). At 25^{o}C, *rbo*^{ts} cells appear indistinguishable from wildtype cells in all respects (Figure 17A). In stark contrast, dramatic endocytic changes are observed in *rbo*^{ts} mutants following upshift for just a few minutes from 25^{o}C to restrictive 37^{o}C. The labyrinthine channels become elongated and drastically engorged in *rbo*^{ts} at 37^{o}C, compared to mutants at 25^{o}C, or wildtype at either temperature (Figure 17B). In the mutant, vacuolar structures develop within the engorged channels. In *shi*^{ts1} mutants at 37^{o}C, labyrinthine channels similarly elongate and accumulate irregular pits as a result of failure to pinch off membrane from the surface (Kosaka and Ikeda, 1983; Narita et al., 1989). These common defects suggest this *rbo*^{ts} phenotype arises from a block of endocytosis from labyrinthine channel plasma membrane. At 37^{o}C, *rbo*^{ts} cells also contain fewer endosomal alpha vacuoles, and the few present appear enlarged and of more irregular shape (Figure. 17C). These defects are consistent with a failure to form endosomes from the labyrinthine channel plasma membrane following acute removal of RBO function.

Horse radish peroxidase (HRP) provides an excellent electron microscopy tracer for Garland cell endocytosis (Lloyd et al., 2002). Garland cells were

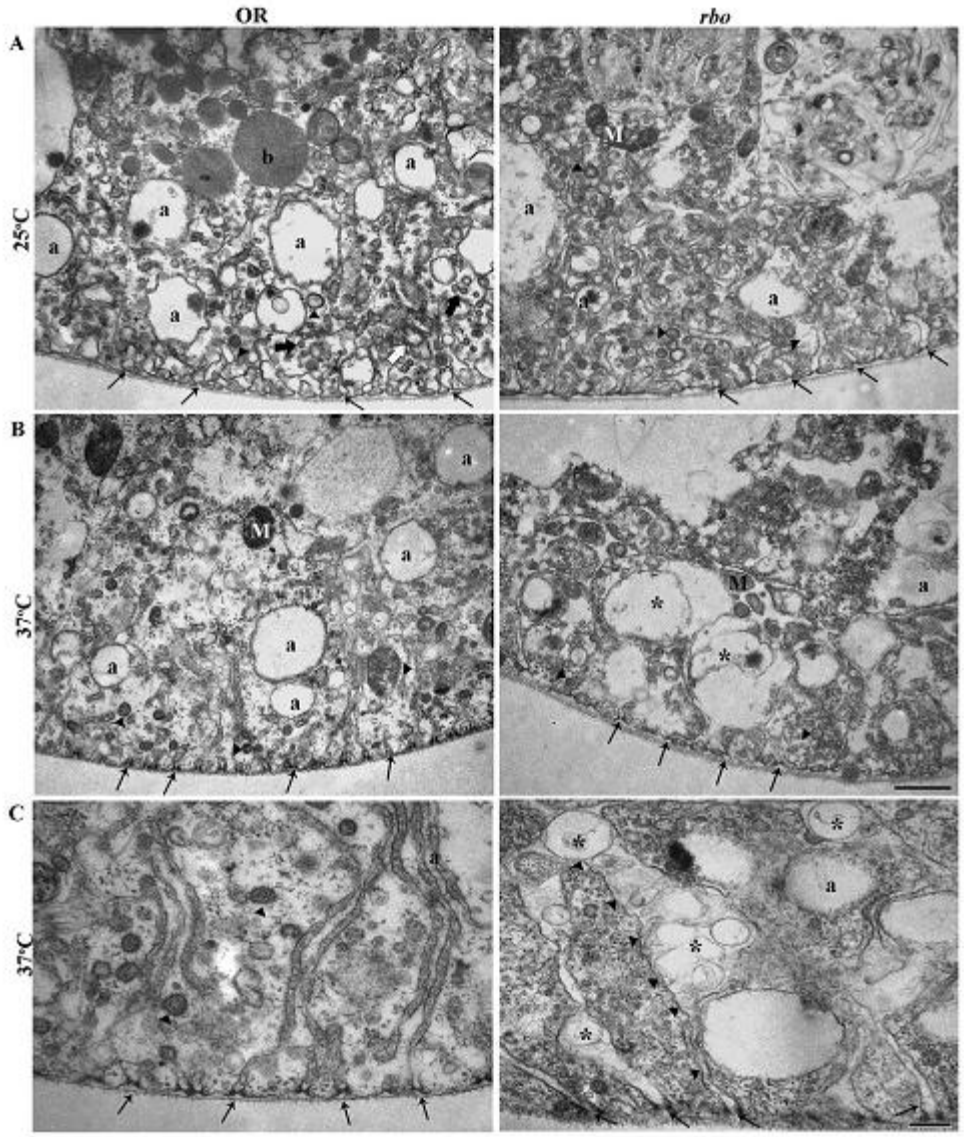

Figure 17: **Ultrastructure of Garland cells in wildtype and *rbo*^{ts} mutants.**
A, Wildtype and *rbo*^{ts} cells at 25°C. Labyrinthine channels (thin black arrows). Alpha vacuoles (a), longitudinal (white arrows) and transverse tubular elements (thick black arrows), and coated vesicles/pits (black arrows heads), mitochondria (M), and beta vacuoles (b) are indicated.**B,** Following 10 minutes at 37°C, *rbo*^{ts} alpha vacuoles are reduced, with remnant vacuoles larger and more irregular. Labyrinthine channels distend with many vacuolar structures (*). Scale 1μm. **C,** Higher magnification images at 37°C. In *rbo*^{ts}, very elongated labyrinthine channels extend, containing many vacuolar structures (*). Thin black arrows show the origin of the labyrinthine channels. Scale 250nm.

dissected and incubated with HRP at 25°C or following 10 minutes at 37°C (Figure 18). At permissive temperature, HRP is clearly observed in the lumen and internal membrane of peripherally located large endosomal alpha vacuoles in both *rbo*^{ts} and wildtype cells (data not shown).

However, when the number of endosomes was quantified, even at permissive temperature *rbo*^{ts} cells display >50% decrease in endosomes labeled with HRP (Figure 18E). Following 10 minutes at 37°C, wildtype cells clearly endocytose HRP tracer into alpha vacuoles (Figure 18A,B; left). In sharp contrast, almost no HRP is observed in *rbo*^{ts} endosomes (Figure 18A,B; right), indicating a near complete block in endocytosis. The alpha vacuoles present in the mutant clearly were made under the permissive condition, as they never contain the HRP tracer. Consistent with an endocytic block, use of tannic acid (TA) as a label to impregnate membrane contiguous with the extracellular space, shows these labyrinthine channels to be abnormally elongated and ramified in *rbo*^{ts} compared to control (Figure 18C). Quantification of cell area shows no change at 25°C but a highly significant increase in *rbo*^{ts} at 37°C (OR 266 $\pm$ 21 μm^2, *rbo*^{ts} 345 $\pm$ 33 μm^2; p=0.009). Area is significantly increased in *rbo*^{ts} by the 10 minute temperature shift (25°C, 229 $\pm$ 22 μm^2; 37°C, 345 $\pm$ 33 μm^2; p=0.007; Figure 18D). Quantification of HRP loaded endosomes per section shows a significant reduction in *rbo*^{ts} at 25°C (OR 32 $\pm$ 1.4, *rbo*^{ts} 14 $\pm$ 0.8; p=0.0001) and near complete loss at 37°C (OR 28 $\pm$ 6.8, *rbo*^{ts} 0.2 $\pm$ 0.14; p<0.0001; Figure 18E).

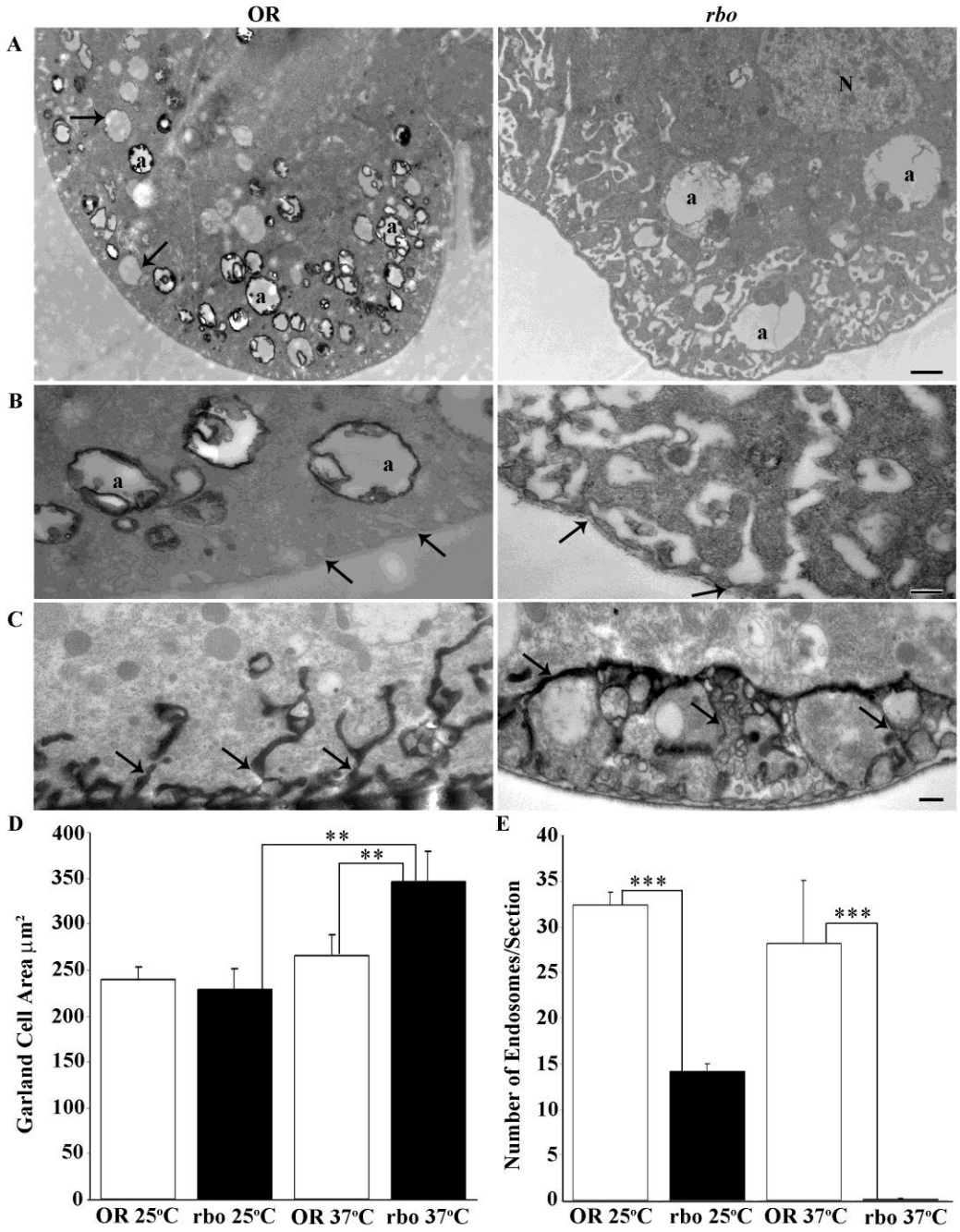

Figure 18: **Block in HRP endocytosis in *rbo*^{ts} Garland cells.**
A, Garland cell endocytic activity visualized using HRP uptake in wildtype (OR) and *rbo*^{ts} at 37°C. alpha vacuoles (a) are labeled in wildtype (left), amongst pre-existing unlabeled alpha vacuoles (black arrows). The mutant (right) shows no HRP uptake into alpha vacuoles (a); nucleus (N). Scale 1µm. **B,** Higher magnification images of alpha vacuoles (a) and labyrinthine channels (black arrows). The mutant (right) shows an absence of labeling, with swollen labyrinthine channels. Scale 250nm. **C,** Tannic acid impregnation shows labyrinthine channels in *rbo*^{ts} fused with many vacuolar inclusions. Scale 250nm. **D,** Quantification of cell area. A significant increase in *rbo*^{ts} at 37°C. **E,** Quantification of loaded endosomes per section. A significant reduction in *rbo*^{ts} at 25°C and near complete loss at 37°C.

These results show that RBO is essential in the endocytosis mechanism that generates endosomes.

RBO Is Required For Bulk Endocytic Formation Of Endosomes At The Synapse

The role of endosome trafficking at the synapse has long been controversial (Heuser and Reese, 1973; Takei et al., 1996; Teng et al., 2007). Based on the insights derived from the Garland cell analyses, we formed the hypothesis that RBO may have a select function in a subset of the endocytosis pathways, specifically the bulk endocytosis that forms endosomes. The functional defects observed at the larval NMJ based on our FM imaging studies (Figures 11,and12) and our previous electrophysiological studies (Huang et al., 2006) also appear consistent with a role for RBO in the bulk endocytosis pathway. To test this hypothesis, we performed ultrastructural experiments at the NMJ synapse, at rest and following stimulation (Figure 19), and also using FM1-43 photoconversion to track different endocytosis pathways (Figure 20).

Wildtype and *rbo*^{ts} are indistinguishable based on any ultrastructural criteria in unstimulated synapses at the 25^{o}C permissive temperature (data not shown). Following 10 minutes at 37^{o}C, mutant and control boutons remain remarkably similar, although some slight changes in synaptic vesicle pools become apparent (Figure19A). The total number of vesicles per bouton profile in *rbo*^{ts} (250 ± 32 SVs/bouton profile) appears elevated compared to control (200 ± 23), although the increase is not quite statistically significant (Figure 19C). In addition, there is a significant ($p<0.05$) increase is the number of synaptic

vesicles clustered (<250 nm) at the presynaptic active zone (OR 13.0 ± 1.4, *rbo*^{ts} 17.2 ± 1.2) and closely docked (<20 nm) at the t-bar (OR 1.2 ± 0.28, *rbo*^{ts} 2.3 ± 0.33; Figure 19C). The unstimulated terminals also contain cisternae (>60 nm in diameter) presumed to be endosomes. The number of these structures does not differ significantly between *rbo*^{ts} and wildtype after 10 minutes at 37^{o}C (OR 4.4 ± 1.3, *rbo*^{ts} 5.3 ± 0.84). Thus, acute removal of RBO function leads to a relatively mild accumulation of synaptic vesicles in the presynaptic bouton.

Synaptic ultrastructure was next assayed following depolarizing stimulation at 37^{o}C; 10 or 20 minute incubation with 60 mM [K^{+}] saline (Figure 19B). This condition is known to place a high demand on the SV cycle, driving high rates of exocytosis and endocytosis (see Figures 11 and 12). Stimulation eliminates the overall accumulation of SVs in *rbo*^{ts} mutants, but the elevated clustered and docked vesicle pools persist under these conditions of intense demand (Figure 19B,C). The number of clustered vesicles remains significantly ($p<0.01$) elevated (OR 10.5 ± 0.60, *rbo*^{ts} 16.6 ± 1.1) and the number of docked vesicles also remains slightly greater (OR 1.7 ± 0.26, *rbo*^{ts} 2.1 ± 0.23). Importantly, significant vesicle depletion does not occur, such as characterizes the endocytic mutants of the direct SV pathway(Gonzalez-Gaitan and Jackle, 1997; Poodry and Edgar, 1979; Verstreken et al., 2003). The striking effect of high [K^{+}] stimulation is massive production of large (>60 nm) cisternae, endosomal-like organelles in control boutons (Figure 19B, arrows). Although these structures exist in *rbo*^{ts} mutants at permissive temperatures, as expected since RBO is functional, stimulation in the absence of RBO function completely

fails to induce the production of more cisternae (Figure 19B, right). After 10 minutes at 37^{o}C, wildtype synapses produce nearly 4-fold more cisternae (at rest, 4.4 ± 1.3; stimulated, 15.1 ± 2.4), whereas *rbo*^{ts} synapses do not display any activity-dependent cisternae production (at rest, 5.3 ± 0.84; stimulated, 3.25 ± 0.56; Figure19D). These results suggest that RBO is essential for stimulus-induced production of endosomal-like cisternae. The FM dye uptake defects reported above are presumably due to the loss of dye internalization specifically within these cisternae, produced by bulk endocytosis from the plasma membrane under conditions of intense demand (Heerssen et al., 2008; Teng et al., 2007). To test this hypothesis, we performed FM1-43 dye uptake experiments, as above (Figure 11), and then photoconverted the label into an electron-dense marker for viewing with electron microscopy (Figure 20). In control synapses, recently endocytosed dye is observed in two locations; 1) small (<40 nm diameter) synaptic vesicles (arrows in Figure 20A, left) and 2) large (>60 nm diameter) endosomes (asterix in Figure 20A, left). In sharp contrast, *rbo*^{ts} synaptic boutons at 37^{o}C show all endocytosed FM dye in small synaptic vesicles without dye in endosomes (Figure 20 A, right). We quantified the number of electron-dense labeled at SVs (Figure 18B) and endosomes (Figure 20C). Following 10 minutes at 37^{o}C labeled SVs than examples observed among all the sections assayed. Control (OR 67.9 ± 15.2, *rbo*^{ts} 130.1 ± 16.3; Figure 20B). Under the same conditions, *rbo*^{ts} boutons contain essentially no labeled endosomes, with only a couple examples observed among all the sections assayed. The result is a very

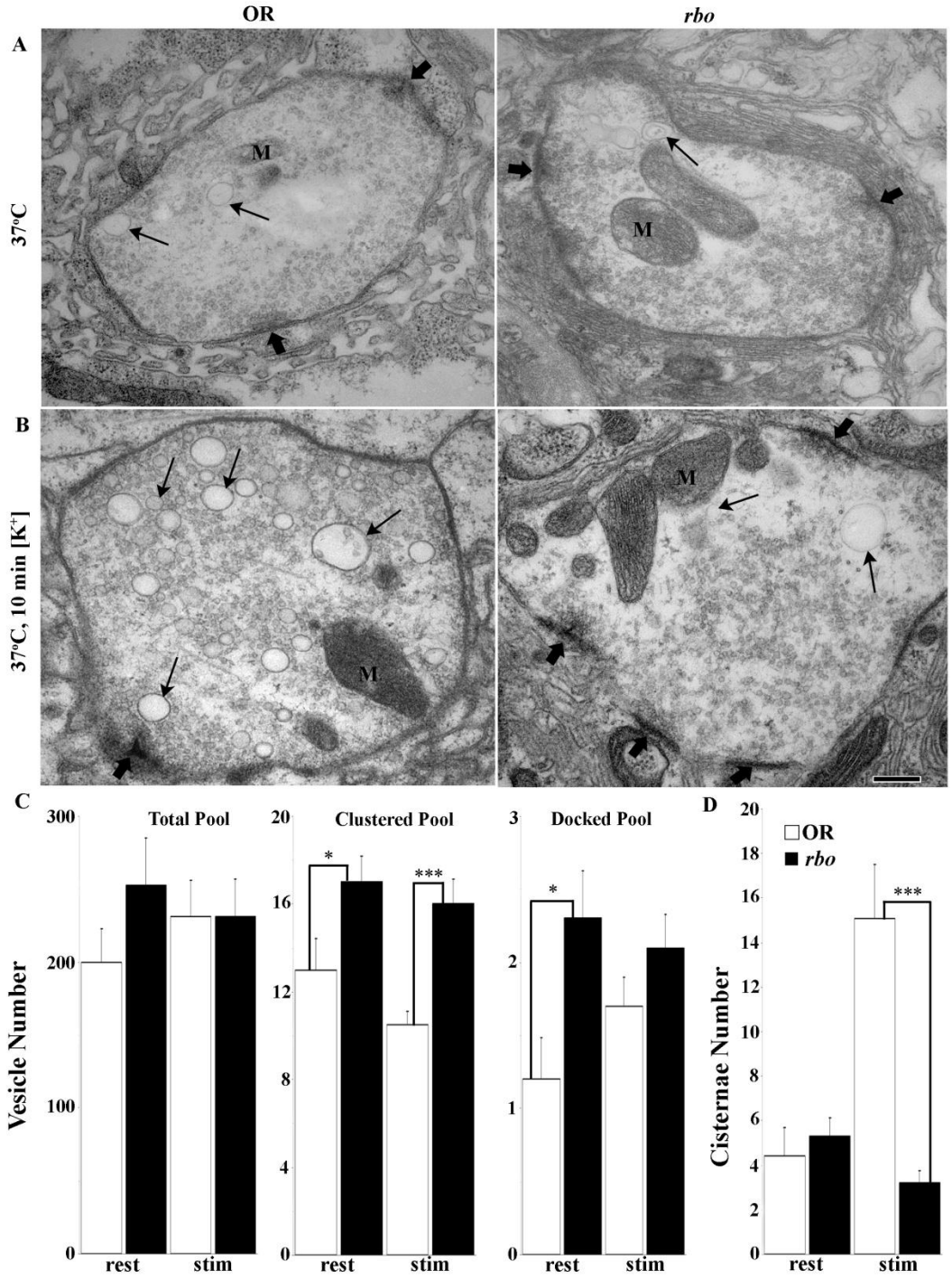

Figure 19: **RBO function is specific for bulk endocytosis at the NMJ. A,** Wildtype (OR) and *rbo*^{ts} at 37°C display similar NMJ ultrastructure. Boutons contain SVs, clustered near active zones (thick black arrows), mitochondria (M) and a few larger (>60 nm) cisternae (thin black arrows). **B,** Terminals challenged for 10 minutes with depolarizing 60 mM [K^+] saline. In wildtype (left), there is production of cisternae (thin black arrows). In *rbo*^{ts} (right), new cisternae fail to form. Scale 250nm. **C,** Synaptic vesicle number quantification in conditions of rest and high [K^+] stimulation (stim). **D,** Number of cisternae is very significantly increased by activity only in OR.

significant loss of endosome production in the mutant (OR 5.8 ± 0.8, *rbo*^{ts} 0.4 ± 0.2; Figure 20C). Thus, RBO is specifically required for endosome formation at the synapse.

Discussion

The conditional *rolling blackout* mutant (*rbo*^{ts}) paralyzes within minutes at 37^{o}C (Huang et al., 2006). Of numerous double mutant combinations with other temperature-sensitive paralytic mutants, *rbo*^{ts} displays a unique synergistic interaction with the t-SNARE Syntaxin-1A allele *syx*$^{3\text{-}69}$. We therefore hypothesized that RBO and Syntaxin-1A act together in synaptic vesicle exocytosis. However, recent re-evaluation of *syx*$^{3\text{-}69}$ forced us to radically reinterpret our previous conclusion. In the original paper (Littleton et al., 1998), the *syx*$^{3\text{-}69}$ T254I mutation was shown to block SV exocytosis due to a failure to form 7S SNARE complexes. In stark contrast, the new *syx*$^{3\text{-}69}$ study (Lagow et al., 2007) utterly contradicts the earlier report, showing that the mutant T-I substitution confers a dominant positive effect on Syntaxin-1A, promoting 7S SNARE complex formation and increasing SV fusion. This is not at all compatible with an additive defect with *rbo*^{ts} in blocking SV exocytosis. In evaluating this inconsistency, we found that *rbo*^{ts} has a temperature-dependent defect in FM1-43 endocytosis at the NMJ synapse, a defect fully rescued by reintroducing the wildtype *rbo* gene. Moreover, *rbo*^{ts};*syx*$^{3\text{-}69}$ double mutants display a severe synergistic defect in FM endocytosis at permissive temperature. These new results, together with Lagow et al. 2007, lead us to conclude a RBO requirement

in endocytosis, becoming more demanding in *rbo*^{ts};*syx*$^{3\text{-}69}$ double mutants due to increased need to recycle SVs to keep up with increased fusion rate. This new conclusion would seem incompatible with our earlier analyses at the adult dorsal longitudinal muscle (DLM) synapse (Huang et al., 2006). Is it possible that RBO has different requirements at different places? Supporting this possibility is the fact that RBO is acutely required to maintain neurotransmission at the adult DLM synapse, with a *rbo*^{ts} block in <3 minutes, but shows no such role at the larval NMJ synapse, even after *rbo*^{ts} is at the restrictive temperature for >30 minutes (Huang et al., 2006). To determine if RBO function is stage-specific (larval vs. adult), or synapse-specific (e.g. central vs. peripheral), we performed FM assays on pupal central brain primary cultured neurons, which contain many classes of synapse (Campusano et al., 2007; Jiang et al., 2005; Su and O'Dowd, 2003). In central synapses, RBO clearly localizes to synaptic varicosities, together with synaptic markers such as Cysteine String Protein, Synapsin and Bruchpilot. These RBO-positive varicosities are clearly presynaptic specializations, which take up and release FM dye in a depolarization-dependent manner. In *rbo*^{ts} neurons, there is a clear, temperature-dependent requirement for RBO in endocytosis. Although some mutant synapses are able to load dye, and a few show strong labeling, many fail to load any dye at detectable levels. Overall, there is a significant reduction in endocytosis in *rbo*^{ts} synapses, strongly supporting a conserved endocytic function for RBO in different developmental stages and classes of synapse. Nevertheless, the fact that some *rbo*^{ts} neurons show comparatively normal FM dye cycling and others show none, might signify

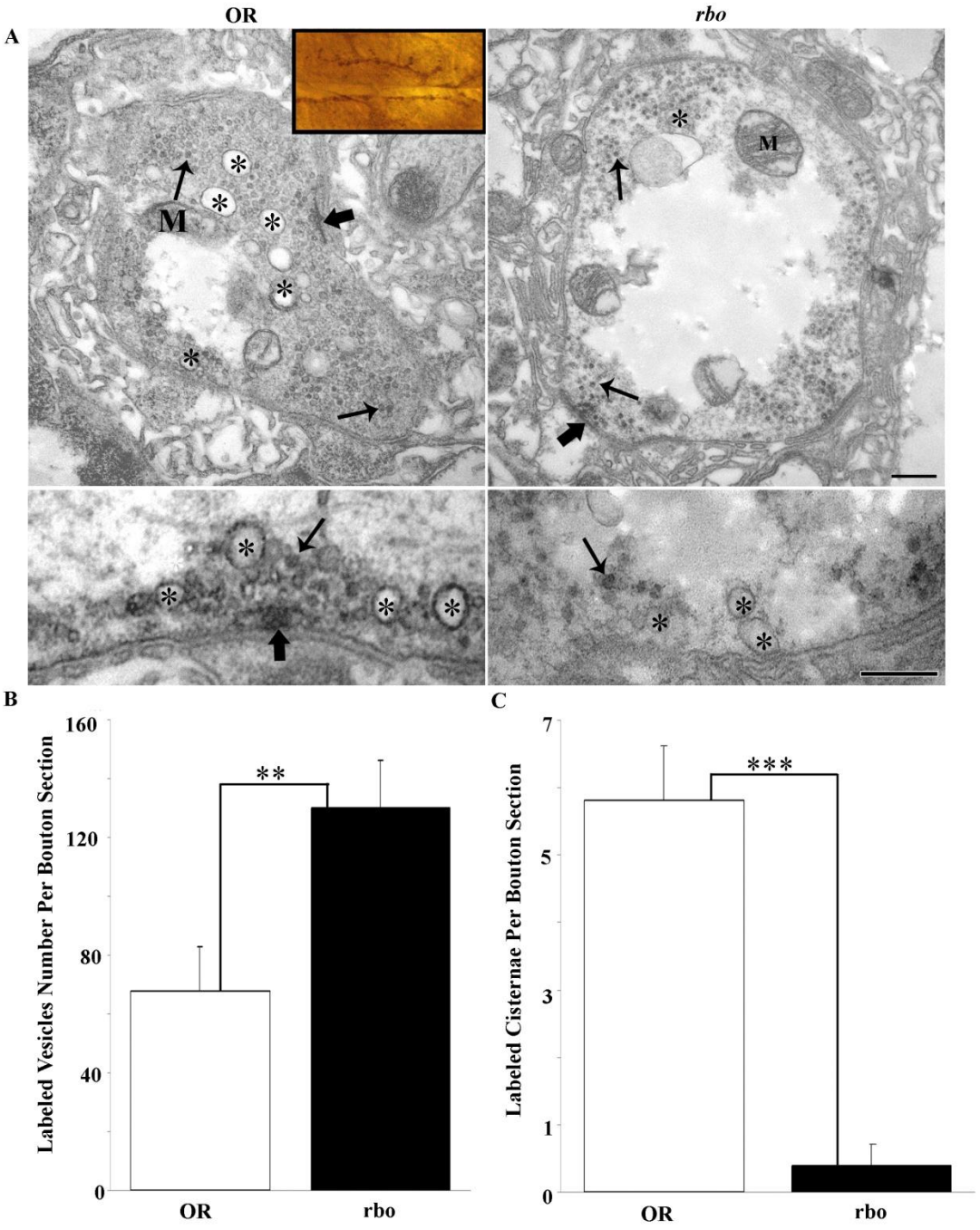

Figure 20: **RBO required for activity-dependent endosome formation in synapses.** FM1-43 photoconversion generates an electron-dense marker visible by electron microscopy. Dye incorporated into NMJ synapses by high [K^+] stimulation at 37°C, photoconverted and examined in wildtype (OR) and *rbo*^{ts}. **A,** Top left inset shows light microscopy image of photoconverted muscle 6/7 NMJ;. Top panels show representative images of control and mutant bouton profiles. Many FM-labeled vesicles and endosomes can be seen throughout the boutons. Asterisks (*) mark labeled endosomes in wildtype compared to absence of label in *rbo*^{ts}. Lower panels show higher magnification images of endosomes (*) and synaptic vesicles (thin black arrow). In *rbo*^{ts}, no labeling of endosomes was observed (*), but abundant synaptic vesicles are labeled. Scale 250nm. **B,** Quantification of FM-labeled synaptic vesicles per bouton. **C,** Quantification of FM-labeled endosomes per bouton. Significance indicated; $p<0.01$ (**), $p<0.001$ (***).

that some neuron classes are more sensitive to disruption of RBO function. This is the first study ever to do FM assays in a brain culture system or analyze genetic mutants in culture in the *Drosophila* system. Thus, these analyses represent a significant technical advance.

To dissect the endocytic RBO mechanism, we first turned to the large, accessible Garland cells, which maintain a high, constitutive rate of vesicular endocytosis (Kosaka and Ikeda, 1983; Narita et al., 1989). In *rbo*^{ts} cells, there is a severe decrease in texas red-conjugated avidin uptake, just as the synapse shows a decrease in FM dye uptake. Ultrastructural analysis reveals a dramatic enlargement and vacuolization of plasma membrane labyrinthine channels and loss of endosomes. Use of HRP as an endocytic tracer revealed a defect of plasma membrane endocytosis into endosomes. Formation of tracer-labeled endosomes is already somewhat impaired at 25^{o}C and is blocked at the 37^{o}C restrictive temperature. A similar block in uptake is observed in the *shibire*^{ts} Dynamin mutant, consistent with a similar endocytic defect (Narita et al., 1989). Moreover, enlarged alpha vacuoles appear in *rbo*^{ts} cells, similar to the phenotype of the hepatocyte growth factor-regulated tyrosine kinase substrate (HRS) mutant (Lloyd et al., 2002), which is defective in endosomal membrane invagination. Based on ultrastructural analyses, RBO function appears to be required for membrane curvature/budding during this endocytic mechanism, prior to Dynamin function.

In several neuronal systems, strong stimulation drives formation of endosomes, taken in from the plasma membrane by an activity-dependent bulk

endocytosis (Holt et al., 2003; Royle and Lagnado, 2003). In synaptosomal preparations and cultured hippocampal neurons, fluid phase tracers such as HRP localize to these structures, showing they are an immediate product of the synaptic terminal surface endosomal system (Leenders et al., 2002; Takei et al., 1996). In the *Drosophila* NMJ synapse, high [K^+] depolarization for just 10 minutes causes a nearly 4-fold increase in the number of these endosomes. Their formation is totally blocked in *rbo*^{ts} at 37^{o}C, revealing an absolute RBO requirement in activity-dependent endosome formation. Since no SV depletion is observed, this suggests that RBO is specifically required in the endosome formation pathway. The best means of testing this hypothesis is to determine whether acutely endocytosed FM dye localizes to these structures, and whether this uptake is specifically blocked in the acute absence of RBO function. We therefore performed FM1-43 dye labeling for just 2 minutes with depolarizing high [K^+] stimulation, and then photoconverted the dye using photoillumination with DAB to visualize the internalized dye ultrastructurally (Harata et al., 2001; Schikorski and Stevens, 2001). To our knowledge, this powerful technique has never before been used in *Drosophila*. Dye is observed in small SVs internalized by CME, in both controls and *rbo*^{ts} mutants, indicating that CME is not dependent on RBO function. In contrast, internalized dye is clearly observed in the enlarged endosomes in wildtype synapses, but is effectively never observed in *rbo*^{ts} synapses. This argues that endosomes are formed by direct uptake from plasma membrane during strong stimulation and that this form of uptake is specifically disrupted in the absence of RBO. Interestingly dye internalized by CME in *rbo*^{ts} is

exocytosed, whereas dye internalized by bulk endocytosis following clathrin inactivation is not re-released (Heerssen et al., 2008). One model is that bulk endocytosis is totally RBO-dependent, but direct CME of synaptic vesicles does not require RBO. In this model, a presumed increased rate of CME endocytosis is a compensatory response to the loss of bulk endocytosis in the absence of RBO function. An alternative model is that vesicles internalized by CME fail to fuse to form endosomes, because the fusion step requires RBO. In this model, the accumulation of small vesicles in *rbo*^{ts} mutants would represent an arrest in the endosomal formation pathway following endocytosis.

Contrary to expectations, *rbo*^{ts} synapses actually show a higher SV density than control, even after 20 minutes at restrictive temperature. We previously reported a similar phenotype at the adult DLM synapse (Huang et al., 2006). In both larval and adult synapses, there is an increase in clustered/docked vesicle pools at the active zone, a phenotype always interpreted as an exocytosis block. However, it has been suggested that SV endocytosis and exocytosis can both occur at the active zone (Koenig and Ikeda, 1989; Koenig and Ikeda, 1999), so it is possible that SVs accumulated at this location may also represent a defect in SV fission or maturation. Consistent with this idea, we clearly observe photoconverted FM dye in vesicles under the T-bar active zone. However, given the limited temporal resolution with our 2 minute loading protocol, it is possible that these vesicles are already docked ready to undergo exocytosis (e.g. assuming a SV cycle <30 seconds). Note also that FM assays show comparable levels of SV exocytosis in *rbo*^{ts} and *syx*$^{3\text{-}69}$ mutants relative to wildtype controls.

How does a synapse maintain exocytosis with impaired endocytosis in the absence of RBO function? Why are SVs not depleted, but actually slightly accumulated in the mutant synapse? The reason presumably is that bulk retrieval plays only a small facilitatory role in acute synaptic function, as has been established at the *Drosophila* NMJ (Heerssen et al., 2008). Indeed, direct CME of SVs appears enhanced in *rbo*^{ts} and may partially compensate for loss of SVs from the RBO-dependent endosomal pathway. These results suggest a delicate balance between CME and bulk endocytosis mechanisms under conditions of high demand, and possibly the ability for cross-talk among different endocytosis mechanisms.

Our previous work has shown that RBO functions in PLC-dependent PIP_2-DAG signaling (Huang et al., 2004). Consistently, the local turnover of phosphoinositides by PLC and PI3 kinase activities has been suggested to regulate membrane curvature and related processes during bulk membrane endocytosis (Araki et al., 2006; Wucherpfennig et al., 2003). We have proposed that RBO may modify $PI4,5P_2$ acyl side chains, making it inaccessible to subsequent conversion to other phospholipid species, which may in turn be required for bulk endocytosis. RBO is thus hypothesized to synthesize or locally concentrate phospholipid species at foci mediating nucleation of membrane retrieval. An alternative model is that endocytic defects could be due to decreased DAG levels in *rbo*^{ts} mutants (Huang et al., 2004). DAG regulates ADP ribosylation factor (ARF) in vesicle budding (Antonny et al., 1997) DAG also activates PKC, UNC-13, RasGrp and chimaerins (Yang and Kazanietz, 2003)

DAG Kinase δ (DGKδ), which converts DAG to phosphatidic acid, has also been implicated in plasma membrane endocytosis (Kawasaki et al., 2008). In the absence of RBO function, these lipids may be absent or aberrantly distributed in the plasma membrane and therefore unable to trigger membrane invagination. Our on-going studies are aimed at addressing the mechanistic interaction between RBO and phospholipids/DAG in the plasma membrane.

Materials and Methods

Drosophila Stocks

Drosophila stocks were maintained on standard food under standard rearing conditions at 25^{o}C. Animals were shifted between permissive (25^{o}C) and restrictive (37^{o}C) temperatures as indicated in individual experiments. Oregon-R (OR) was used as the wildtype control. The *rbo*^{2} allele is a null, the TS allele *rbo*^{ts1} contains a G487D missense mutation, and *rbo-egfp* is driven by the native *rbo* promoter in the *rbo*^{2} background (Huang et al., 2004; Huang et al., 2006). The *syntaxin*$^{3\text{-}69}$ T254I (Lagow et al., 2007; Littleton et al., 1998) and *shibire*^{ts1} containing a G-A transition resulting in a glycine to aspartate substitution (van der Bliek and Meyerowitz, 1991), lines were provided by Barry Ganetzky, University of Wisconsin, Madison, WI.

Immunocytochemistry

RBO-eGFP imaging was performed on *rbo^2/rbo^2; rbo-egfp/rbo-egfp* transgenic rescue animals (Huang et al., 2004, Huang et al., 2006). Coverslips were fixed in 4% paraformaldehyde for 30 minutes, washed 3 times in PBS with 0.1% Triton-X (PBS-TX) and blocked in PBS-TX containing 2.5% BSA for 1 hour. The following antibodies were used overnight at 4^{o}C; anti-GFP 5450 (1:250, goat, Abcam), anti-Synapsin (Syn; 1:100 mouse, DSHB), anti-Bruchpilot (BRP; 1:100, mouse, provided by Hugo Bellen**,** Baylor College of Medicine, Houston, TX), and anti-Cysteine String Protein (CSP; 1:200, mouse, provided by Konrad Zinsmaier, University of Arizona, Tucson, AZ). Secondary antibodies conjugated to TritC or Alexa 488 were used at 1:250 (Jackson Immunolabs, Molecular Probes). Images were captured with a Zeiss 510 Meta confocal microscope and processed with Adobe Photoshop CS8.

FM Dye Imaging Assays

FM1-43 dye loading/unloading assays were performed on wandering 3rd instar NMJ as previously described (Fergestad and Broadie, 2001). Briefly, FM1-43 dye (10 µM; Molecular Probes, Eugene, Oregon) was applied in 60 mM depolarizing K^+ saline in 1.8 mM Ca^{2+} for 2 minutes at 25^{o}C. Preparations were subsequently washed in Ca^{2+}-free saline before imaging. For restrictive temperature experiments, preparations were incubated for 10 minutes at 37^{o}C and then a 2 minute pulse of FM1-43 dye was applied in 60 mM K^+ saline. Samples were then washed at 37^{o}C in Ca^{2+}-free saline and imaged. To assay

exocytosis, loaded terminals were stimulated for 2 minutes with 60 mM K^+ saline, either at 25^{o}C or 37^{o}C. Equidistant confocal slices were scanned from muscle 6/7 NMJs, 4 NMJs per animal, two each from segments A3 and A4. Quantification was done using Image J (NIH), with average pixel intensity for the entire Z-stack 3D bouton determined. Mean pixel intensity was calculated for 10 boutons per NMJ and averaged across each animal (N = number of animals). Pupal neurons were cultured based on the protocol described by Jiang et al., 2005. 5-8 day cultures were incubated with FM1-43 dye for 45 seconds, either at 25^{o}C or following 10 minutes at 37^{o}C. Synapse fields were selected using DIC optics, with 20 fields imaged per coverslip. For quantification, the total number of DIC puncta, and number of dye-loaded puncta were each counted per 20 μm distance of axonal processes using LSM software (N = number of coverslips). A 63 X, 0.95W water immersion objective on a Zeiss LSM 510 confocal microscope was used for image acquisition.

Garland Cell Tracer Endocytosis Assays

Endocytic tracer assays were performed on Garland cells as described (Dermaut et al., 2005). Briefly, Garland cells were dissected from wandering 3rd instars in Schneider's culture medium (Gibco) and incubated at 25^{o}C or 37^{o}C for 10 minutes. Texas red-conjugated avidin (0.2 mg/ml; Sigma Aldrich) was applied for 5 minutes, followed by fixation with 4% paraformaldehyde for 15 minutes. Quantification of tracer uptake was done using Image J (NIH). An outline of the cell was drawn and total fluorescence intensity measured. A second circle was

similarly drawn in the cell interior. Subtracting this value from the whole cell value generated the peri-membrane fluorescence. Imaging was done using a Zeiss LSM 510 Meta confocal microscope.

Electron Microscopy

Analyses of NMJ synapse and Garland cell ultrastructure were performed as reported previously (Pan et al., 2004; Rohrbough et al., 2007). Briefly; for stimulated and unstimulated assays, dissected wandering 3rd instars were incubated at 37^{o}C in 60 mM K^+ saline with 1.8 mM Ca^{2+} or Ca^{2+}-free saline, respectively. Specimens were fixed in 2% glutaraldehyde for 1 hour, washed in PBS for 10 minutes and transferred into 1% OsO_4 in dH_20 for 1 hour. Preparations were stained *en bloc* in 1% aqueous uranyl acetate for 1 hour, dehydrated using a graded series of ethanol followed by propylene oxide for 30 minutes and then embedded in araldite. Ultrathin (<60nm) sections were obtained using a Leica Ultracut UCT 54 ultramicrotome, and transferred to formvar-coated slot grids placed on Synaptiek grid-sticks to be blocked stained with lead nitrate and uranyl acetate. Sections were imaged using a Phillips CM10 TEM at 80V with images from a 2-megapixel AMT CCD camera.

Tannic Acid Impregnation And Horseradish Peroxidase Uptake Methods

Following the method of Kosaka and Ikeda (1983), tannic acid (TA) was used to mark internalized lumens continuous to the extracellular space. After the osmification step in the TEM methods above, specimens were rinsed twice for 5

minutes with 1% tannic acid and then immersed for 1 hour with agitation at room temperature. Horseradish peroxidase (HRP) in modified Bodenstein saline (0.7% HRP solution) was used to assay endocytotic activity in Garland cells (Kosaka and Ikeda, 1983). Garland cells were incubated in HRP solution for 10 minutes, either at 25^{o}C or 37^{o}C. The cells were then fixed in 1.6% paraformaldehyde, 2% glutaraldehyde in PBS for 20 minutes. Samples were rinsed overnight in 0.1 M phosphate buffer at 4^{o}C and then incubated in 0.15% 3,3'-Diaminobenzidine (DAB, DEKO) for 20 minutes at room temperature. All samples were further processed for electron microscopy using the standard protocol, as described above.

FM1-43 Photoconversion

FM1-43 dye loading was done as described above and then preparations were fixed for 5 minutes in 1.6% paraformaldehyde/2% glutaraldehyde in PBS. Samples were washed for 20 minutes in Tris buffered saline (TBS, pH 7.5) and then incubated in 0.15% 3,3'-Diaminobenzidine (DAB, DEKO) in TBS for 5 minutes. The DAB solution was refreshed and samples were then illuminated using a 100 W mercury lamp, a 63X, 0.95W objective, and a standard FITC filter for 20 minutes. The photoconverted samples (see Figure. 20A; inset) were post-fixed overnight in 2% glutaraldehyde at 4^{o}C. Samples were placed in osmium (1% OsO_4) at RT for 30 minutes, washed and then placed in uranyl acetate at RT for 30 minutes. Samples were dehydrated through ethanol and then propylene oxide for 30 minutes, placed in a 1:1 ratio of propylene oxide and Spurr's resin

for 30 minutes, and finally 1 hour in pure resin in a vacuum oven. Samples were taken out and further dissected so that only muscles 6 and 7 were embedded for thin sectioning. Ultra thin (<60nm) sections of were cut on a Leica ultra cut UCT microtome. Samples were then processed for electron microscopy using the standard protocol, as described above.

CHAPTER III

ROLLING BLACKOUT POSSESSES LIPASE DOMAIN-DEPENDENT AND INDEPENDENT ENDOCYTIC FUNCTIONS DOWNSTREAM OF DYNAMIN

Introduction

The lipid composition of the plasma membrane determines its flexibility, curvature and trafficking properties. Membrane retrieval endocytosis mechanisms are critically dependent on the temporally-regulated focal accumulation of specific lipids. Numerous endocytic proteins have selective domains that recognize different membrane lipids. Pleckstrin homology (PH) and AP180 N-terminal homology/Epsin N terminal homology (ANTH/ENTH) domains bind acidic phospholipids such as PIP_2. PIP_2 is required for several steps in endocytic vesicle retrieval including clathrin coat nucleation, vesicle budding, scission and uncoating (Cremona et al., 1999; Di Paolo et al., 2004). The recruitment of endocytic adaptor proteins AP2 and AP180 requires PIP_2. Bar domain containing proteins such as endophilin and amphyphysin also bind negatively charged membrane lipids and facilitate membrane curvature during vesicle formation (Gallop et al., 2006; Peter et al., 2004). The PH domain of GTPase dynamin also binds PIP_2 (Zheng et al., 1996), and PH domain mutations inhibit dynamin function to block vesicle endocytosis (Lee et al., 1999; Vallis et al., 1999). Mutations that decrease brain PIP_2 levels, result in delayed endocytosis and slower vesicle recycling kinetics (Di Paolo et al., 2004).

We previously reported the cloning and characterization of the *Drosophila* EFR3 (Pho eighty five requiring 3) *rolling blackout* (*rbo*) (Huang et al., 2004; Huang et al., 2006). Null *rbo* mutants are 100% late embryonic lethal with no escapers, whereas a conditional temperature-sensitive mutant (*rbo*^{ts}) paralyzes within minutes at restrictive temperature and acutely blocks synaptic transmission. Conditional *rbo*^{ts} mutants display an activity-dependent complete loss of PLC-mediated phototransduction and, at the molecular level, rapidly accumulate phosphatidyl inositol 4 phosphate (PI4P) and $PIP_{2,}$ and concomitantly lose DAG, within minutes after exposure to restrictive temperature (Huang et al., 2004). RBO shows local domain homology to membrane lipases. The protein contains the pentapeptide motif G-X-S-X-G, with the central serine (358) functioning as a catalytic active site along with a histidine (H289) and an aspartate (D719), forming a serine esterase catalytic triad similar to sn-1 DAG lipase and neuropathy target esterase/swiss cheese (Bisogno et al., 2003; Muhlig-Versen et al., 2005). These data suggest that RBO may function directly as a lipase in the PIP_2-DAG pathway. On the other hand, the yeast RBO homolog EFR3 is proposed to function as a scaffolding protein required for recruiting PI4P kinase, and thus indirectly regulating plasma membrane phosphoinositide signaling (Baird et al., 2008). In the absence of yeast EFR3, cells fail to assemble the membrane kinase complex and thereby accumulate altered levels of PI4P and PIP_2 (Baird et al., 2008). These data suggest that RBO may have critical scaffolding function independent of an enzymatic activity.

RBO is expressed in both neurons and non-neuronal tissues. Conditional *rbo*^{ts} mutants demonstrate a temperature-dependent defect in vesicle endocytosis in both non-neuronal cells and neuronal synapses (Vijayakrishnan et al., 2009). Non-neuronal Garland cells show a complete endocytic block in tracer uptake assays. Ultrastructurally, there is a specific defect in tracer uptake into endosomes. Neuronal synapse show a defect in styryl FM dye endocytosis, with a ~50% reduction in dye uptake. However, there is a total blockade of endosome formation at synapses via activity-dependent bulk endocytosis (Vijayakrishnan et al., 2009). At the same time, *rbo*^{ts} mutant synapses display a significant elevation in the number and density of synaptic vesicles at the restrictive temperature. These data led us to speculate on several mechanistic hypotheses. RBO function may be required for the direct uptake of large portions of plasma membrane to form endosomal –like structures by bulk endocytosis, such that at restrictive temperature, there is a block in the formation of these structures. Alternatively, RBO function may be required for the fusion of synaptic vesicles internalized by CME, to form endosomal-like structures. This model explains the presence of increased number of synaptic vesicles at 37^{o}C. *shibire*^{ts1} is a dominant positive temperature-sensitive mutation in the GTPase dynamin. Prolonged incubation of mutants at restrictive temperature produce empty boutons devoid of vesicles due to an inability to pinch-off vesicles (Koenig and Ikeda, 1989). We made *shi*^{ts1};*rbo*^{ts} double mutants to determine if the number of synaptic vesicles formed at restrictive temperature decreased (as seen in *shi*^{ts1}) or remained elevated (as

seen in *rbo*^{ts}) and thereby determine if RBO functions up or downstream of vesicle scission.

In the present study, we first investigate the effects of a point mutation targeting the predicted catalytic active site of RBO. In the null *rbo* mutant, the lipase-dead protein is normally expressed and localized, but provides no rescue of embryonic lethality, indicating that RBO may be a lipase with essential function. Consistently, the RBO lipase domain is completely required for vesicle endocytosis in non-neuronal cells in the TS background, indicating that the lipase activity is fully required for membrane trafficking. On the other hand, the lipase-dead RBO rescues both the paralytic behavior and the endocytic defect at *rbo*^{ts} neuronal synapses, showing that lipase domain is not essential in neurons presumably due to a neural-specific compensating pathway. Secondly, to investigate the RBO endocytic mechanism, we examine genetic interactions between *rbo*^{ts} and the well-characterized GTPase dynamin TS mutant (*shi*^{ts1}). A synthetic lethal interaction occurs between *rbo*^{ts} and *shi*^{ts1}, indicating that they function in a common pathway required for viability. Consistently, the *rbo*^{ts};*shi*^{ts1} double mutants phenocopy the *shi*^{ts1} single mutant in all neuronal and non-neuronal membrane trafficking assays, indicating that *shi*^{ts1} is epistatic to *rbo*^{ts1}. We therefore conclude that dynamin functions upstream of RBO in vesicle endocytosis, and that RBO has both lipase activity and membrane scaffolding functions differentially required in neurons and non-neuronal cells.

Materials and Methods

Drosophila Stocks

All *Drosophila* stocks were maintained on standard cornmeal, agar, molasses medium in a 18^{o}C/25^{o}C cycling incubator. The wildtype strain Oregon-R was used as control. Mutant combinations containing *shi*^{ts1} mutation were maintained in the hemizygous condition, due to the lethal interaction with *rbo* in the homozygous condition. Assays were performed at 18^{o}C. *shi*^{ts1} and *shi*^{ts2} stocks were kindly provided by Dr.Mani Ramaswami, University of Arizona. Lipase-dead mutants were generated by embryonic injection of *w1118* embyros. Red-eyed adult flies from injected embryos containing the transgene (mini white w^{+} gene), were collected and crossed to a doubly balanced animals carrying cyo, mkrs (on the 2nd and 3rd chromosomes respectively), xasta markers. Animals with the transgene on the third chromosome were collected and crossed into the *rbo*^{ts} or Δ background. *rbo*S-A:GFP transgene is recessive lethal.

Molecular Techniques

Genomic *rbo* along with native promoter was tagged with a 3' terminal GFP sequence, and cloned into pUAST plasmid (Huang et al., 2004). The serine in position 358 was mutated to alanine in *rbo*S-A:GFP using the Quick Change Site-Directed Mutagenesis Kit (Stratagene, La Jolla, California) with forward 5'CGAAAATTATAGCTATTGCAGCGGGAGAAGCTGTCGGTCCCTCGGCCCTG G3' and reverse 5' CCA GGG CCG AGG GAC CGA CAGCTT CTC CCG CTG

CAA TAG CTA TAA TTT TCG 3' primers and *rbo* genomic sequence as template for PCR. Clones were selected by blue/white selection, and the presence of the mutation was verified by sequencing. The construct was injected into embryos and transgenic animals were produced by P-element mediated germ line transformations.

Behavioral Assays

For embryo hatching rate assays, animals of all genotypes shown in Figure 19 (Δ*rbo*/cyoGFP and Δ*rbo*/cyoGFP;*rbo*S-A/mkrs) were allowed to lay eggs in apple juice agar plates supplemented with yeast paste over a 10 hour period. After eggs were aged for 48 hours at 25^{o}C, the number of GFP positive and GFP negative hatched and unhatched embyos was counted, and a percentage calculated for every 100 eggs.

Paralysis assays were done as described in (Huang et al., 2006). 5 animals of each genotype were placed at a time in a pre-warmed empty plastic vial. The vials were placed in a water bath set to 37^{o}C, and time taken to paralyze was counted. The vials were tapped from time to time, and animals that fell to the bottom of the vials, lay on their backs and displayed a complete cessation of all movement were deemed to be paralyzed. Trials of paralyses for each genotype were repeated 3 times, with a fresh set of animals. A total of 15 animals were used per genotype.

Immunohistochemistry

Embryos were collected on apple juice agar plates supplemented with yeast and rinsed with water on to a mesh sieve. Embryos were dechorionated in 50% bleach for 2-3 minutes. The embryos were washed in water to remove bleach and mounted on slides with coverslips for imaging. Images were captured with a Zeiss 510 Meta confocal microscope. An argon 488nm laser was used to excitation, with a 505-530 bandpass filter and a 40X, 1.3 oil-immersion lens was used for image collection. Images were collected at a single focal plane with the pinhole kept at 670μm. Images were processed with Adobe Photoshop CS8.

FM1-43 Dye Loading Assays

Activity-dependent FM dye labeling assays were performed as previously described (Fergestad and Broadie, 2001; Vijayakrishnan et al., 2009). Briefly, wandering 3rd instar larvae were dissected in buffered, Ca^{2+}-free saline with the dorsal side facing up and pinned using Vetbond (3M) glue on sylgard coated coverslips in 0 Ca^{2+} saline. (2 mM K^{+}, 120 mM Na^{+}, 70 mM sucrose, 3 mM HEPES, pH 7.2). Larvae were incubated at 37^{o}C for 10 minutes in 0 Ca^{2+} saline, and a 2 minute pulse of FM1-43 dye (10 μM; Molecular Probes, Eugene, Oregon) was applied in 60mM high [K^{+}] saline (Vijayakrishnan et al., 2009). The coverslips were then washed in 0 Ca^{2+} saline at 37^{o}C before imaging in 0 Ca^{2+} saline at 25^{o}C. Confocal slices were scanned from muscle 6/7 NMJs, 4 NMJs per animal, two each from segments A3 and A4. Quantification was done using Image J (NIH), with average pixel intensity for the entire Z-stack 3D bouton

determined. Mean pixel intensity was calculated for 10 boutons per NMJ and averaged across each animal (N = number of animals). A 63 X, 0.95W water immersion objective on a Zeiss LSM 510 confocal microscope was used for image acquisition. Images were processed using Adobe photoshop CS8.

Garland Cell Tracer Assays

Endocytic tracer assays were performed on Garland cells as described (Dermaut et al., 2005; Vijayakrishnan et al., 2009). Briefly, Garland cells were dissected from wandering 3rd instars in Schneider's culture medium (Gibco) and incubated at 25^{o}C or 37^{o}C for 10 minutes. Texas red-conjugated avidin (0.2 mg/ml; Sigma Aldrich) was applied for 2 or 5 minutes (Vijayakrishnan et al., 2009). All *shibire* experiments were done at 18^{o}C. Quantification of tracer uptake was done using Image J (NIH). The total number of tracer-labeled vesicles inside the cell was counted for each condition. Imaging was done using a Zeiss LSM 510 Meta confocal microscope. Images were processed using Adobe photoshop CS8.

Results

Putative Lipase-Dead RBO Does Not Rescue *rbo* Null Embryonic Lethality

Lipase-dead RBO was generated by mutating the G-X-S-X-G enzyme active site in the genomic *rbo* sequence (Figure 21A, top). An EGFP tag was added at the carboxy terminus of the transgene to track transgene expression.

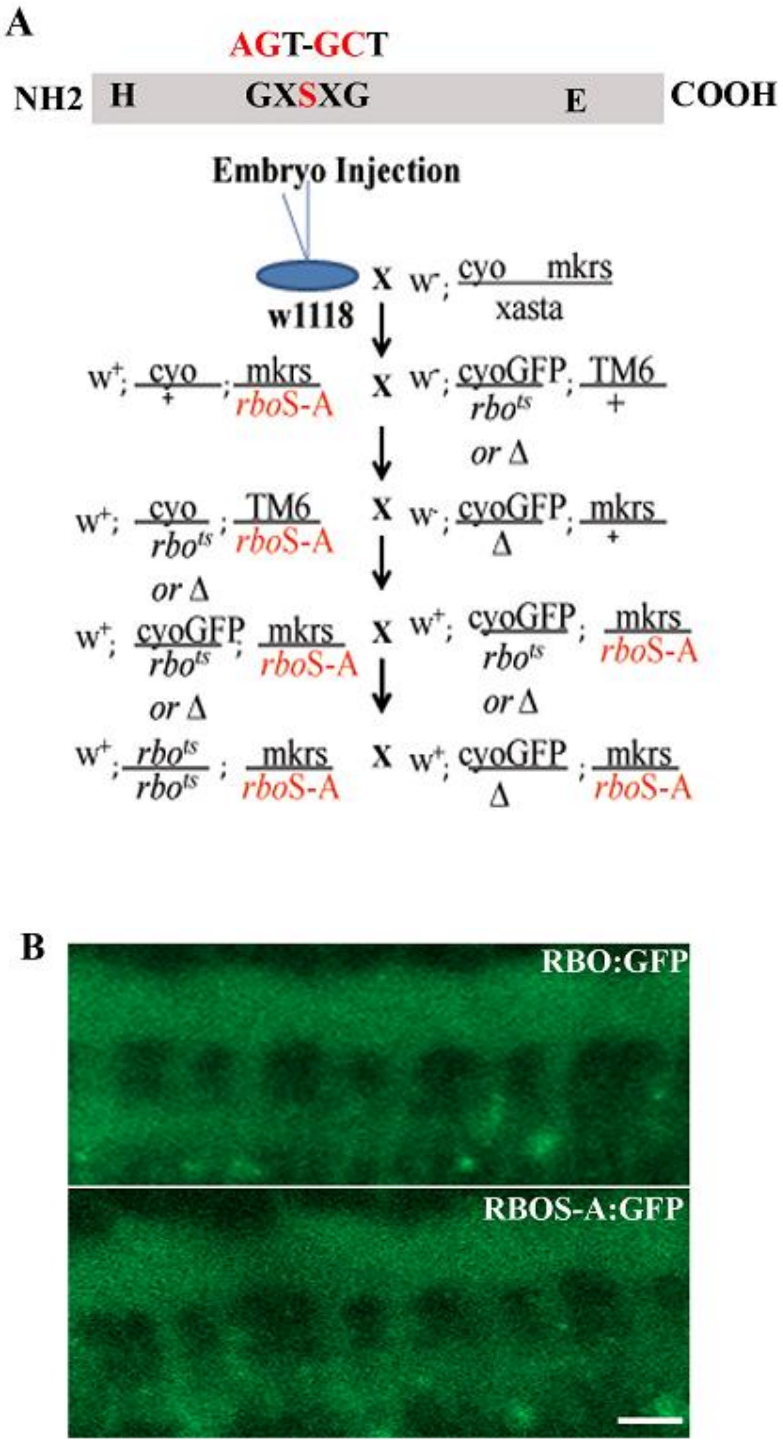

Figure 21: **Putatuve lipase-dead RBO fails to rescue the lethality of the null mutant. A,** Schematic diagram showing the primary sequence of RBO with the histidine and glutamate catalytic sites and the peptide motif of the predicted serine active site. The serine was mutated to an alanine by substituting two nucleotides in the native gene shown above the protein structure. Scheme to generate transgenic lines expressing lipase-dead RBOGFP in both TS and null mutant background. **B,** Representative images showing WT RBOGFP and RBOS-AGFP in the embryonic ventral nerve cord. Scale 20μm.

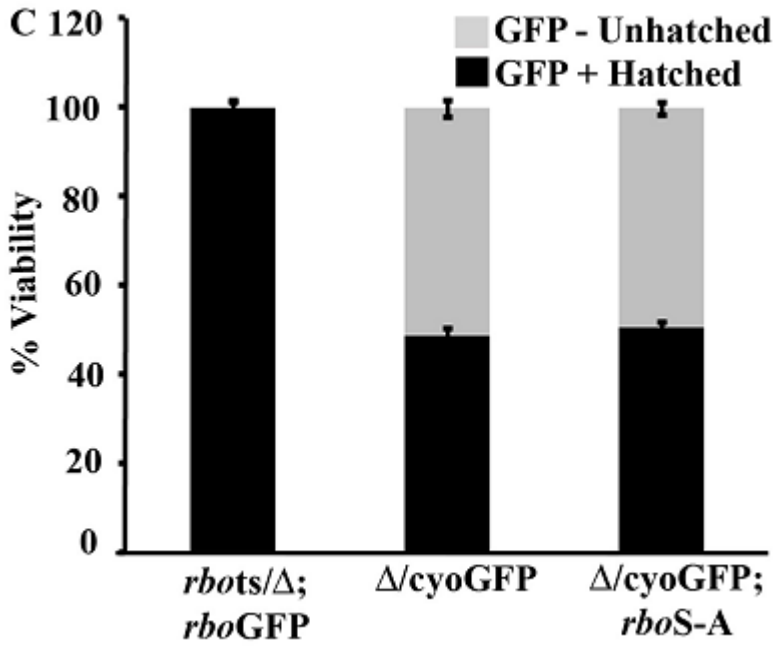

Figure 21: **Putatuve lipase-dead RBO fails to rescue the lethality of the null mutant. C,** Quantification of embryo hatching and first instar larva viability. GFP negative embryos are null for *rbo*, due to the absence of CyoGFP balancer. Error bars show SD.

The tagged transgene along with native promoter and 5' regulatory sequences was cloned into the pUAST vector. The construct was microinjected into control w^{1118} embryos (Figure 21A, middle). Stably integrated genomic lines were recovered and self-perpetuating stocks were generated. For ease of manipulation, a third chromosome transformant was selected over mkrs balancer and crossed to animals bearing balanced rbo^{ts} and the *rbo* deficiency (Δ) chromosome over cyo or cyoGFP (Figure 21A, bottom). This cross scheme produced a self-perpetuating stock containing either the *rbo* null allele over balancer or homozygous rbo^{ts} with a single copy of the transgene over balancer. Homozygous animals bearing the transgene are not viable.

Transgene expression driven by the native promoter was examined by imaging RBO:GFP (Figure 21B). Wildtype RBO:GFP expression can be detected in the embryonic ventral nerve cord (VNC) as early as stage 9 (Huang et al., 2004). The protein is rapidly restricted to the synaptic neuropil in the ladder-like array typical of synaptic markers (Figure 21B). In order to compare RBOS-A:GFP expression to wildtype RBO:GFP expression, age-matched embryos bearing a single copy of either the mutant transgene or the wildtype transgene driven by the same endogenous native promoter were dechorionated and examined in parallel. Similar to wildtype protein, the mutant protein is expressed in the embryonic VNC neuropil (Figure 21B). When imaged under identical conditions, the level and cellular distribution of RBOS-A:GFP was indistinguishable from wildtype RBO:GFP, indicating that the transgene is expressed and targeted

properly. Note that a single copy of the wildtype transgene rescue the late stage embryonic lethality of the null mutant (Huang et al., 2004).

Null *rbo* mutants die as mature embryos. In order to determine if the RBO S-A transgen can rescue the lethality of the null condition, embryo hatching was quantified (Figure 21C). Hatching of GFP negative and positive larvae was scored, and compared between animals carrying the null allele over CyoGFP balancer, and the balanced null with a single copy if the *rbo*SA transgene (Δ/CyoGFP and Δ/CyoGFP; *rbo*SA). Hatching efficiency in a rescued stock carrying wildtype RBO was used as control (Figure 21C). The percentage hatching of GFP-positive embryos (with cyoGFP, carrying wildtype *rbo* on the balancer) was not significantly different between Δ/CyoGFP and Δ/CyoGFP; *rbo*-SA (rescue, 98.75% ± 1.5, Δ/CyoGFP, 45.5% ± 2.64 and 49.75% ± 1.70). The percentage of GFP negative unhatched embryos (*rbo* null, with or without *rbo*S-A transgene) was also not significantly different between the two groups (Δ/Δ, 47.6% ±3.14, Δ/Δ;*rbo*S-A, 48.6%± 1.51). Therefore the presence of a single copy of the *rbo*S-A transgene in the null background is unable to rescue the lethality of the null at the mature embryonic stage (Figure 21C). These data indicate that mutant protein made from the RBOS-A:GFP transgene expressed at normal locations at normal levels identical to the wildtype during development is unable to provide a wildtype function.

Putative Lipase-Dead RBO Is Unable To Rescue Garland Cell Endocytosis Defects

Drosophila Garland cells (or “wreath” cells) encircle the anterior end of oesophagous above the proventriculous (Chang et al., 2002; Kosaka and Ikeda, 1983; Narita et al., 1989), and act as nephrocytes analogous to the kidneys of higher animals. These cells are highly specialized for clathrin-mediated fluid phase endocytic uptake from the haemolymph. Mainly due to their large size and ease of visualization, these cells are used as a model system to understand the mechanistic aspects of endocytic trafficking (Aggarwal and King, 1967; Kosaka and Ikeda, 1983; Narita et al., 1989). We previously showed that RBO is expressed in the plasma membrane of garland cells, and that *rbo*^{ts} mutants show a temperature-dependent block in texas-red avidin tracer uptake (Vijayakrishnan et al., 2009). Ultrastructurally, the surface area of garland cells is increased by deep invaginations called labyrinthine channels, from which vesicles are pinched off by CME (Aggarwal and King, 1967). Typically these channels are short because the endocytic pinch-off rate far exceeds the membrane re-insertion rate (Narita et al., 1989). However, in *rbo*^{ts} mutants at restrictive temperature, labyrinthine channels become much elongated and engorged, similar to defects seen in other endocytic mutants, with a failure to pinch-off while membrane insertion continues (Narita et al., 1989).

In order to determine how the presence of the lipase-dead *rbo*S-A transgene affects the *rbo*^{ts} endocytic block, we performed tracer uptake assays in garland cells isolated from *rbo*^{ts} animals expressing *rbo*S-A (Figure 22). Following TR-avidin uptake of 2 minutes at permissive 25^{o}C, both wildtype

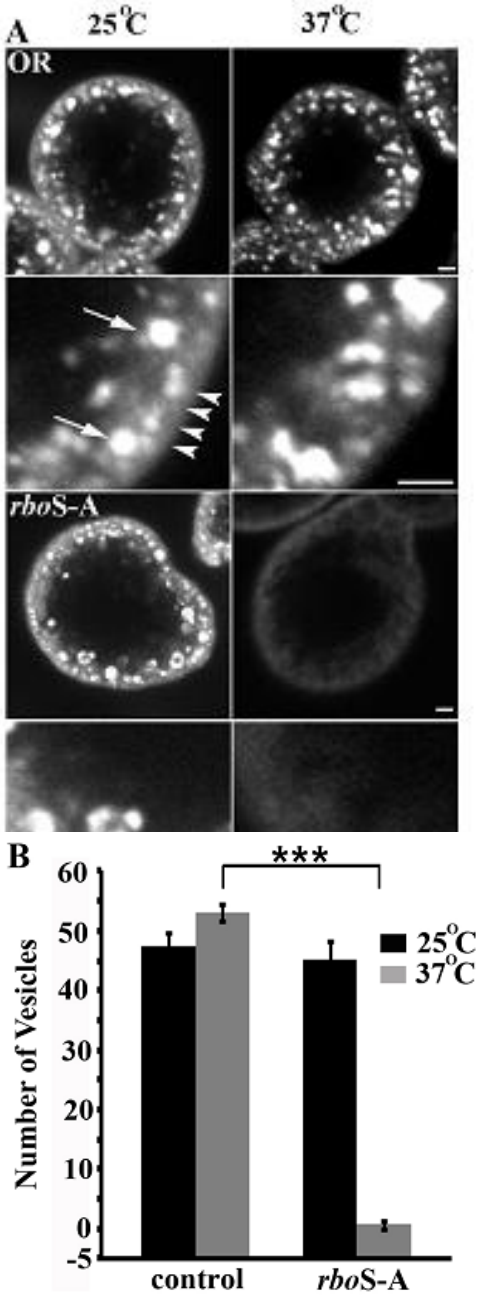

Figure 22: **Putative lipase-dead rbo fails to rescue garland cell endocytic defects**. **A,** Representative images showing texas-red avidin uptake in garland cells of indicated genotypes loaded at permissive (25°C) or restrictive temperatures (37°C). Lower panels in each case showing higher magnification region below the plasma membrane. Scale 2 μm. White arrows point to vesicles and arrow heads point to plasma membrane of the garland cell **B,** Quantification of number of texas-red avidin positive vesicles inside the cell in OR and rbo-S-A garland cells following permissive and restrictive temperature loading. Error bars show mean ± SEM. Significance of $p<0.001$ is indicated (***)

control OR cells and *rbo*-SA cells take up tracer into discrete puncta/vesicles within the cell (Figure 22A, left column; plasma membrane and internalized vesicles shown with white arrowheads and arrows, respectively). At permissive temperature, the total number of endocytosed vesicles in control and *rbo*S-A is indistinguishable (wildtype OR, 47.42 ± 2.26; *rbo*S-A, 41.67 ± 2.93; Figure 22B). At the restrictive 37^{o}C, however, while wildtype cells continue to display robust tracer uptake (OR, 53.11 ± 1.39; Figure 22A,B), no tracer positive vesicles appear in *rbo*S-A cells (*rbo*S-A, 0.62 ±0.59, $p<0.001$; Figure 22A,B). These data show there is a complete block in garland cell endocytosis in the *rbo*^{ts};*rbo*S-A animals, similar to that seen in *rbo*^{ts} alone (Vijayakrishnan et al., 2009). The *rbo*S-A transgene is unable to provide a rescue of function.

Putative Lipase-Dead RBO Rescues Endocytic Defects At The NMJ

rbo^{ts} animals display conditional temperature-sensitive paralysis (Huang et al., 2006). In adult animals there is a reversible loss of excitatory junction potential from the dorsal longitudinal muscle following presynaptic nerve stimulation suggesting that this is due to a synaptic transmission defect (Huang et al., 2006). The 3rd instar larval neuromuscular junction is a well studied model for assays of synaptic function(Fergestad and Broadie, 2001). Previously we showed that *rbo*^{ts} larvae show a temperature-dependent defect in depolarization-dependent lipophilic styryl dye FM1-43 uptake into motor neuron NMJs indicative of a defect in membrane endocytosis (Vijayakrishnan et al., 2009). This defect is

due to the *rbo*^{ts} mutation and is completely rescued by a single copy of a wildtype *rbo* transgene driven by its endogenous promoter (Vijayakrishnan et al., 2009).

In order to determine how the presence of the *rbo*S-A transgene affected paralysis and endocytic trafficking defects in *rbo*^{ts} NMJ, we performed paralysis assays in *rbo*^{ts} adults and FM1-43 dye uptake assays in dissected 3rd instar larvae (Fergestad and Broadie, 2001; Trotta et al., 2004). *rbo*^{ts} larvae display a FM-43 dye loading defect at 37^{o}C (Vijayakrishnan et al., 2009). Three genotypes were analyzed, control OR, *rbo*^{ts} and *rbo*^{ts}; *rbo*S-A.

100% of *rbo*^{ts}/Δ animals paralyze within 5 minutes of shift to 37^{o}C. Under the same conditions *rbo*^{ts}/Δ; *rbo*S-A/mkrs animals are still able to walk/climb the walls of the vials similar to control OR animals. The presence of the *rbo*S-A transgene is able to rescue the paralytic phenotype seen in *rbo*^{ts}.

FM1-43 dye was loaded for 2 minutes in 60mM [K^{+}] depolarizing saline following 10 minutes of incubation in 0 Ca^{2+} saline at 37^{o}C. As shown previously *rbo*^{ts} larvae show a significant decrease ($p<0.0001$) in dye loading compared to controls at restrictive temperature (OR 78.24 ± 4.068 (N=5) *rbo*^{ts}35.59 ± 3.11 (N=5), $p<0.001$, Figure 23B, left). However dye loading in the presence of a single copy of the *rbo*S-A transgene is not significantly different from that seen in controls ($p=0.285$). The transgene is able to rescue the endocytic defect seen in *rbo*^{ts} background (*rbo*^{ts};*rbo*S-A 71.74 ± 3.99 (N=6), Figure 23B, right). These data suggest that lipase function is not required for its endocytic role at the larval NMJ. RBO may function as a hetero/oligomer, such that the presence of one wildtype TS regions and one wildtype G-X-S-X-G region the two mutant proteins can

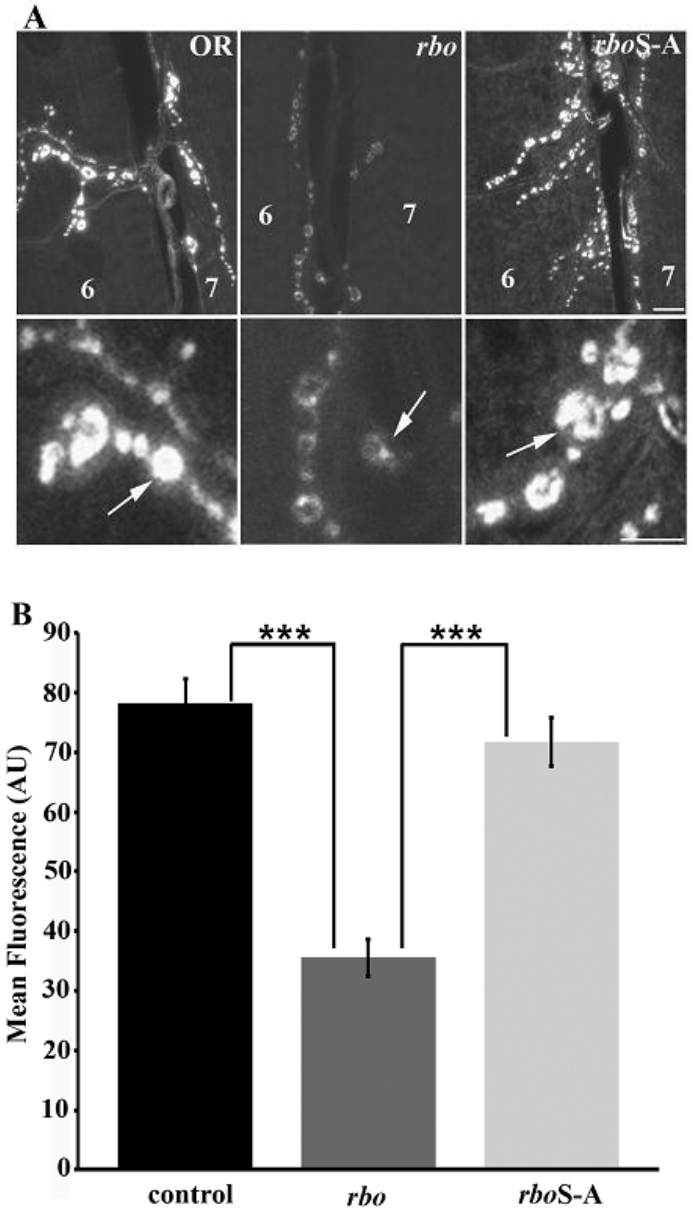

Figure 23: **Putative lipase-dead RBO rescues synaptic endocytic defects . A,** Representative images of 3rd instar larval NMJ terminals in control (OR), *rbo*^{ts} and *rbo*^{ts};*rbo*S-A larvae with FM1-43 dye at 37^{o}C. Scale 2μm. Lower panel shows higher magnification view of boutons from the terminals shown above, scale 1μm. **B,** Quantification of FM1-43 dye loading. The presence of *rbo*S-A in the *rbo*^{ts} background is able to rescue the endocytic defect seen in *rbo*^{ts} at restrictive temperature. Error bars show mean ± SEM. Significance of $p<0.001$ is indicated (***).

come together and provide near normal function. Alternatively, if the TS phenotype is simply the result of decreased levels of RBO protein, the presence of an extra copy of RBOS-A is able to rescue the defect.

shibire^{ts1} Is Epistatic To *rbo*^{ts} In Synaptic Endocytosis

The GTPase dynamin is one of the most well studied endocytic proteins. It is required for all forms of endocytosis at the *Drosophila* NMJ. (Hinshaw and Schmid, 1995; Koenig and Ikeda, 1989; Sever et al., 2000; van der Bliek and Meyerowitz, 1991). The temperature-sensitive *Shibire*^{ts1} mutation first helped establish dynamin's cellular role in endocytosis (Koenig and Ikeda, 1989; Kosaka and Ikeda, 1983). There is ample physiological and ultrastructural evidence to show defective cycling in these mutants (Kawasaki et al., 2000; Kosaka and Ikeda, 1983). Exposure to temperatures >29^{o}C leads to a loss of styryl dye loading indicative of a strong defect in endocytosis under these conditions (Ramaswami et al., 1994). Ultrastructurally synaptic terminals of these animals are completely depleted of synaptic vesicles. Upon return to 22^{o}C, recycling resumes in these mutants and nerve terminals are refilled with synaptic vesicles (Koenig et al., 1983; Poodry and Edgar, 1979).

To determine if RBO acts in a dynamin-dependent or independent mechanism, we attempted to make *shi*^{ts1};*rbo*^{ts} double homozygous mutants. However, even when reared at 16-18^{o}C this combination produces synthetic lethality in double homozygous animals. No double homozygous female third instar larvae could be recovered indicating that lethality occurs at the second

instar stage or earlier. *shi*^{ts1}/y;*rbo*^{ts}/Δ males can be seen as third instars but die at a late larval or early pupal stage. All adult males recovered contain balancer over y and females have either one or two copies of balancer chromosome with wildtype *shibire*. In order to assay endocytosis at the larval NMJ, *shi*^{ts1};*rbo*^{ts} larvae were maintained in a hemizygous condition by maintaining the *shi*^{ts1} over an FM7GFP balancer. *shi*^{ts1}/y;*rbo*^{ts}/Δ (non GFP males) and *shi*^{ts1}/y larvae were selected for FM1-43 dye loading experiments. To test if the presence of the *rbo*^{ts} mutation worsened dye loading phenotypes in the *shi*^{ts1} background, FM 1-43 dye was loaded with a 60 mM [K^+] stimulus for 4 minutes at 18^{o}C. Under these conditions both *shi*^{ts1}/y and *shi*^{ts1}/y;*rbo*^{ts}/Δ larvae showed significantly decreased loading compared to wildtype controls (OR, 106.63 ±10.23, (N=4), *shi*^{ts1}/y, 64.69 ± 7.596 (p=0.009), (N=10), *shi*^{ts1}/y; *rbo*^{ts}/Δ, 53.53 ± 5.46,(p=0.0004)(N=9), Figure 24A and B), but not significantly different from each other (p=0.258). These data suggest that since the endocytic phenotype in *shi*^{ts1}/y is not worsened in *shi*^{ts1}/y;*rbo*^{ts}/Δ, RBO acts in a dynamin-dependent endocytic pathway at the NMJ. There is a general requirement for RBO in dynamin-dependent endocytosis at the neuronal synapse. In order to determine if this requirement is also there in non-neuronal cells we next analyzed garland cells in the double mutants.

shibire Is Epistatic To *rbo*^{ts} In Non-Neuronal Cell Endocytosis

Garland cell endocytosis is well studied in *shi*^{ts1} mutants. Temperature-dependent structural changes have been reported in *shi*^{ts1} garland cells

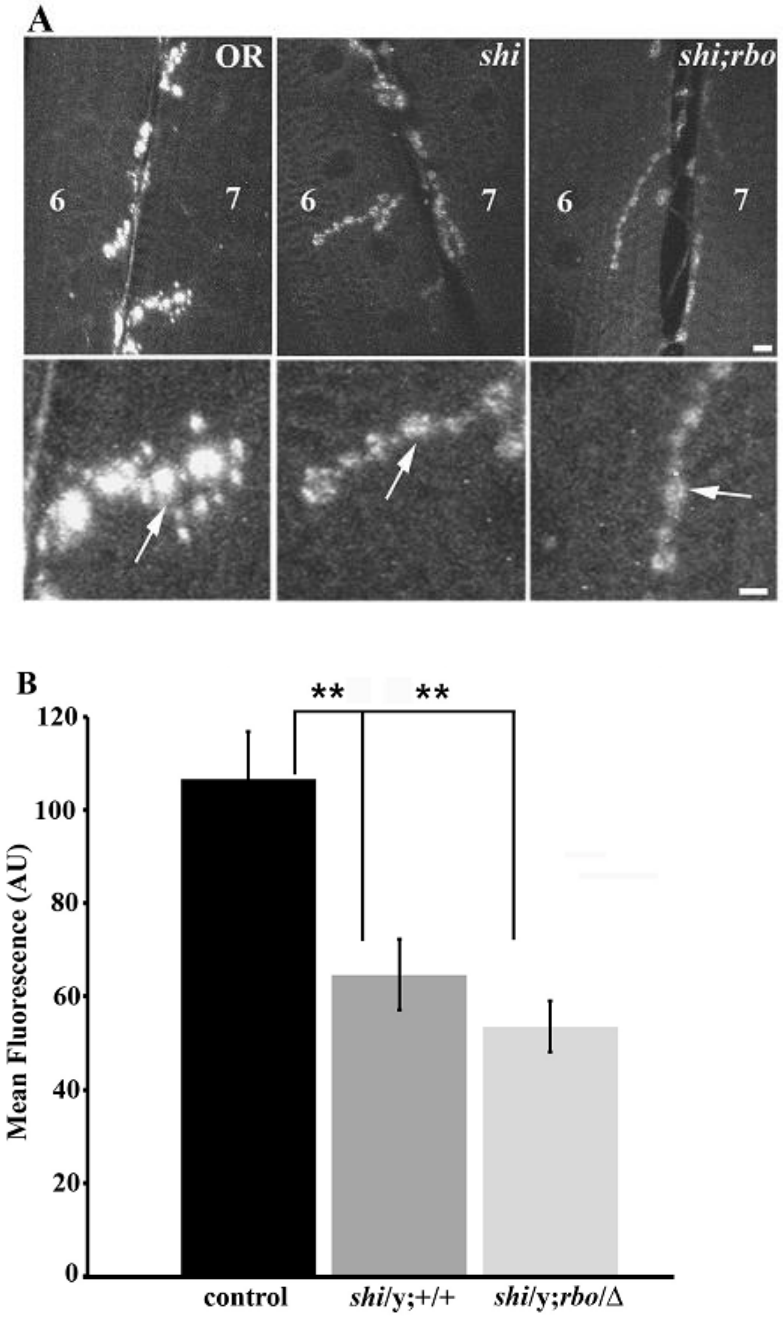

Figure 24: **Interaction of RBO with Dynamin-dependent endocytosis at the NMJ. A,** Representative images showing FM1-43 dye loading in 3rd instar larval NMJ preparation. Loaded in depolarizing saline for 4 minutes at 18°C. Scale 2μm. Lower panel shows higher magnification of boutons from terminals shown in above panel. Scale 1μm. **B,** Quantification of FM1-43 dye loading showing relative dye loading intensity between OR, shi^{ts1}/y, and shi^{ts1}/y; rbo^{ts}/Δ.Error bars show mean ± SEM. Significance of $p<0.01$ is indicated (**)

(Narita et al., 1989). Previous ultrastructural analyses of *shi*^{ts1} garland cells revealed a doubling of whole cell caparitance, suggestive on an increase in cell area due to

the endocytic block, and elongation of the labyrinthine channels that increase endocytic surface area (Kosaka and Ikeda, 1983; Narita et al., 1989). Further, there is a block in the uptake of fluorescent tracers at the level of the light microscope. Ultrastructurally there is a block in the the uptake of horse radish peroxidase at restrictive temperature. Coated pits are present but no coated vesicles are formed, indicative of a block at the pinching-off stage (Kosaka and Ikeda, 1983; Vijayakrishnan et al., 2009).

In order to analyze the interaction between dynamin and RBO function we performed garland cell Texas-red avidin uptake assays on *shi*^{ts1}/y and *shi*^{ts1}/y;*rbo*^{ts}/Δ. Garland cells were dissected and Texas-Red avidin was applied for 5 minutes at the permissive temperature, 18^{o}C. The total number of internalized puncta were counted and found to be significantly different between wildtype controls and *shi*^{ts1}/y and *shi*^{ts1}/y;*rbo*^{ts}/Δ, (OR, 47.94 ±3.95*, shi*^{ts1}/y, 31.267±4.57 (p=0.0487), *shi*^{ts1}/y;*rbo*^{ts}/Δ, 32.23 ± 5.05, (p=0.043), Figure 25A and B). There was no significant difference between *shi*^{ts1}/y and *shi*^{ts1}/y;*rbo*^{ts}/Δ (p=0.801). These data suggest that as seen in the NMJ RBO may be acting in a dynamin-dependent pathway to facilitate endocytosis in garland cells similar to that seen in neuronal synapses.

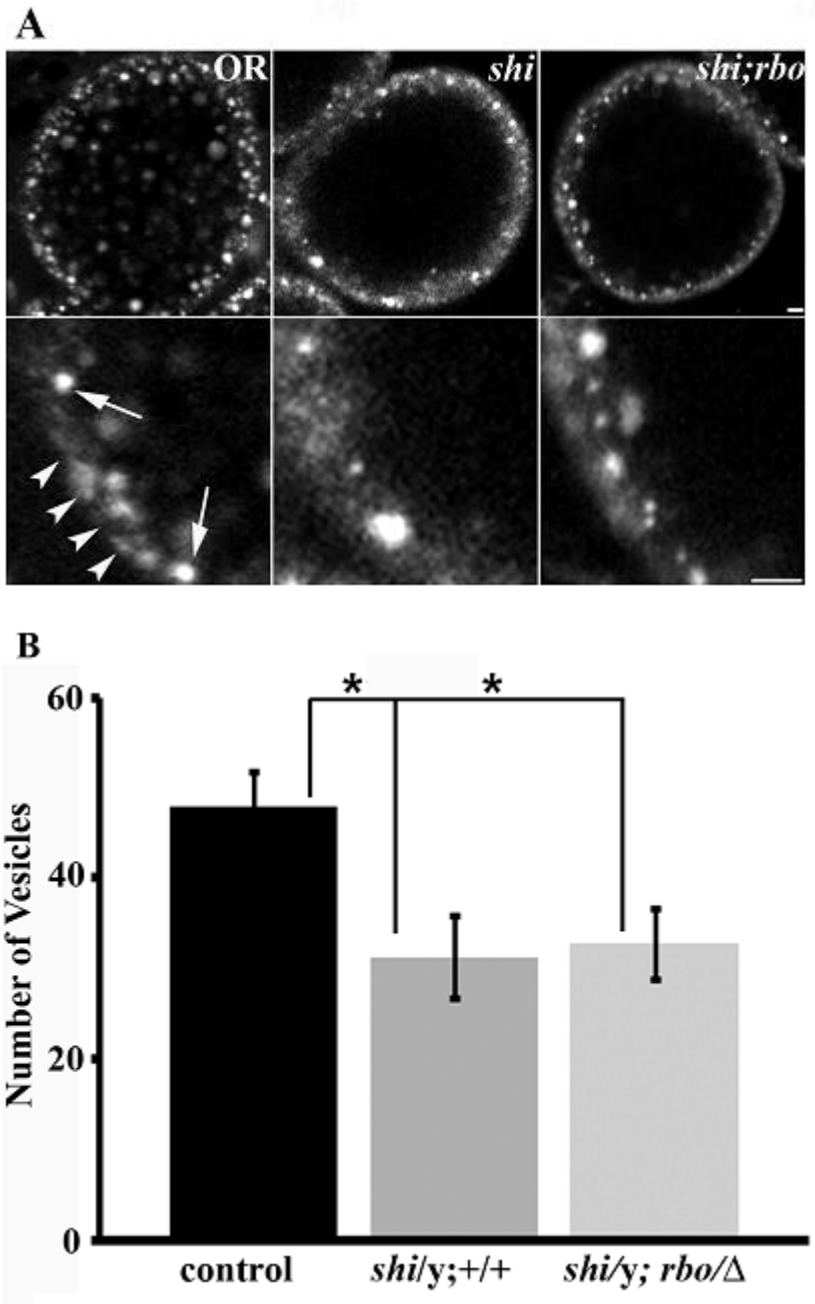

Figure 25: **Interaction of RBO with Dynamin-dependent endocytosis in garland cells. A,** Representative images showing texas-red avidin uptake in garland cells of shi^{ts1}/y, and shi^{ts1}/y;*rbo*/Δ larvae at 18°C for 5 minutes. Scale 5μm. Lower panel shows higher magnification view of garland cell plasma membrane from cells shown in upper panel, scale 2.5μm. **B,** Quantification of garland cell endocytosis. Error bars show mean ± SEM. Significance of $p<0.05$ is indicated (*).

Discussion

A growing body of evidence suggests that lipid modifying enzymes play a vital role in cellular endocytic processes (Haucke, 2005; Rohrbough and Broadie, 2005; Wenk and De Camilli, 2004; Yakir-Tamang and Gerst, 2009). The *Drosophila* EFR3 *rolling blackout* is an integral plasma membrane protein and predicted lipase that we have previously shown to be required for phototransduction and synaptic transmission (Huang et al., 2004; Huang et al., 2006). RBO was initially described as homologous to sn-1 DAG lipase (Bisogno et al., 2003; Huang et al., 2004). However, recently the *Drosophila* homolog of sn-1 DAG lipase, INAE (Inactivation no afterpotential E), has been cloned and shown to hydrolyze DAG at the sn1 position (Leung et al., 2008). Thus, the lipolytic function came in question. Mechanistically, we have shown that RBO plays a role in endocytic trafficking in non-neuronal cells and in neuronal synapses (Vijayakrishnan et al., 2009). In order to test the hypothesis that *rbo* functions as a lipase in endocytosis, we generated a point mutation in the putative catalytic active site of RBO, a mutation predicted to render the lipase inactive (Gronke et al., 2005; Muhlig-Versen et al., 2005). Since our attempts to characterize the enzymatic activity of heterologously expressed RBO protein where unsuccessful (Vijayakrishnan and Broadie, 2006), the genetic disruption of the catalytic active S-A 358 provides the best possible alternate method to elucidate of the importance of the predicted lipase function in vesicle endocytosis.

rbo is an essential gene required for cell viability (Faulkner et al., 1998) and lack of of widtype *rbo* causes completely penetrant embryonic lethality. The transgene with the S-A 358 point mutation by itself is 100% lethal, showing that the mutation alters an essential function of the protein. This result indicates the S358 residue has an essential function. Importantly, the presence of the TS mutation can rescue the lethal phenotype in *rbo* null embryos (Figure 21C), while conferring conditional paralysis and defects in cellular endocytosis as shown by tracer uptake assays in neuronal and non neuronal cells at larval and adult stages (Huang et al., 2004; Huang et al., 2006; Vijayakrishnan et al., 2009). These data show that the TS mutant allele contains sufficient RBO activity to provide for the essential function. The rbo^{ts} mutant carrying the S-A 358 point mutation do not display any FM-143 dye loading defects at the larval NMJ (Figure 23) and, in accordance with the lack of synaptic endocytosis phenotype, these animals do not paralyze at the restrictive temperature ($37^{o}C$). RBO may function as a dimer/oligomer such that the functionally intact TS site in RBO S-A can come together with the intact Serine 358 site to provide a rescue of function. While more structural data on the domain structure of RBO will be required to provide a definitive explanation for this phenotypic suppression, genetic analysis of intragenic suppressors provides a powerful tool to study the contributions of individual domains of a protein to its biochemical activity (Shin et al., 2002). Several such examples of intragenic suppressors exist in Drosophila. A temperature-sensitive allele of the ATPase NSF (N-ethymaleimide-sensitive factor), $comt^{st53}$ containing a S-L483 substitution is suppressed by a A-T279

substitution in the *comt*^{su1} allele such that double mutants take almost twice as long to paralyze at the same temperature. In this case since both mutations occur in the D1 ATPase domain it is hypothesized that the complementarity of these mutations could restore some intramolecular interaction disrupted in the *comt*^{st53} mutant. *comt*^{su1} might alter ATP binding or suppress *comt*^{st53} paralysis by stimulating ATP hydrolysis (Dellinger et al., 2000). All known TS phenotypes seen in a temperature-sensitive *shibire* allele, *shi*^{ts2} with a G-S146 substitution in GTPase domain, believed to affect GTP binding affinity, are rescued by three intragenic suppressors, known as suppresors of *shibire* (sushi) (Narayanan et al., 2005). One occurring in another region of the GTPase domain, and two in a C terminal GTPase effector domain (GED), these sushi mutations reduce both the basal and assembly-stimulated rate of GTP hydrolysis without affecting GTP binding. It is therefore proposed that the phenotypic rescue is brought about by functional interactions between the various domains of dynamin. A reduction in the GTP hydrolysis rate compensates for reduced binding (Narayanan et al., 2005). However, the *rbo*^{ts}; *rbo*S-A larvae continue to show the full mutant defects in garland cell tracer uptake assays at 37^{o}C, with a complete loss of plasma membrane endocytosis. These data show that the predicted lipase-inactive mutant disrupts this vital aspect of RBO function, and this activity cannot be compensated for in the requirement for embryonic viability, or the endocytic requirements at least in non-neuronal tissues like garland cells.

A more controversial possibility is that the lipase activity of RBO is not required for its endocytic role at neuronal synapses. In support of this idea, other

synaptic enzymes with known activities have been shown to modulate cellular processes independent of that activity. For example, CamKII acts both as a calcium-dependent kinase and also via non-kinase related activities. It mediates short term synaptic plasticity in hippocampus by scaffolding presynaptic vesicle docking independently of its ability to phosphorylate itself or other presynaptic targets (Hojjati et al., 2007). The yeast RBO homolog, EFR3/Ymr212c functions as an integral plasma membrane scaffolding protein (Baird et al., 2008). In yeast, the RBO homolog function is required to recruit and maintain plasma membrane phosphatidylinositiol 4 kinase (PI4K) patches which, in turn, regulates membrane PI4P and $PI4,5P_2$ levels (Baird et al., 2008). Thus, both *Drosophila* and yeast proteins regulate plasma membrane lipid levels, but by completely different proposed mechanisms. It remains possible that, independent of lipase activity, the S-A358 mutations affects protein phosphorylation or some other posttranslational modification which then affects protein function.

To analyze the exact mechanistic role of RBO in membrane trafficking during endocytosis, we compared the RBO requirement with the hallmark Dynamin function. Dynamin belongs to a superfamily of GTPases and participates in a number of membrane trafficking events such as the formation of endocytic and secretory vesicles, intracellular organelle fission, and regulation of the actin cytoskeleton (McNiven et al., 2000; Orth and McNiven, 2003). It is believed to act as a mechanochemical enzyme or scaffolding protein during endocytosis, that either directly severs the necks of endocytosing vesicles by GTP hydrolysis-driven constriction, or recruit other proteins that may participate

in the fission of the necks (Sever et al., 2000; Stowell et al., 1999; Sweitzer and Hinshaw, 1998). Work done on *shi*^{ts1} mutation, a G273D substitution in the GTPase domain of dynamin that affects its ability to pinch-off endocytosing vesicles in a temperature-dependent manner, has greatly facilitated our current understanding of the mechanism of endocytic scission (Chen et al., 1991; Grigliatti et al., 1973; van der Bliek and Meyerowitz, 1991). The temperature-sensitive paralytic behavior of these animals is translated at the ultrastructural level by the appearance of synaptic boutons devoid of vesicles, containing apparently arrested coated collared endocytic intermediates both in neuronal synapses and non-neuronal cells such as garland cells (Koenig and Ikeda, 1996; Kosaka and Ikeda, 1983; Poodry and Edgar, 1979). Based on our previous work, we hypothesized that RBO function is required for endocytic trafficking. In *rbo*^{ts} boutons, we see an endocytic dye loading defect. At the ultrastructural level, even after conditions of high [K^+] stimulation known to deplete vesicles in other endocytic mutants, we fail to see vesicle depletion. The number of small vesicles (40nm diameter) internalized by CME is always slightly higher than that seen in controls. However, only under conditions of stimulation, at restrictive temperature in control boutons we see the appearance of large cisternae (60nm in diameter) that form in *rbo*^{ts} at permissive temperature but completely fail to form at restrictive temperature. These cisternae are known to form in *shi*^{ts1} boutons prior to depletion (Poodry and Edgar, 1979). In order to determine if these cisternae that fail to form in *rbo*^{ts} boutons represent a defect in bulk uptake, where large portions of synaptic terminal membrane invaginate to form an endosomal-like

structure, or alternatively if there is a failure of vesicles internalized by CME to coalesce and form these structures, we made *shi*^{ts1}/y;*rbo*^{ts}/Δ double mutants. If dynamin functions upstream of RBO function, then the overall number of vesicles internalized by CME should be decreased following stimulation at restrictive temperature in the double mutants.

The double homozygous mutant combination results in synthetic lethality at a late larval or early pupal stage. No adult *shi*^{ts1}/*shi*^{ts1};*rbo*^{ts}/Δ animals were recovered. Therefore all assays with *shibire* were performed on male larvae hemizygous for *shi*^{ts1}. Other examples of endocytic mutants showing synthetic lethality with *shi*^{ts1} include a TS allele of *stoned* (*stn*^{ts}) and Eps15 (Majumdar et al., 2006; Petrovich et al., 1993). However *stoned* and *eps*15 mutants also display synergistic interactions with weaker *shibire* alleles (Majumdar et al., 2006; Stimson et al., 2001). Synergism between Eps15 and dynamin has also been reported in C.*elegans* (Salcini et al., 2001). Interestingly Eps15 also shows a synthetic lethal interaction with stoned TS allele and at the protein level can be pulled down with dynamin and Stn B (Majumdar et al., 2006). Mammalian stoned homolog, stonin 2 has been reported to bind Eps15 (Martina et al., 2001). Therefore this synthetic lethal interaction between RBO and dynamin may be due to overlap in function.

Here we report the characterization of *shi*^{ts}/y;*rbo*^{ts} mutant larvae using dye and tracer uptake assays in garland cells and in the neuromuscular junction. Both at the NMJ and in garland cells, while *shi*^{ts1} and *shi*^{ts1};*rbo*^{ts} display strongly reduced dye loading and tracer uptake compared to wildtype, a synergistic

exacerbation of the *shi*^{ts1} phenotype was not seen in the double mutant. These data suggest that Dynamin acts upstream of RBO function during endocytosis.

Based on these data we propose that the disruption of the lipase domain impairs some vital requirements of RBO but not others and RBO is a component of dynamin-dependent endocytosis both in neurons and non-neuronal cells. Further biochemical experiments are needed to determine if RBO is a lipase and what its substrate specificity is. Biochemical assays to identify substrate specificity showing that a heterologously expressed wildtype RBO protein but not the lipase dead version has the aforesaid hydrolase activity. Once the specific substrate is identified, the levels of PLC pathway lipids will need to be assayed in a temperature-dependent manner to determine how they change in *rbo*^{ts}. The interaction with dynamin can be further tested by identifying synergistic interactions with weaker *shibire* alleles. The identification of new protein or genetic interactors will help further elucidate the pathway.

CHAPTER IV

CONCLUSIONS AND FUTURE DIRECTIONS

The *rolling blackout* gene was originally identified 25 years ago as a TS paralytic mutant named stambha A (*stm*A) in an EMS-screen (Shyngle and Sharma, 1985). The gene was mapped using three genomic deficiencies by complementation failure to the cytological position 44D2-8 on the 2nd chromosome and cloned in the Broadie Lab (Huang et al., 2004). An intragenic deficiency *rev*499 failed to complement *rbo* and proved that *rbo* is allelic to a Drosophila gene previously named conserved membrane protein 44E (*cmp*44E) (Faulkner et al., 1998; Huang et al., 2004). The TS paralysis was shown to be due to a missense mutation (G487D) and all observed defects in *rbo*^{ts} are rescued by a single copy of the wildtype *rbo* gene (Huang et al., 2004). Two transcripts have been observed by Northern Blot analysis (Faulkner et al., 1998) and three transcripts of sizes 2.78kb (isoform A), 3.10kb (isoform B) and 3.16kb (isoform C) are predicted to exist (pubmed). Sequence analysis reveals that RBO is predicted to encode a protein of 91 kDa (molecular weight) in *Drosophila*, *C.elegans* (CD32D5.3) and Humans (KIAA0143). In Drosophila the three splice variants are predicted to have 794 (isoform A), 820 (isoform B) and 834 (isoform C) amino acids. Drosophila RBO protein shows 34% identity to the human KIAA0143 (Faulkner et al., 1998). RBO is predicted to be an integral transmembrane-spanning plasma membrane protein. Hydrophobicity analyses of RBO protein have predicted varying number of membrane-spanning domains for

the various homologs- human RBO 5, *Drosophila* RBO 2 or 3, *C.elegans* RBO 3 and yeast RBO 2 (Faulkner et al., 1998; Huang et al., 2004; Kyte and Doolittle, 1982; Nagase et al., 1995). However upon further analysis only 3 predicted transmembrane domains are conserved between *Drosophila* RBO and Human RBO and 2 are conserved between the more closely related *Drosophila* and C.*elegans* homologs (Faulkner et al., 1998). To determine the transmembrane topology of RBO and the orientation of each of the termini, multiple flag-tagged versions of the protein can be made. The constructs can be transfected into S2 cells and expression checked with anti-flag antibodies. Comparing westerns from permeabilized and nonpermeabilized cells will determine if the flag tags at various positions on the protein are intracellular or extracellular. Determining the transmembrane topology of the protein would be an important in addressing RBO function, if RBO is a lipase. If on the other hand, RBO is a scaffolding protein, mapping the transmembrane, extracellular and intracellular domains may be useful for future biochemical assays. Portions of the protein may be expressed heterologously to identify binding partners.

Subcellular fractionation experiments have revealed that RBO can be extracted from a membrane fraction only following detergent (1% Nonidet P-40) treatment, but not following treatment with high salt (1M NaCl) or alkaline conditions (pH 10, 0.1M $NaCO_3$) indicating that is it is an integral membrane protein (Huang et al., 2004). Furthermore epitope tagged heterologously expressed RBO can be biotinylated with a membrane impermeable version of biotin proving that portions of the protein are exposed to the outside of the cell

(Huang et al., 2004). Further immunoEM experiments and subcellular fractionation experiments with synptosomal preparations can provide a more precise localization (pre and or postsynaptic terminal plasma membrane, intracellular organelles, such as SV membrane or endosomal membranes) of RBO in synaptic terminals.

A synergistic interaction between *rbo*^{ts} and a TS mutation in the t-SNARE syntaxin, *syx*$^{3\text{-}69}$ was previously identified (Huang et al., 2004). *syx*$^{3\text{-}69}$ or *rbo*^{ts};*syx*$^{3\text{-}69}$ larvae surprisingly do not show defects in evoked release or FM exocytosis following restrictive temperature incubation. However, since *rbo*^{ts};*syx*$^{3\text{-}69}$ larvae showed behavioral paralysis at 33^{o}C, lower than the paralysis temperature of the *rbo*^{ts} or *syx*$^{3\text{-}69}$ mutants, and an FM1-43 dye loading phenotype at 25^{o}C, we reasoned that, the presence of the *syx*$^{3\text{-}69}$ mutation made the requirement for RBO more pronounced. Endocytic assays were then performed at restrictive temperature. Although the *rbo*^{ts};*syx*$^{3\text{-}69}$ phenotype did not worsen following 37^{o}C incubation, this condition revealed an endocytic dye loading phenotype in *rbo*^{ts} mutants. The *syx*$^{3\text{-}69}$ mutation is believed to function as a dominant positive that increases the fusion rate. However, if this synergism is due to increased vesicle fusion, such an interaction was not observed with a TS allele of *snap*25, known to have increased vesicular release (Rao et al., 2001). Syntaxin1A adopts a closed conformation in solution (Dulubova et al., 1999). Mutating 2 highly conserved residues (L165A, E166A, in rat syntaxin1A, L166A,E167A in C.e*legans*) converts closed syntaxin1A into a constitutively open syntaxin (Dulubova et al., 1999; Richmond et al., 2001).These 2 residues are

conserved across species. In *Drosophila* syntaxin1A these residues correspond to L168, and E169. These two amino acids can be mutated to alanines to generate constitutively open *Drosophila* syntaxin1A. Work in mice has shown that in the syntaxin 1A knockout background, open syntaxin1B dramatically enhances fusion (Gerber et al., 2008). In *Drosophila* it is to be determined if overexpression of constitutively open syntaxin can rescue lethality and/or suppress phenotypes seen in the *syntaxin* null background. If overexpression leads to increased spontaneous and evoked vesicle fusion, as seen in other model systems, it can be expressed in the *rbo*^{ts} background to determine if a synergism similar to that observed with *syx*$^{3\text{-}69}$ occurs. This will determine if the exacerbation of the endocytic phenotype in the *rbo*^{ts};*syx*$^{3\text{-}69}$ double mutants at permissive temperature, is indeed due to increased fusion.

Ultrastructurally *rbo*^{ts} mutants do not show vesicle depletion in unstimulated or stimulated conditions, (Huang et al., 2006; Vijayakrishnan et al., 2009). However, voltage clamp recordings from the DLM reveal a loss of muscle response following nerve stimulation at restrictive temperature (Huang et al., 2006). If this is not, as previously thought, due to a post-docking block in fusion, in the absence of empty boutons, what could be the explanation for the observed loss of muscle response? Given that there is a temperature-dependent endocytic phenotype at the larval NMJ, it would be interesting to determine if larval high frequency stimulation (10-12Hz for 5 minutes) of the muscle 6/7 NMJ) produces synaptic depression. This condition has been shown to induce depression in

several endocytic mutants. High frequency experiments can also be used to test function in adult giant fiber synapses.

Our previous work has shown that RBO function is required for endocytic trafficking in both neuronal and non-neuronal cells. Is RBO function required for other types of endocytosis? Many cell signaling events and developmental processes are regulated by endocytosis. Larval imaginal discs have been used to study the dynamin-dependent endocytosis of the transmembrane boss protein. Boss is expressed in R8 photoreceptor cells. Following binding to sevenless boss is endocytosed into the neighboring R7 photoreceptor cells. Dissected third instar larval eye imaginal discs can be fixed and stained with the boss antibody and a HRP-conjugated secondary to determine relative localization of the receptor at permissive and restrictive temperature (a 2 hour incubation of rbo^{ts} larvae at $37^{o}C$) This will facilitate a detection of defects in boss endocytosis at the level of the light microscope (only on the surface of R8 or also internalized into R7). If a requirement for RBO is seen in boss internalization further antibody staining can be done with other ligands (such as delta) which also undergo transendocytosis. A chimeric HRP-boss construct, containing an N terminal extracellular HRP tag, introduced into the genome by germline transformation, was shown to rescue all defects seen in a boss null mutants proving that it is functional and is expressed and targeted properly. *shibire*^{ts1} mutants show defects in HRP-boss internalization following a 2 hour incubation at restrictive temperature. Ultrastructural analyses of DAB treated imaginal dics was used to analyze the stage at which endocytic arrest of the internalized HRP-boss receptor occurs

(Sunio et al., 1999). Such an ultrastructural analysis will elucidate the nature of the trafficking defect in *rbo*^{ts} through better visualization of endosomes, lysosomes and multivesicular bodies.

Further immunoprecipitation experiments can be carried out using RBO-GFP animals and probing with antibodies to endocytic proteins such as dynamin, endophilin, synaptojanin, α adaptin, AP180, DAP160, clathrin, epsin and eps15. TAP-MS (Tandem affinity purification mass spectrometry) can be used to identify RBO interactors in a non-biased way (Puig et al., 2001). A TAP tag consisting of calmodulin binding peptide and two IgG binding domains of *Staphylococcus aureus* protein A, separated by a TEV (tobacco etch virus) protease cleavage site, can be added to RBO to facilitate purification and MS-based analysis either form cell culture or transgenic animals. *Drosophila* vectors with N and C terminal TAP tags for expression *in vivo* (pUAST inducible by GAL4) and for cell culture are available (Veraksa et al., 2005).

What is the molecular role for this novel membrane protein? The most informative clue is that RBO contains a well-conserved lipolytic enzyme domain, with the canonical catalytic triad consisting of a histidine, a serine and an acidic residue in the predicted active site. RBO protein shows 42% sequence identity with a rat transmembrane *sn*-1 DAG (diacylglycerol) lipase, based on local alignment. These comparisons predict that that *rbo* could encode either a DAG lipase or related lipase. Analyses of whole heads from mutants brains revealed a temperature-dependent increase in PIPs and PIP_2 and decrease in DAG (Huang et al., 2004). These alterations could be due to a decreased PLC function *in vivo*

in *rbo*^{ts} animals. Alternatively, if acyl side chains on phospholipids are modified in *rbo*^{ts}, it could prevent proper substrate recognition and cleavage by PLC.

Matrix assisted laser desorption ionization (MALDI) mass spectrometry can be used to directly quantify the levels of lipids from tissue. In order to demonstrate this we used a *Drosophila* lipid pathway mutant, *easily shocked* (*eas*), hypomorphic for a phosphatidylethanomamine (PE) pathway biosynthetic enzyme ethanolamine kinase (Nyako et al., 2001; Pavlidis et al., 1994). The first step in PE biosynthesis in the CDP-ethanolamine pathway requires ethanolamine kinase. *Drosophila* possesses only a single ethanolamine kinase gene encoded by the *eas* locus (Pavlidis et al., 1994). Mutants were isolated in a classic behavioral genetic screen for bang-sensitive paralysis (Benzer, 1971). Adult *eas* mutant animals are homozygous viable but display brief hyperactivity followed by complete paralysis when given a mechanical shock such as banging on a bench top or vortex shaking (Reynolds et al., 2004) The seizure-induced paralysis is transitory and is repeatedly manifest upon mechanical shock. PE is a major constituent of neuronal membranes. This *eas* mutant epileptic behavior results from defects in membrane neuronal excitability causing a burst of unregulated action potentials followed by neuronal transmission failure upon stimulation (Glasscock et al., 2005; Hekmat-Scafe et al., 2005), and compensatory mutations that decrease neuronal excitability eliminate the *eas* mutant defect (Song and Tanouye, 2006). Previous studies showed an overall decrease in PE in *eas* mutants using thin layer chromatography (TLC) (Nyako et al., 2001).

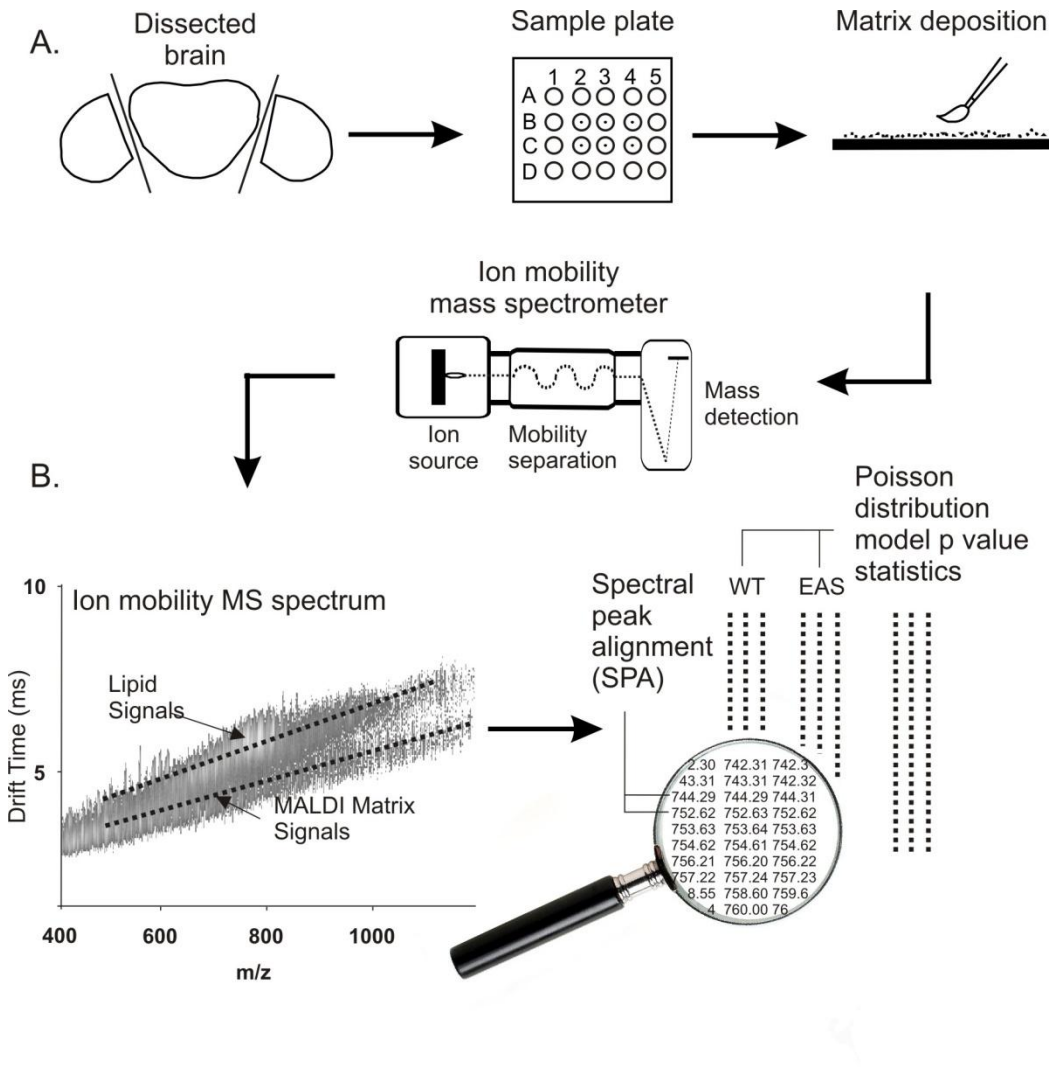

Figure 26: **MALDI MS of phospholipids from the microdissected *Drosophila* brain. A)** The *Drosophila* central brain microdissected and spotted on a frozen MALDI plate. Finely crushed nanometer crystal size MALDI matrix was deposited on the brain. Lipid signals were measured on MALDI MS instrument. **B)** Lipid MS data was extracted and aligned across three experimental sets using peak alignment macro. Changes between control and mutant conditions determined using Poisson model statistics.

We have developed a novel mass spectrometry methodology using electrospray ionization (ESI) MALDI for the relative quantitation of intact phospholipid signals directly from isolated brain tissue. This new approach paints a much more detailed picture of the entire lipid profile within the brain proper, with dramatically improved sensitivity as well as decreased processing time for evaluating changes across the phospholipid spectrum, including PE, and previously unreported changes in PI and phosphatidylcholine (PC) lipid species.

The schematic shown in Figure 26 was used to obtain and analyze lipid signals from intact *Drosophila* brain. With further optimization, this method might be applicable to the detection of lower abundance species such as PIPs and neutral lipids such as DAG and to the quantitative analysis these lipids from *rbo*^{ts} brain tissue.

The yeast model predicts that RBO functions as a transmembrane scaffolding protein that recruits PI4K to the membrane. The mouse homolog of *Drosophila* RBO, KIAA0143, can be introduced into flies by germline transformation. If this is able to rescue lethality of the *rbo* null embryos, TS paralysis, ERG defects of adults and endocytic defects at the larval NMJ, other putative homologs of RBO binding or interacting proteins shown by the yeast model can be studied in *Drosophila*. Yeast ypp1 is a tetratricopeptide repeat (TPR) domain containing protein. It has been shown to bind the C terminal portion of yeast RBO. Mutational deletion of the TPR domain in the putative mouse homolog TTC7a, produces a flaky skin phenotype with pleiotropic defects such as autoimmunity, skin abnormalities and anemia (Helms et al., 2005). The

putative drosophila homolog, lethal (2)K14710, is also predicted to have 2 C terminal TPR domains. The putative drosophila homolog of yeast stt4 is SD12145P. RNAi-mediated knock down or UAS-GAL4 driven overexpression of these genes in the *rbo*^{ts} background can be examined to determine if there is an exacerbation of the endocytic phenotype. Tagged versions of the cDNA for these genes can be introduced into *Drosophila* S2 cells to determine if these proteins associate with or can be pulled down with RBO-GFP. Yeast RBO (EFR3) was originally identified in screen for genes that require pho85 for viability. Pho85 is a homolog of CDK5, an atypical cyclin-dependent kinase. It is not required for transition through cell cycle check points but has varied roles in post-mitotic neurons ranging from neuronal migration, neurite outgrowth and regulation of the actin cytoskeleton, synaptic plasticity, neurotransmitter receptor stabilization, dynamin phosphorylation and SV endocytosis (Hellmich et al., 1992; Morabito et al., 2004; Nikolic et al., 1996; Tan et al., 2003; Tomizawa et al., 2003; Tsai et al., 1993). In *Drosophila* CDK5 expression is enriched in neurons, and is controlled by regulatory subunits p35 and p39 also primarily expressed in neurons (Tang et al., 1995). *cdk*5 null animals are viable, but show locomotion and flight defects as adults, and larval NMJ overgrowth phenotypes (Kissler et al., 2009). Age-dependent loss of motor neuron function also seen in p35 null mutants (Connell-Crowley et al., 2007).These mutants can be crossed into the *rbo*^{ts} background to determine if there is a genetic interaction in *Drosophila*.

In conclusion, this work demonstrates that RBO is required for a form of dynamin-dependent endocytic trafficking in neurons and non-neuronal cells in

Drosophila. Further experiments will be required to demonstrate the exact requirement for RBO in endocytosis (bulk endocytosis or fusion of vesicles internalized by CME). Genetic and biochemical assays will help identify other proteins required for RBO-dependent endocytosis and thereby elucidate the pathway better. This may help explain the mechanistic basis of the synthetic lethal interaction with *shibire*. In the absence of conclusive experiments to prove lipase activity and the identification of a substrate, it remains to be seen if RBO functions as a lipase to directly modify membrane lipids during endocytosis, or functions as a scaffolding protein to recruit other proteins that may then affect membrane lipids levels indirectly. The lipids changes seen in RBO will have to be further examined by mass spectrometry or high performance liquid chromatography, to identify what PIP species is changing and the time course of these changes. The development of optical imaging tools such as fluorescently tagged lipid binding domains may facilitate detection of lipid changes in whole brain tissue and in individual synapses.

REFERENCES

Aggarwal, S.K., and R.C. King. 1967. The ultrastructure of the wreath cells of Drosophila melanogaster larvae. *Protoplasma*. 63:343-52.

Ahle, S., and E. Ungewickell. 1986. Purification and properties of a new clathrin assembly protein. *Embo J*. 5:3143-9.

Alawi, A.A., V. Jennings, J. Grossfield, and W.L. Pak. 1972. Phototransduction mutants of Drosophila melanogaster. *Adv Exp Med Biol*. 24:1-21.

Alloway, P.G., L. Howard, and P.J. Dolph. 2000. The formation of stable rhodopsin-arrestin complexes induces apoptosis and photoreceptor cell degeneration. *Neuron*. 28:129-38.

Antonny, B., I. Huber, S. Paris, M. Chabre, and D. Cassel. 1997. Activation of ADP-ribosylation factor 1 GTPase-activating protein by phosphatidylcholine-derived diacylglycerols. *J Biol Chem*. 272:30848-51.

Araki, N., M. Hamasaki, Y. Egami, and T. Hatae. 2006. Effect of 3-methyladenine on the fusion process of macropinosomes in EGF-stimulated A431 cells. *Cell Struct Funct*. 31:145-57.

Aravamudan, B., T. Fergestad, W.S. Davis, C.K. Rodesch, and K. Broadie. 1999. Drosophila UNC-13 is essential for synaptic transmission. *Nat Neurosci*. 2:965-71.

Baird, D., C. Stefan, A. Audhya, S. Weys, and S.D. Emr. 2008. Assembly of the PtdIns 4-kinase Stt4 complex at the plasma membrane requires Ypp1 and Efr3. *J Cell Biol*. 183:1061-74.

Bao, H., R.W. Daniels, G.T. MacLeod, M.P. Charlton, H.L. Atwood, and B. Zhang. 2005. AP180 maintains the distribution of synaptic and vesicle proteins in the nerve terminal and indirectly regulates the efficacy of Ca2+-triggered exocytosis. *J Neurophysiol*. 94:1888-903.

Bennett, M.K., N. Calakos, and R.H. Scheller. 1992. Syntaxin: a synaptic protein implicated in docking of synaptic vesicles at presynaptic active zones. *Science*. 257:255-9.

Benzer, S. 1971. From the gene to behavior. *Jama*. 218:1015-22.

Beramendi, A., S. Peron, G. Casanova, C. Reggiani, and R. Cantera. 2007. Neuromuscular junction in abdominal muscles of Drosophila melanogaster during adulthood and aging. *J Comp Neurol*. 501:498-508.

Berridge, M.J. 1993. Cell signalling. A tale of two messengers. *Nature*. 365:388-9.

Betz, A., M. Okamoto, F. Benseler, and N. Brose. 1997. Direct interaction of the rat unc-13 homologue Munc13-1 with the N terminus of syntaxin. *J Biol Chem*. 272:2520-6.

Binns, D.D., B. Barylko, N. Grichine, M.A. Atkinson, M.K. Helms, D.M. Jameson, J.F. Eccleston, and J.P. Albanesi. 1999. Correlation between self-association modes and GTPase activation of dynamin. *J Protein Chem*. 18:277-90.

Bisogno, T., F. Howell, G. Williams, A. Minassi, M.G. Cascio, A. Ligresti, I. Matias, A. Schiano-Moriello, P. Paul, E.J. Williams, U. Gangadharan, C. Hobbs, V. Di Marzo, and P. Doherty. 2003. Cloning of the first sn1-DAG lipases points to the spatial and temporal regulation of endocannabinoid signaling in the brain. *J Cell Biol*. 163:463-8.

Broadie, K., A. Prokop, H.J. Bellen, C.J. O'Kane, K.L. Schulze, and S.T. Sweeney. 1995. Syntaxin and synaptobrevin function downstream of vesicle docking in Drosophila. *Neuron*. 15:663-73.

Brodsky, F.M., C.Y. Chen, C. Knuehl, M.C. Towler, and D.E. Wakeham. 2001. Biological basket weaving: formation and function of clathrin-coated vesicles. *Annu Rev Cell Dev Biol*. 17:517-68.

Campusano, J.M., H. Su, S.A. Jiang, B. Sicaeros, and D.K. O'Dowd. 2007. nAChR-mediated calcium responses and plasticity in Drosophila Kenyon cells. *Dev Neurobiol*. 67:1520-32.

Carter, L.L., T.E. Redelmeier, L.A. Woollenweber, and S.L. Schmid. 1993. Multiple GTP-binding proteins participate in clathrin-coated vesicle-mediated endocytosis. *J Cell Biol*. 120:37-45.

Ceccarelli, B., W.P. Hurlbut, and A. Mauro. 1973. Turnover of transmitter and synaptic vesicles at the frog neuromuscular junction. *J Cell Biol*. 57:499-524.

Chang, H.C., S.L. Newmyer, M.J. Hull, M. Ebersold, S.L. Schmid, and I. Mellman. 2002. Hsc70 is required for endocytosis and clathrin function in Drosophila. *J Cell Biol*. 159:477-87.

Chatterjee, S., and S. Mayor. 2001. The GPI-anchor and protein sorting. *Cell Mol Life Sci*. 58:1969-87.

Chen, M.S., R.A. Obar, C.C. Schroeder, T.W. Austin, C.A. Poodry, S.C. Wadsworth, and R.B. Vallee. 1991. Multiple forms of dynamin are encoded by shibire, a Drosophila gene involved in endocytosis. *Nature*. 351:583-6.

Chyb, S., P. Raghu, and R.C. Hardie. 1999. Polyunsaturated fatty acids activate the Drosophila light-sensitive channels TRP and TRPL. *Nature*. 397:255-9.

Collins, B.M., A.J. McCoy, H.M. Kent, P.R. Evans, and D.J. Owen. 2002. Molecular architecture and functional model of the endocytic AP2 complex. *Cell*. 109:523-35.

Connell-Crowley, L., D. Vo, L. Luke, and E. Giniger. 2007. Drosophila lacking the Cdk5 activator, p35, display defective axon guidance, age-dependent behavioral deficits and reduced lifespan. *Mech Dev*. 124:341-9.

Cook, B., M. Bar-Yaacov, H. Cohen Ben-Ami, R.E. Goldstein, Z. Paroush, Z. Selinger, and B. Minke. 2000. Phospholipase C and termination of G-protein-mediated signalling in vivo. *Nat Cell Biol*. 2:296-301.

Cousin, M.A., and P.J. Robinson. 2001. The dephosphins: dephosphorylation by calcineurin triggers synaptic vesicle endocytosis. *Trends Neurosci*. 24:659-65.

Couteaux, R., and M. Pecot-Dechavassine. 1970. [Synaptic vesicles and pouches at the level of "active zones" of the neuromuscular junction]. *C R Acad Sci Hebd Seances Acad Sci D*. 271:2346-9.

Cremona, O., G. Di Paolo, M.R. Wenk, A. Luthi, W.T. Kim, K. Takei, L. Daniell, Y. Nemoto, S.B. Shears, R.A. Flavell, D.A. McCormick, and P. De Camilli. 1999. Essential role of phosphoinositide metabolism in synaptic vesicle recycling. *Cell*. 99:179-88.

Damke, H., T. Baba, A.M. van der Bliek, and S.L. Schmid. 1995. Clathrin-independent pinocytosis is induced in cells overexpressing a temperature-sensitive mutant of dynamin. *J Cell Biol*. 131:69-80.

Damke, H., D.D. Binns, H. Ueda, S.L. Schmid, and T. Baba. 2001. Dynamin GTPase domain mutants block endocytic vesicle formation at morphologically distinct stages. *Mol Biol Cell*. 12:2578-89.

David, C., P.S. McPherson, O. Mundigl, and P. de Camilli. 1996. A role of amphiphysin in synaptic vesicle endocytosis suggested by its binding to dynamin in nerve terminals. *Proc Natl Acad Sci U S A*. 93:331-5.

de Lange, R.P., A.D. de Roos, and J.G. Borst. 2003. Two modes of vesicle recycling in the rat calyx of Held. *J Neurosci*. 23:10164-73.

de Wit, H., L.N. Cornelisse, R.F. Toonen, and M. Verhage. 2006. Docking of secretory vesicles is syntaxin dependent. *PLoS One*. 1:e126.

Dellinger, B., R. Felling, and R.W. Ordway. 2000. Genetic modifiers of the Drosophila NSF mutant, comatose, include a temperature-sensitive paralytic allele of the calcium channel alpha1-subunit gene, cacophony. *Genetics*. 155:203-11.

Dermaut, B., K.K. Norga, A. Kania, P. Verstreken, H. Pan, Y. Zhou, P. Callaerts, and H.J. Bellen. 2005. Aberrant lysosomal carbohydrate storage accompanies endocytic defects and neurodegeneration in Drosophila benchwarmer. *J Cell Biol*. 170:127-39.

Di Paolo, G., H.S. Moskowitz, K. Gipson, M.R. Wenk, S. Voronov, M. Obayashi, R. Flavell, R.M. Fitzsimonds, T.A. Ryan, and P. De Camilli. 2004. Impaired PtdIns(4,5)P2 synthesis in nerve terminals produces defects in synaptic vesicle trafficking. *Nature*. 431:415-22.

Dulubova, I., S. Sugita, S. Hill, M. Hosaka, I. Fernandez, T.C. Sudhof, and J. Rizo. 1999. A conformational switch in syntaxin during exocytosis: role of munc18. *Embo J*. 18:4372-82.

Evans, G.J., and M.A. Cousin. 2007. Activity-dependent control of slow synaptic vesicle endocytosis by cyclin-dependent kinase 5. *J Neurosci*. 27:401-11.

Faulkner, D.L., T.C. Dockendorff, and T.A. Jongens. 1998. Clonal analysis of cmp44E, which encodes a conserved putative transmembrane protein, indicates a requirement for cell viability in Drosophila. *Dev Genet*. 23:264-74.

Fergestad, T., and K. Broadie. 2001. Interaction of stoned and synaptotagmin in synaptic vesicle endocytosis. *J Neurosci*. 21:1218-27.

Fernandez, I., J. Ubach, I. Dulubova, X. Zhang, T.C. Sudhof, and J. Rizo. 1998. Three-dimensional structure of an evolutionarily conserved N-terminal domain of syntaxin 1A. *Cell*. 94:841-9.

Fesce, R., F. Grohovaz, F. Valtorta, and J. Meldolesi. 1994. Neurotransmitter release: fusion or 'kiss-and-run'? *Trends Cell Biol*. 4:1-4.

Ford, M.G., B.M. Pearse, M.K. Higgins, Y. Vallis, D.J. Owen, A. Gibson, C.R. Hopkins, P.R. Evans, and H.T. McMahon. 2001. Simultaneous binding of PtdIns(4,5)P2 and clathrin by AP180 in the nucleation of clathrin lattices on membranes. *Science*. 291:1051-5.

Gad, H., P. Low, E. Zotova, L. Brodin, and O. Shupliakov. 1998. Dissociation between Ca2+-triggered synaptic vesicle exocytosis and clathrin-mediated endocytosis at a central synapse. *Neuron*. 21:607-16.

Gaidarov, I., and J.H. Keen. 1999. Phosphoinositide-AP-2 interactions required for targeting to plasma membrane clathrin-coated pits. *J Cell Biol*. 146:755-64.

Gallop, J.L., C.C. Jao, H.M. Kent, P.J. Butler, P.R. Evans, R. Langen, and H.T. McMahon. 2006. Mechanism of endophilin N-BAR domain-mediated membrane curvature. *Embo J*. 25:2898-910.

Gandhi, S.P., and C.F. Stevens. 2003. Three modes of synaptic vesicular recycling revealed by single-vesicle imaging. *Nature*. 423:607-13.

Gerber, S.H., J.C. Rah, S.W. Min, X. Liu, H. de Wit, I. Dulubova, A.C. Meyer, J. Rizo, M. Arancillo, R.E. Hammer, M. Verhage, C. Rosenmund, and T.C. Sudhof. 2008. Conformational switch of syntaxin-1 controls synaptic vesicle fusion. *Science*. 321:1507-10.

Gerona, R.R., E.C. Larsen, J.A. Kowalchyk, and T.F. Martin. 2000. The C terminus of SNAP25 is essential for Ca(2+)-dependent binding of synaptotagmin to SNARE complexes. *J Biol Chem*. 275:6328-36.

Glasscock, E., A. Singhania, and M.A. Tanouye. 2005. The mei-P26 gene encodes a RING finger B-box coiled-coil-NHL protein that regulates seizure susceptibility in Drosophilia. *Genetics*. 170:1677-89.

Gonzalez-Gaitan, M., and H. Jackle. 1997. Role of Drosophila alpha-adaptin in presynaptic vesicle recycling. *Cell*. 88:767-76.

Grigliatti, T.A., L. Hall, R. Rosenbluth, and D.T. Suzuki. 1973. Temperature-sensitive mutations in Drosophila melanogaster. XIV. A selection of immobile adults. *Mol Gen Genet*. 120:107-14.

Gronke, S., A. Mildner, S. Fellert, N. Tennagels, S. Petry, G. Muller, H. Jackle, and R.P. Kuhnlein. 2005. Brummer lipase is an evolutionary conserved fat storage regulator in Drosophila. *Cell Metab*. 1:323-30.

Guha, A., V. Sriram, K.S. Krishnan, and S. Mayor. 2003. Shibire mutations reveal distinct dynamin-independent and -dependent endocytic pathways in primary cultures of Drosophila hemocytes. *J Cell Sci*. 116:3373-86.

Haffner, C., G. Di Paolo, J.A. Rosenthal, and P. de Camilli. 2000. Direct interaction of the 170 kDa isoform of synaptojanin 1 with clathrin and with the clathrin adaptor AP-2. *Curr Biol*. 10:471-4.

Hao, W., Z. Luo, L. Zheng, K. Prasad, and E.M. Lafer. 1999. AP180 and AP-2 interact directly in a complex that cooperatively assembles clathrin. *J Biol Chem*. 274:22785-94.

Harata, N., T.A. Ryan, S.J. Smith, J. Buchanan, and R.W. Tsien. 2001. Visualizing recycling synaptic vesicles in hippocampal neurons by FM 1-43 photoconversion. *Proc Natl Acad Sci U S A*. 98:12748-53.

Hasan, G., and M. Rosbash. 1992. Drosophila homologs of two mammalian intracellular Ca(2+)-release channels: identification and expression patterns of the inositol 1,4,5-triphosphate and the ryanodine receptor genes. *Development*. 116:967-75.

Hata, Y., C.A. Slaughter, and T.C. Sudhof. 1993. Synaptic vesicle fusion complex contains unc-18 homologue bound to syntaxin. *Nature*. 366:347-51.

Haucke, V. 2005. Phosphoinositide regulation of clathrin-mediated endocytosis. *Biochem Soc Trans*. 33:1285-9.

Heerssen, H., R.D. Fetter, and G.W. Davis. 2008. Clathrin dependence of synaptic-vesicle formation at the Drosophila neuromuscular junction. *Curr Biol*. 18:401-9.

Heisenberg, M. 1971. Separation of receptor and lamina potentials in the electroretinogram of normal and mutant Drosophila. *J Exp Biol*. 55:85-100.

Hekmat-Scafe, D.S., K.N. Dang, and M.A. Tanouye. 2005. Seizure suppression by gain-of-function escargot mutations. *Genetics*. 169:1477-93.

Hellmich, M.R., H.C. Pant, E. Wada, and J.F. Battey. 1992. Neuronal cdc2-like kinase: a cdc2-related protein kinase with predominantly neuronal expression. *Proc Natl Acad Sci U S A*. 89:10867-71.

Helms, C., S. Pelsue, L. Cao, E. Lamb, B. Loffredo, P. Taillon-Miller, B. Herrin, L.M. Burzenski, B. Gott, B.L. Lyons, D. Keppler, L.D. Shultz, and A.M. Bowcock. 2005. The Tetratricopeptide repeat domain 7 gene is mutated in flaky skin mice: a model for psoriasis, autoimmunity, and anemia. *Exp Biol Med (Maywood)*. 230:659-67.

Heuser, J.E., and T.S. Reese. 1973. Evidence for recycling of synaptic vesicle membrane during transmitter release at the frog neuromuscular junction. *J Cell Biol*. 57:315-44.

Hinshaw, J.E. 2000. Dynamin and its role in membrane fission. *Annu Rev Cell Dev Biol*. 16:483-519.

Hinshaw, J.E., and S.L. Schmid. 1995. Dynamin self-assembles into rings suggesting a mechanism for coated vesicle budding. *Nature*. 374:190-2.

Hojjati, M.R., G.M. van Woerden, W.J. Tyler, K.P. Giese, A.J. Silva, L. Pozzo-Miller, and Y. Elgersma. 2007. Kinase activity is not required for alphaCaMKII-dependent presynaptic plasticity at CA3-CA1 synapses. *Nat Neurosci*. 10:1125-7.

Holt, M., A. Cooke, M.M. Wu, and L. Lagnado. 2003. Bulk membrane retrieval in the synaptic terminal of retinal bipolar cells. *J Neurosci*. 23:1329-39.

Honing, S., D. Ricotta, M. Krauss, K. Spate, B. Spolaore, A. Motley, M. Robinson, C. Robinson, V. Haucke, and D.J. Owen. 2005. Phosphatidylinositol-(4,5)-bisphosphate regulates sorting signal recognition by the clathrin-associated adaptor complex AP2. *Mol Cell*. 18:519-31.

Huang, F.D., H.J. Matthies, S.D. Speese, M.A. Smith, and K. Broadie. 2004. Rolling blackout, a newly identified PIP2-DAG pathway lipase required for Drosophila phototransduction. *Nat Neurosci*. 7:1070-8.

Huang, F.D., E. Woodruff, R. Mohrmann, and K. Broadie. 2006. Rolling blackout is required for synaptic vesicle exocytosis. *J Neurosci*. 26:2369-79.

Hunt, J.M., K. Bommert, M.P. Charlton, A. Kistner, E. Habermann, G.J. Augustine, and H. Betz. 1994. A post-docking role for synaptobrevin in synaptic vesicle fusion. *Neuron*. 12:1269-79.

Jiang, S.A., J.M. Campusano, H. Su, and D.K. O'Dowd. 2005. Drosophila mushroom body Kenyon cells generate spontaneous calcium transients mediated by PLTX-sensitive calcium channels. *J Neurophysiol*. 94:491-500.

Kawasaki, F., M. Hazen, and R.W. Ordway. 2000. Fast synaptic fatigue in shibire mutants reveals a rapid requirement for dynamin in synaptic vesicle membrane trafficking. *Nat Neurosci*. 3:859-60.

Kawasaki, T., T. Kobayashi, T. Ueyama, Y. Shirai, and N. Saito. 2008. Regulation of clathrin-dependent endocytosis by diacylglycerol kinase delta: importance of kinase activity and binding to AP2alpha. *Biochem J*. 409:471-9.

Kirschfeld, K., and N. Franceschini. 1969. [A mechanism for the control of the light flow in the rhabdomeres of the complex eye of Musca]. *Kybernetik*. 6:13-22.

Kissler, A.E., N. Pettersson, A. Frolich, S.J. Sigrist, and B. Suter. 2009. Drosophila cdk5 is needed for locomotive behavior and NMJ elaboration, but seems dispensable for synaptic transmission. *Dev Neurobiol*. 69:365-77.

Koenig, J.H., and K. Ikeda. 1989. Disappearance and reformation of synaptic vesicle membrane upon transmitter release observed under reversible blockage of membrane retrieval. *J Neurosci*. 9:3844-60.

Koenig, J.H., and K. Ikeda. 1996. Synaptic vesicles have two distinct recycling pathways. *J Cell Biol*. 135:797-808.

Koenig, J.H., and K. Ikeda. 1999. Contribution of active zone subpopulation of vesicles to evoked and spontaneous release. *J Neurophysiol*. 81:1495-505.

Koenig, J.H., K. Saito, and K. Ikeda. 1983. Reversible control of synaptic transmission in a single gene mutant of Drosophila melanogaster. *J Cell Biol*. 96:1517-22.

Kosaka, T., and K. Ikeda. 1983. Reversible blockage of membrane retrieval and endocytosis in the garland cell of the temperature-sensitive mutant of Drosophila melanogaster, shibirets1. *J Cell Biol*. 97:499-507.

Kumari, S., V. Borroni, A. Chaudhry, B. Chanda, R. Massol, S. Mayor, and F.J. Barrantes. 2008. Nicotinic acetylcholine receptor is internalized via a Rac-dependent, dynamin-independent endocytic pathway. *J Cell Biol*. 181:1179-93.

Kumari, S., and S. Mayor. 2008. ARF1 is directly involved in dynamin-independent endocytosis. *Nat Cell Biol*. 10:30-41.

Kuppers-Munther, B., J.J. Letzkus, K. Luer, G. Technau, H. Schmidt, and A. Prokop. 2004. A new culturing strategy optimises Drosophila primary cell cultures for structural and functional analyses. *Dev Biol*. 269:459-78.

Kuromi, H., and Y. Kidokoro. 1998. Two distinct pools of synaptic vesicles in single presynaptic boutons in a temperature-sensitive Drosophila mutant, shibire. *Neuron*. 20:917-25.

Kyte, J., and R.F. Doolittle. 1982. A simple method for displaying the hydropathic character of a protein. *J Mol Biol*. 157:105-32.

Lagow, R.D., H. Bao, E.N. Cohen, R.W. Daniels, A. Zuzek, W.H. Williams, G.T. Macleod, R.B. Sutton, and B. Zhang. 2007. Modification of a hydrophobic layer by a point mutation in syntaxin 1A regulates the rate of synaptic vesicle fusion. *PLoS Biol*. 5:e72.

Lee, A., D.W. Frank, M.S. Marks, and M.A. Lemmon. 1999. Dominant-negative inhibition of receptor-mediated endocytosis by a dynamin-1 mutant with a defective pleckstrin homology domain. *Curr Biol*. 9:261-4.

Lee, S.Y., S. Voronov, K. Letinic, A.C. Nairn, G. Di Paolo, and P. De Camilli. 2005. Regulation of the interaction between PIPKI gamma and talin by proline-directed protein kinases. *J Cell Biol*. 168:789-99.

Leenders, A.G., G. Scholten, R.P. de Lange, F.H. Lopes da Silva, and W.E. Ghijsen. 2002. Sequential changes in synaptic vesicle pools and endosome-like organelles

during depolarization near the active zone of central nerve terminals. *Neuroscience*. 109:195-206.

Leung, H.T., J. Tseng-Crank, E. Kim, C. Mahapatra, S. Shino, Y. Zhou, L. An, R.W. Doerge, and W.L. Pak. 2008. DAG lipase activity is necessary for TRP channel regulation in Drosophila photoreceptors. *Neuron*. 58:884-96.

Lichte, B., R.W. Veh, H.E. Meyer, and M.W. Kilimann. 1992. Amphiphysin, a novel protein associated with synaptic vesicles. *Embo J*. 11:2521-30.

Littleton, J.T., R.J. Barnard, S.A. Titus, J. Slind, E.R. Chapman, and B. Ganetzky. 2001. SNARE-complex disassembly by NSF follows synaptic-vesicle fusion. *Proc Natl Acad Sci U S A*. 98:12233-8.

Littleton, J.T., E.R. Chapman, R. Kreber, M.B. Garment, S.D. Carlson, and B. Ganetzky. 1998. Temperature-sensitive paralytic mutations demonstrate that synaptic exocytosis requires SNARE complex assembly and disassembly. *Neuron*. 21:401-13.

Llorente, A., A. Rapak, S.L. Schmid, B. van Deurs, and K. Sandvig. 1998. Expression of mutant dynamin inhibits toxicity and transport of endocytosed ricin to the Golgi apparatus. *J Cell Biol*. 140:553-63.

Lloyd, T.E., R. Atkinson, M.N. Wu, Y. Zhou, G. Pennetta, and H.J. Bellen. 2002. Hrs regulates endosome membrane invagination and tyrosine kinase receptor signaling in Drosophila. *Cell*. 108:261-9.

Loughney, K., R. Kreber, and B. Ganetzky. 1989. Molecular analysis of the para locus, a sodium channel gene in Drosophila. *Cell*. 58:1143-54.

Macia, E., M. Ehrlich, R. Massol, E. Boucrot, C. Brunner, and T. Kirchhausen. 2006. Dynasore, a cell-permeable inhibitor of dynamin. *Dev Cell*. 10:839-50.

Majumdar, A., S. Ramagiri, and R. Rikhy. 2006. Drosophila homologue of Eps15 is essential for synaptic vesicle recycling. *Exp Cell Res*. 312:2288-98.

Marks, B., M.H. Stowell, Y. Vallis, I.G. Mills, A. Gibson, C.R. Hopkins, and H.T. McMahon. 2001. GTPase activity of dynamin and resulting conformation change are essential for endocytosis. *Nature*. 410:231-5.

Martina, J.A., C.J. Bonangelino, R.C. Aguilar, and J.S. Bonifacino. 2001. Stonin 2: an adaptor-like protein that interacts with components of the endocytic machinery. *J Cell Biol*. 153:1111-20.

Marxen, M., W. Volknandt, and H. Zimmermann. 1999. Endocytic vacuoles formed following a short pulse of K+ -stimulation contain a plethora of presynaptic membrane proteins. *Neuroscience*. 94:985-96.

McNiven, M.A., H. Cao, K.R. Pitts, and Y. Yoon. 2000. The dynamin family of mechanoenzymes: pinching in new places. *Trends Biochem Sci*. 25:115-20.

Merrifield, C.J., M.E. Feldman, L. Wan, and W. Almers. 2002. Imaging actin and dynamin recruitment during invagination of single clathrin-coated pits. *Nat Cell Biol*. 4:691-8.

Morabito, M.A., M. Sheng, and L.H. Tsai. 2004. Cyclin-dependent kinase 5 phosphorylates the N-terminal domain of the postsynaptic density protein PSD-95 in neurons. *J Neurosci*. 24:865-76.

Morgan, J.R., X. Zhao, M. Womack, K. Prasad, G.J. Augustine, and E.M. Lafer. 1999. A role for the clathrin assembly domain of AP180 in synaptic vesicle endocytosis. *J Neurosci*. 19:10201-12.

Muhlberg, A.B., D.E. Warnock, and S.L. Schmid. 1997. Domain structure and intramolecular regulation of dynamin GTPase. *Embo J*. 16:6676-83.

Muhlig-Versen, M., A.B. da Cruz, J.A. Tschape, M. Moser, R. Buttner, K. Athenstaedt, P. Glynn, and D. Kretzschmar. 2005. Loss of Swiss cheese/neuropathy target esterase activity causes disruption of phosphatidylcholine homeostasis and neuronal and glial death in adult Drosophila. *J Neurosci*. 25:2865-73.

Munn, A.L., B.J. Stevenson, M.I. Geli, and H. Riezman. 1995. end5, end6, and end7: mutations that cause actin delocalization and block the internalization step of endocytosis in Saccharomyces cerevisiae. *Mol Biol Cell*. 6:1721-42.

Nagase, T., N. Seki, A. Tanaka, K. Ishikawa, and N. Nomura. 1995. Prediction of the coding sequences of unidentified human genes. IV. The coding sequences of 40 new genes (KIAA0121-KIAA0160) deduced by analysis of cDNA clones from human cell line KG-1. *DNA Res*. 2:167-74, 199-210.

Nankoe, S.R., and S. Sever. 2006. Dynasore puts a new spin on dynamin: a surprising dual role during vesicle formation. *Trends Cell Biol*. 16:607-9.

Narayanan, R., M. Leonard, B.D. Song, S.L. Schmid, and M. Ramaswami. 2005. An internal GAP domain negatively regulates presynaptic dynamin in vivo: a two-step model for dynamin function. *J Cell Biol*. 169:117-26.

Narita, K., T. Tsuruhara, J.H. Koenig, and K. Ikeda. 1989. Membrane pinch-off and reinsertion observed in living cells of Drosophila. *J Cell Physiol*. 141:383-91.

Neves, G., A. Gomis, and L. Lagnado. 2001. Calcium influx selects the fast mode of endocytosis in the synaptic terminal of retinal bipolar cells. *Proc Natl Acad Sci U S A*. 98:15282-7.

Nicoziani, P., F. Vilhardt, A. Llorente, L. Hilout, P.J. Courtoy, K. Sandvig, and B. van Deurs. 2000. Role for dynamin in late endosome dynamics and trafficking of the cation-independent mannose 6-phosphate receptor. *Mol Biol Cell*. 11:481-95.

Nikolic, M., H. Dudek, Y.T. Kwon, Y.F. Ramos, and L.H. Tsai. 1996. The cdk5/p35 kinase is essential for neurite outgrowth during neuronal differentiation. *Genes Dev*. 10:816-25.

Nonet, M.L., A.M. Holgado, F. Brewer, C.J. Serpe, B.A. Norbeck, J. Holleran, L. Wei, E. Hartwieg, E.M. Jorgensen, and A. Alfonso. 1999. UNC-11, a Caenorhabditis elegans AP180 homologue, regulates the size and protein composition of synaptic vesicles. *Mol Biol Cell*. 10:2343-60.

Nyako, M., C. Marks, J. Sherma, and E.R. Reynolds. 2001. Tissue-specific and developmental effects of the easily shocked mutation on ethanolamine kinase activity and phospholipid composition in Drosophila melanogaster. *Biochem Genet*. 39:339-49.

Oh, H.W., J.M. Campusano, L.G. Hilgenberg, X. Sun, M.A. Smith, and D.K. O'Dowd. 2008. Ultrastructural analysis of chemical synapses and gap junctions between Drosophila brain neurons in culture. *Dev Neurobiol*. 68:281-94.

Orth, J.D., and M.A. McNiven. 2003. Dynamin at the actin-membrane interface. *Curr Opin Cell Biol*. 15:31-9.

Owen, D.J., Y. Vallis, B.M. Pearse, H.T. McMahon, and P.R. Evans. 2000. The structure and function of the beta 2-adaptin appendage domain. *Embo J*. 19:4216-27.

Pak, W.L., J. Grossfield, and K.S. Arnold. 1970. Mutants of the visual pathway of Drosophila melanogaster. *Nature*. 227:518-20.

Pan, L., Y.Q. Zhang, E. Woodruff, and K. Broadie. 2004. The Drosophila fragile X gene negatively regulates neuronal elaboration and synaptic differentiation. *Curr Biol*. 14:1863-70.

Pavlidis, P., M. Ramaswami, and M.A. Tanouye. 1994. The Drosophila easily shocked gene - A mutation in a phospholipid synthetic pathway causes seizure, neuronal failure and paralysis. *Cell*. 79:23-33.

Pavlidis, P., M. Ramaswami, and M.A. Tanouye. 1994. The Drosophila easily shocked gene: a mutation in a phospholipid synthetic pathway causes seizure, neuronal failure, and paralysis. *Cell*. 79:23-33.

Peter, B.J., H.M. Kent, I.G. Mills, Y. Vallis, P.J. Butler, P.R. Evans, and H.T. McMahon. 2004. BAR domains as sensors of membrane curvature: the amphiphysin BAR structure. *Science*. 303:495-9.

Petrovich, T.Z., J. Merakovsky, and L.E. Kelly. 1993. A genetic analysis of the stoned locus and its interaction with dunce, shibire and Suppressor of stoned variants of Drosophila melanogaster. *Genetics*. 133:955-65.

Poodry, C.A., and L. Edgar. 1979. Reversible alteration in the neuromuscular junctions of Drosophila melanogaster bearing a temperature-sensitive mutation, shibire. *J Cell Biol*. 81:520-7.

Praefcke, G.J., and H.T. McMahon. 2004. The dynamin superfamily: universal membrane tubulation and fission molecules? *Nat Rev Mol Cell Biol*. 5:133-47.

Puig, O., F. Caspary, G. Rigaut, B. Rutz, E. Bouveret, E. Bragado-Nilsson, M. Wilm, and B. Seraphin. 2001. The tandem affinity purification (TAP) method: a general procedure of protein complex purification. *Methods*. 24:218-29.

Raghu, P., K. Usher, S. Jonas, S. Chyb, A. Polyanovsky, and R.C. Hardie. 2000. Constitutive activity of the light-sensitive channels TRP and TRPL in the Drosophila diacylglycerol kinase mutant, rdgA. *Neuron*. 26:169-79.

Ramaswami, M., K.S. Krishnan, and R.B. Kelly. 1994. Intermediates in synaptic vesicle recycling revealed by optical imaging of Drosophila neuromuscular junctions. *Neuron*. 13:363-75.

Rao, S.S., B.A. Stewart, P.K. Rivlin, I. Vilinsky, B.O. Watson, C. Lang, G. Boulianne, M.M. Salpeter, and D.L. Deitcher. 2001. Two distinct effects on neurotransmission in a temperature-sensitive SNAP-25 mutant. *Embo J*. 20:6761-71.

Razzaq, A., I.M. Robinson, H.T. McMahon, J.N. Skepper, Y. Su, A.C. Zelhof, A.P. Jackson, N.J. Gay, and C.J. O'Kane. 2001. Amphiphysin is necessary for organization of the excitation-contraction coupling machinery of muscles, but not for synaptic vesicle endocytosis in Drosophila. *Genes Dev*. 15:2967-79.

Ren, G., P. Vajjhala, J.S. Lee, B. Winsor, and A.L. Munn. 2006. The BAR domain proteins: molding membranes in fission, fusion, and phagy. *Microbiol Mol Biol Rev*. 70:37-120.

Renden, R.B., and K. Broadie. 2003. Mutation and activation of Galpha s similarly alters pre- and postsynaptic mechanisms modulating neurotransmission. *J Neurophysiol*. 89:2620-38.

Reynolds, E.R., E.A. Stauffer, L. Feeney, E. Rojahn, B. Jacobs, and C. McKeever. 2004. Treatment with the antiepileptic drugs phenytoin and gabapentin ameliorates seizure and paralysis of Drosophila bang-sensitive mutants. *J Neurobiol*. 58:503-13.

Richards, D.A., C. Guatimosim, and W.J. Betz. 2000. Two endocytic recycling routes selectively fill two vesicle pools in frog motor nerve terminals. *Neuron*. 27:551-9.

Richmond, J.E., R.M. Weimer, and E.M. Jorgensen. 2001. An open form of syntaxin bypasses the requirement for UNC-13 in vesicle priming. *Nature*. 412:338-41.

Ringstad, N., H. Gad, P. Low, G. Di Paolo, L. Brodin, O. Shupliakov, and P. De Camilli. 1999. Endophilin/SH3p4 is required for the transition from early to late stages in clathrin-mediated synaptic vesicle endocytosis. *Neuron*. 24:143-54.

Rizo, J., and T.C. Sudhof. 2002. Snares and Munc18 in synaptic vesicle fusion. *Nat Rev Neurosci*. 3:641-53.

Rohde, G., D. Wenzel, and V. Haucke. 2002. A phosphatidylinositol (4,5)-bisphosphate binding site within mu2-adaptin regulates clathrin-mediated endocytosis. *J Cell Biol*. 158:209-14.

Rohrbough, J., and K. Broadie. 2005. Lipid regulation of the synaptic vesicle cycle. *Nat Rev Neurosci*. 6:139-50.

Rohrbough, J., E. Rushton, E. Woodruff, 3rd, T. Fergestad, K. Vigneswaran, and K. Broadie. 2007. Presynaptic establishment of the synaptic cleft extracellular matrix is required for post-synaptic differentiation. *Genes Dev*. 21:2607-28.

Royle, S.J., and L. Lagnado. 2003. Endocytosis at the synaptic terminal. *J Physiol*. 553:345-55.

Salcini, A.E., M.A. Hilliard, A. Croce, S. Arbucci, P. Luzzi, C. Tacchetti, L. Daniell, P. De Camilli, P.G. Pelicci, P.P. Di Fiore, and P. Bazzicalupo. 2001. The Eps15 C. elegans homologue EHS-1 is implicated in synaptic vesicle recycling. *Nat Cell Biol*. 3:755-60.

Satoh, A.K., and D.F. Ready. 2005. Arrestin1 mediates light-dependent rhodopsin endocytosis and cell survival. *Curr Biol*. 15:1722-33.

Schikorski, T., and C.F. Stevens. 2001. Morphological correlates of functionally defined synaptic vesicle populations. *Nat Neurosci*. 4:391-5.

Schulze, K.L., K. Broadie, M.S. Perin, and H.J. Bellen. 1995. Genetic and electrophysiological studies of Drosophila syntaxin-1A demonstrate its role in nonneuronal secretion and neurotransmission. *Cell*. 80:311-20.

Sever, S., H. Damke, and S.L. Schmid. 2000. Garrotes, springs, ratchets, and whips: putting dynamin models to the test. *Traffic*. 1:385-92.

Shao, X., C. Li, I. Fernandez, X. Zhang, T.C. Sudhof, and J. Rizo. 1997. Synaptotagmin-syntaxin interaction: the C2 domain as a Ca2+-dependent electrostatic switch. *Neuron*. 18:133-42.

Shin, B.S., D. Maag, A. Roll-Mecak, M.S. Arefin, S.K. Burley, J.R. Lorsch, and T.E. Dever. 2002. Uncoupling of initiation factor eIF5B/IF2 GTPase and translational activities by mutations that lower ribosome affinity. *Cell*. 111:1015-25.

Shupliakov, O., P. Low, D. Grabs, H. Gad, H. Chen, C. David, K. Takei, P. De Camilli, and L. Brodin. 1997. Synaptic vesicle endocytosis impaired by disruption of dynamin-SH3 domain interactions. *Science*. 276:259-63.

Shyngle, J., and R.P. Sharma. 1985. Studies on paralysis and development of second chromosome temperature sensitive paralytic mutants of Drosophila melanogaster. *Indian J Exp Biol*. 23:235-40.

Siddiqi, O., and S. Benzer. 1976. Neurophysiological defects in temperature-sensitive paralytic mutants of Drosophila melanogaster. *Proc Natl Acad Sci U S A*. 73:3253-7.

Sihra, T.S., E. Bogonez, and D.G. Nicholls. 1992. Localized Ca2+ entry preferentially effects protein dephosphorylation, phosphorylation, and glutamate release. *J Biol Chem*. 267:1983-9.

Slepnev, V.I., and P. De Camilli. 2000. Accessory factors in clathrin-dependent synaptic vesicle endocytosis. *Nat Rev Neurosci*. 1:161-72.

Sollner, T., S.W. Whiteheart, M. Brunner, H. Erdjument-Bromage, S. Geromanos, P. Tempst, and J.E. Rothman. 1993. SNAP receptors implicated in vesicle targeting and fusion. *Nature*. 362:318-24.

Song, B.D., D. Yarar, and S.L. Schmid. 2004. An assembly-incompetent mutant establishes a requirement for dynamin self-assembly in clathrin-mediated endocytosis in vivo. *Mol Biol Cell*. 15:2243-52.

Song, J., and M.A. Tanouye. 2006. Seizure suppression by shakB2, a gap junction mutation in Drosophila. *J Neurophysiol*. 95:627-35.

Stimson, D.T., P.S. Estes, S. Rao, K.S. Krishnan, L.E. Kelly, and M. Ramaswami. 2001. Drosophila stoned proteins regulate the rate and fidelity of synaptic vesicle internalization. *J Neurosci*. 21:3034-44.

Stowell, M.H., B. Marks, P. Wigge, and H.T. McMahon. 1999. Nucleotide-dependent conformational changes in dynamin: evidence for a mechanochemical molecular spring. *Nat Cell Biol*. 1:27-32.

Su, H., and D.K. O'Dowd. 2003. Fast synaptic currents in Drosophila mushroom body Kenyon cells are mediated by alpha-bungarotoxin-sensitive nicotinic acetylcholine receptors and picrotoxin-sensitive GABA receptors. *J Neurosci*. 23:9246-53.

Sudhof, T.C. 1995. The synaptic vesicle cycle: a cascade of protein-protein interactions. *Nature*. 375:645-53.

Sudhof, T.C. 2004. The synaptic vesicle cycle. *Annu Rev Neurosci*. 27:509-47.

Sunio, A., A.B. Metcalf, and H. Kramer. 1999. Genetic dissection of endocytic trafficking in Drosophila using a horseradish peroxidase-bride of sevenless chimera: hook is required for normal maturation of multivesicular endosomes. *Mol Biol Cell*. 10:847-59.

Suzuki, D.T., T. Grigliatti, and R. Williamson. 1971. Temperature-sensitive mutations in Drosophila melanogaster. VII. A mutation (para-ts) causing reversible adult paralysis. *Proc Natl Acad Sci U S A*. 68:890-3.

Sweeney, S.T., K. Broadie, J. Keane, H. Niemann, and C.J. O'Kane. 1995. Targeted expression of tetanus toxin light chain in Drosophila specifically eliminates synaptic transmission and causes behavioral defects. *Neuron*. 14:341-51.

Sweitzer, S.M., and J.E. Hinshaw. 1998. Dynamin undergoes a GTP-dependent conformational change causing vesiculation. *Cell*. 93:1021-9.

Takei, K., O. Mundigl, L. Daniell, and P. De Camilli. 1996. The synaptic vesicle cycle: a single vesicle budding step involving clathrin and dynamin. *J Cell Biol*. 133:1237-50.

Tan, T.C., V.A. Valova, C.S. Malladi, M.E. Graham, L.A. Berven, O.J. Jupp, G. Hansra, S.J. McClure, B. Sarcevic, R.A. Boadle, M.R. Larsen, M.A. Cousin, and P.J. Robinson. 2003. Cdk5 is essential for synaptic vesicle endocytosis. *Nat Cell Biol*. 5:701-10.

Tang, D., J. Yeung, K.Y. Lee, M. Matsushita, H. Matsui, K. Tomizawa, O. Hatase, and J.H. Wang. 1995. An isoform of the neuronal cyclin-dependent kinase 5 (Cdk5) activator. *J Biol Chem*. 270:26897-903.

Tebar, F., S.K. Bohlander, and A. Sorkin. 1999. Clathrin assembly lymphoid myeloid leukemia (CALM) protein: localization in endocytic-coated pits, interactions with

clathrin, and the impact of overexpression on clathrin-mediated traffic. *Mol Biol Cell*. 10:2687-702.

Teng, F.Y., Y. Wang, and B.L. Tang. 2001. The syntaxins. *Genome Biol*. 2:REVIEWS3012.

Teng, H., M.Y. Lin, and R.S. Wilkinson. 2007. Macroendocytosis and endosome processing in snake motor boutons. *J Physiol*. 582:243-62.

Tomizawa, K., S. Sunada, Y.F. Lu, Y. Oda, M. Kinuta, T. Ohshima, T. Saito, F.Y. Wei, M. Matsushita, S.T. Li, K. Tsutsui, S. Hisanaga, K. Mikoshiba, K. Takei, and H. Matsui. 2003. Cophosphorylation of amphiphysin I and dynamin I by Cdk5 regulates clathrin-mediated endocytosis of synaptic vesicles. *J Cell Biol*. 163:813-24.

Trotta, N., C.K. Rodesch, T. Fergestad, and K. Broadie. 2004. Cellular bases of activity-dependent paralysis in Drosophila stress-sensitive mutants. *J Neurobiol*. 60:328-47.

Trujillo-Cenoz, O. 1965. Some aspects of the structural organization of the arthropod eye. *Cold Spring Harb Symp Quant Biol*. 30:371-82.

Tsai, L.H., T. Takahashi, V.S. Caviness, Jr., and E. Harlow. 1993. Activity and expression pattern of cyclin-dependent kinase 5 in the embryonic mouse nervous system. *Development*. 119:1029-40.

Vallis, Y., P. Wigge, B. Marks, P.R. Evans, and H.T. McMahon. 1999. Importance of the pleckstrin homology domain of dynamin in clathrin-mediated endocytosis. *Curr Biol*. 9:257-60.

van der Bliek, A.M., and E.M. Meyerowitz. 1991. Dynamin-like protein encoded by the Drosophila shibire gene associated with vesicular traffic. *Nature*. 351:411-4.

Veraksa, A., A. Bauer, and S. Artavanis-Tsakonas. 2005. Analyzing protein complexes in Drosophila with tandem affinity purification-mass spectrometry. *Dev Dyn*. 232:827-34.

Verstreken, P., T.W. Koh, K.L. Schulze, R.G. Zhai, P.R. Hiesinger, Y. Zhou, S.Q. Mehta, Y. Cao, J. Roos, and H.J. Bellen. 2003. Synaptojanin is recruited by endophilin to promote synaptic vesicle uncoating. *Neuron*. 40:733-48.

Vickery, R.G., and M. von Zastrow. 1999. Distinct dynamin-dependent and -independent mechanisms target structurally homologous dopamine receptors to different endocytic membranes. *J Cell Biol*. 144:31-43.

Vijayakrishnan, N., and K. Broadie. 2006. Temperature-sensitive paralytic mutants: insights into the synaptic vesicle cycle. *Biochem Soc Trans*. 34:81-7.

Vijayakrishnan, N., E.A. Woodruff, 3rd, and K. Broadie. 2009. Rolling blackout is required for bulk endocytosis in non-neuronal cells and neuronal synapses. *J Cell Sci*. 122:114-25.

Wald, G. 1968. The molecular basis of visual excitation. *Nature*. 219:800-7.

Weber, T., F. Parlati, J.A. McNew, R.J. Johnston, B. Westermann, T.H. Sollner, and J.E. Rothman. 2000. SNAREpins are functionally resistant to disruption by NSF and alphaSNAP. *J Cell Biol*. 149:1063-72.

Wenk, M.R., and P. De Camilli. 2004. Protein-lipid interactions and phosphoinositide metabolism in membrane traffic: insights from vesicle recycling in nerve terminals. *Proc Natl Acad Sci U S A*. 101:8262-9.

Wu, M.N., T. Fergestad, T.E. Lloyd, Y. He, K. Broadie, and H.J. Bellen. 1999. Syntaxin 1A interacts with multiple exocytic proteins to regulate neurotransmitter release in vivo. *Neuron*. 23:593-605.

Wucherpfennig, T., M. Wilsch-Brauninger, and M. Gonzalez-Gaitan. 2003. Role of Drosophila Rab5 during endosomal trafficking at the synapse and evoked neurotransmitter release. *J Cell Biol*. 161:609-24.

Yakir-Tamang, L., and J.E. Gerst. 2009. Phosphoinositides, exocytosis and polarity in yeast: all about actin? *Trends Cell Biol*. 19:677-84.

Yang, C., and M.G. Kazanietz. 2003. Divergence and complexities in DAG signaling: looking beyond PKC. *Trends Pharmacol Sci*. 24:602-8.

Zelhof, A.C., H. Bao, R.W. Hardy, A. Razzaq, B. Zhang, and C.Q. Doe. 2001. Drosophila Amphiphysin is implicated in protein localization and membrane morphogenesis but not in synaptic vesicle endocytosis. *Development*. 128:5005-15.

Zhang, B., Y.H. Koh, R.B. Beckstead, V. Budnik, B. Ganetzky, and H.J. Bellen. 1998. Synaptic vesicle size and number are regulated by a clathrin adaptor protein required for endocytosis. *Neuron*. 21:1465-75.

Zhang, C., W. Xiong, H. Zheng, L. Wang, B. Lu, and Z. Zhou. 2004. Calcium- and dynamin-independent endocytosis in dorsal root ganglion neurons. *Neuron*. 42:225-36.

Zheng, J., S.M. Cahill, M.A. Lemmon, D. Fushman, J. Schlessinger, and D. Cowburn. 1996. Identification of the binding site for acidic phospholipids on the pH domain

of dynamin: implications for stimulation of GTPase activity. *J Mol Biol*. 255:14-21.